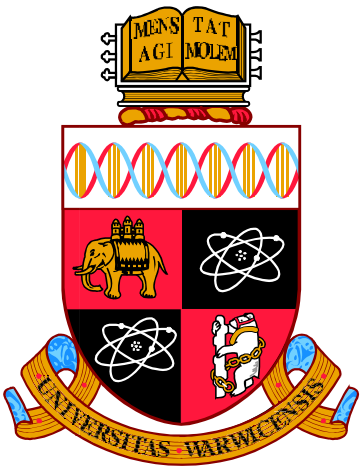

Molecular Communication Systems: Design, Modelling and Experimentation

by

Song Qiu

Thesis

Submitted to the University of Warwick

for the degree of

Doctor of Philosophy

School of Engineering

July 2017

THE UNIVERSITY OF WARWICK

献给我的父母

Contents

List of Tables

List of Figures

Acknowledgments

The most important person I would like to express my great gratitude to, is my primary supervisor, Dr. Weisi Guo. It is Dr. Weisi Guo, who introduced me to the research field and provided me with the valuable guidance as well as the persistent encouragement, helping me go through all difficulties I encountered during my Ph.D. study. His strongest support to both my research and daily life makes me not only grow to be an independent and hard working researcher, but also build up my own well-meaning personality. I can never achieve this level and stage without his supervision. Being his student is the greatest treasure I have ever had.

I would like to express my sincere appreciation to Dr. Mark Leeson, who is my second supervisor, for his time and efforts on continuously providing precious and valuable comments and feedback on my publications as well as my Ph.D. thesis. I would like to present my special thanks to Dr. Michael Chappell, Dr. Christos Mias and Dr. Mike Jennings within School of Engineering, University of Warwick, for their continuously suggestions and support for my Ph.D. study; And to Dr. Siyi Wang (Xi'an Jiaotong-Liverpool University), Dr. Mark D Mcdonnell (University of South Australia), Dr. Nariman Farsad (Stanford University), Professor Andrew Eckford (York University), Dr. Bin Li and Dr. Chenlin Zhao (Beijing University of Posts and Telecommunications), Dr. Yue Wu and Dr. Xiaoli Chu (The University of Sheffield), Dr. Yin Yao Dong (University of Oxford), Dr. Taufiq Asyhari (University of Bradford), Dr. Werner Haselmayr (Johannes Kepler Universitat Linz), for their valuable collaboration and comments on my research, which are indispensable for my research progress. Special thanks to Dr. Yunfei Chen (University of Warwick) and Prof. Arumugam Nallanathan (King's College London) for agreeing to be my

Ph.D. examiners.

My study would not have been completed without the help and the friendship of others, Dr. Kezhi Wang, Dr. Hu Yuan, Dr. Xiayang Wang, Dr. Yi Lu, Dr. Chenyao Bai, Dr. Wei Xing, Dr. Yangze Liao, Dr. Zhichao Rong, Dr. Xin Tong, Dr. Shuyue Lin, Dr. Pengyuan Qi, Dr. Xing Wei. Particularly, I would like to present my sincere thanks to Dr. Nurhan Gunes, Mrs. Elif Gunes, Mr. Osman Gunes and their family, who treat me as one of their family member, continuously supporting me. They always hold a place in my happy memories of my Ph.D. study in University of Warwick. I appreciate their precious friendship.

Finally, with my love and gratitude, I would like to dedicate this thesis to my family who always provides me the unreserved support and the selfishless love, especially to my parents, Mrs Mingqing Gao, Mr Bingwen Qiu, and my fiancee, Ms Fanlin Zhou.

Declarations

I herewith declare that this thesis contains my own research performed under the supervision of Dr Weisi Guo and Dr Mark S. Leeson, without assistance of third parties, unless stated otherwise. No part of this thesis was previously published or submitted for a degree at any other university.

List of Publications

Journals

[A] S. Qiu, W. Haselmayr, B. Li, C. Zhao and W. Guo, "Bacterial Mechanical Relay for Energy Efficient Molecular Communications", *IEEE Transactions on NanoBioscience*, Under Review, 2017.

[B] S. Qiu, T. Asyhari, W. Guo, S. Wang, B. Li, C. Zhao and M. Leeson, "Molecular Channel Fading due to Diffusivity Fluctuations", *IEEE Communication Letters*, vol. 1, pp. 1-4, December, 2016.

[C] S. Qiu, W. Guo, B. Li, Y. Wu, X. Chu, S. Wang and Y. Dong, "Long Range and Long Duration Underwater Localization Using Molecular Messaging", *IEEE Transactions on Molecular, Biological and Multi-Scale Communications*, vol. 1, pp. 363-370, July, 2015.

[D] S. Qiu, S. Wang, and W. Guo, "Experimental Nakagami Distributed Noise Model for Molecular Communication Channels With No Drift", *IET Electronics Letters*, vol. 51,. pp. 611-613, April 2015.

[E] S. Qiu, W. Guo, M. S. Leeson, S. Wang, N. Farsad, and A. W. Eckford, "Nanoparticle Communications: From Chemical Signals in Nature to Wireless Sensor Networks", *Nanotechnology Perceptions*, vol. 10, pp. 29-41, March 2014.

Conferences

[F] S. Qiu, T. Asyhari, and W. Guo, "Mobile Molecular Communications: Positional-Distance Codes", *IEEE International Workshop on Signal Processing Advances in Wireless Communications (SPAWC)*, pp. 1-5, August 2016.

[G] S. Qiu, N. Farsad, Y. Dong, and W. Guo, "Under-water molecular signalling:

A hidden transmitter and absent receivers problem, *IEEE International Conference on Communications (ICC)*, pp. 1085-1090, June 2015.

[H] S. Qiu, W. Guo, S. Wang, N. Farsad and A. W. Eckford, "A Molecular Communication Link for Monitoring in Confined Environments, *IEEE International Conference on Communications (ICC)*, pp. 718-723, June 2014.

[I] S. Wang, W. Guo, **S. Qiu**, and M. D. McDonnell, "Performance of Macro-Scale Molecular Communications With Sensor Cleanse Time, *IEEE International Conference on Telecommunications (ICT)*, pp. 363-368, April 2014.

Abstract

Molecular Communications (MC) is an increasingly attractive technique to enable the communication and networking of devices in environments where traditional communication techniques may not be suitable. MC has been used to convey information in both human society and in animal populations and been studied on both the microscale and the macroscale. On the basis of these studies, this thesis focuses on characterising MC channel models under different environments and examining the impact these models have on the communication performance.

The thesis begins by reviewing the latest developments in MC including communication paradigm, channel models, modulation schemes and forward error correction codes. It then provides the comprehensive research methods used during the PhD, including the construction of complex propagation environments and molecular communication equipments, and explains the procedures of the experimentation. The thesis then goes on to analyse the channel model for static environment. A novel capture probability expression of a finite sized receiver and the performance metrics of bit error rate, throughput and round-trip-time are derived. Experimentally, the additive noise in the channel response was found to conform to a Nakagami distribution. Afterwards, the thesis characterises two dynamic channel models, namely, the fading distribution due to temperature fluctuations, which is validated by numerical simulations, and the mobile channel where both transmitter and receiver are in mobility and in order to combat transposition errors, positional-distance codes are applied. Furthermore, the energy model of the bacteria based mobile relay channel is proposed to demonstrate a superior energy efficiency. Finally, the thesis goes on to propose a potential application of MC to locate a hidden entity with an unknown location in a vast underwater search space. Two molecular messaging methods for location discovery are proposed: a chemical encoding messaging method, and a Rosenbrock gradient ascent algorithm. The two chemical methods are found to offer attractive performance trade-offs in complexity and robustness. To conclude, the

potential future work on MC channel modelling is identified in complex geometric environments.

Abbreviations

1. Abbreviations

AC, Acoustic Communication
AHL, Acylhomoserine Lactone
AIGN, Additive Inverse Gaussian Noise
AIPs, Autoinducing Polypeptides
ATP, Adenosine Triphosphate
AWGN, Additive White Gaussian Noise
BER, Bit Error Rate
CCDF, Complementary Cumulative Distribution Function
CDF, Cumulative Distribution Function
CGL, Chemical Gradient Localizations
CIC, Chemical Information Carrier
CPT, Chemical Plume Tracing
C-RM, Cyclic Reed-Muller
CSK, Concentration Shift Keying
DAQ, Data Acquisition System
DHW, Distinct Hamming-weight Code
DNA, Deoxyribonucleic Acid
DPU, DNA Processing Unit
EG-LDPC, Euclidean Geometry Low Density Parity Check
EM, Electromagnetic
FEC, Forward Error Correction
FPT, First Passage Times
GEV, Generalized Extreme Value
HLA, High Level Architecture
HTAR, Hidden Transmitter and Absent Receiver
ID, Information Delivery
IP, Information Pick-up
ISI, Inter-Symbol Interference
LOC, Lab-On-a-Chip
LOD, Limit of Detection
MAP, Maximum A-Posteriori
MC, Molecular Communication
MCSK, Molecular Concentration Shift Keying
MCvD, Molecular Communication via Diffusion
MEC, Minimum Energy Codes
MEMS, Micro-Electro-Mechanical Systems
MEP, Minimum Error Probability
MIMO, Multiple Input Multiple Output
ML, Maximum Likelihood
MMSE, Minimum Mean Square Error
MoCo, Molecular Coding
MoSK, Molecular Shift Keying
MTSK, Molecular Transition Shift Keying
NBC, Nuclear, Biological and Chemical Defenses
NEMS, Nano-Electro-Mechanical Systems

NRD, Normal Random Deployment
OOK, On-Off Keying
OPDE, Ordinary Partial Differential Equation
PAM, Pulse Amplitude Modulation
PDF, Probability Density Function
PMF, Possison-Binomial Probability Mass Function
PPM, Pulse Position Modulation
RA, Receiver Attractant
RNA, Ribonucleic Acid
RSSI, Received Signal Strength Indication
RTT, Round Trip Time
RW, Random Walk
Rx, Stationary Receiver
SNR, Signal to Noise Ratio
SOCC, Self-Orthogonal Convolution Codes
TA, Transmission Attractant
Tx, Stationary Transmitter
URD, Uniform Random Deployment
UWOC, Underwater Wireless Optical Communication

2. Symbols denotations

$\Delta x_i, \Delta y_i, \Delta z_i, \Delta r_i$, random displacement
η_D, Decision threshold
η, Dynamic viscosity of the fluid
$\mathcal{B}$, Binomial distribution
$\mathcal{C}$, Codebook
$\mathcal{L}$, Laplace transform
$\mathcal{N}$, Normal distribution
ϕ, Channel gain (PDF)
ρ, Energy efficiency
τ, ISI period
τ_{delay}, Delay spread
PL_{radio}, EM propagation loss
θ_{c}, Captured number of molecules
θ_{ISI}, Number of molecules received as ISI
A, Energy attenuation
C, Molecular concentration
C_{Th}, Channel throughput
d, Horizontal distance from origin
D. Diffusion coefficient
d_{MoCo}, MoCo distance
D_{Tx}, Movement speed of Tx
D_x, D_y, D_z, Diffusion coefficients of x, y, z directions
E_{B}, Energy cost of passing one *plasmid* to one bacterium
E_{C}, Energy cost for a single bacterium swimming in the environment
E_{D}, Energy cost of decapsulation
E_{Del}, Total energy cost of producing the delivered plasmids
E_{E}, Energy cost of extraction the information from plasmid
E_{P}, Energy cost of encoding
E_{Total}, Total energy cost
E_{CGL}, Receiver Energy of CGL
E_{CIC}, Receiver Energy of CIC
$E_{p,\text{total}}$, Total molecular received energy from N_R molecular receivers
E_s, The energy of the step response
f_o, Frequency of the light beam
H, Sea depth
h, Vertical distance from origin

I, Molecular ISI strength
I_N, Number of plasmid being picked up by bacteria
k_B, Boltzman constant
L, Initial distance between Tx and Rx
M, Number of transmitted molecules
N, Molecular noise strength
N_N, Number of plasmid been successfully picked and delivered
N_R, Number of molecular receivers
P_e, Error probability
Q, Number of bacteria
r, Receiver deployment radius
R_{L}, Load resistance
R_{S}, Sensor resistance
R_{t}, Transmitter radius
$R_{\mathrm{Rep.}}$, Code rate
R_c, Deployment radius
R_H, Hydraulic radius of the molecule
R_N, Number of information molecules can be received of MCvD
R_r, Radius of receiver
t, Diffusion time
T, Molecules releasing period
$t_{\max}$, Time delay to peak pulse
t_{RTT}, Round trip time (Expected delay)
T_1, Receiver start searching time
T_2, Receiver finish searching time
T_p, Time period of bacteria swimming
T_s, Transmit bit duration
T_T, Temperature
v, Drift velocity
v^{prop}, Bacteria velocity
V_{in}, Input voltage
V_{out}, Output voltage
v_o, Sspeed of light in sea water
$W(\cdot)$, Product log function (*Lambert W* Function)
x, Distance between transmitter and receiver
x_{R}, Equivalent molecular propagation distance
$\Lambda_{1/2}$, Half-life of the message molecule
χ_n, Emitter transmit bit 1 or 0
ρ_p, Probability of bit 1
$\mu, \sigma, \omega, \lambda, \gamma$, Distribution parameters

3. Symbols used as substitutions

i, j, k, m, n, ϑ, ℓ.

Chapter 1

Introduction

1.1 Background

The need to convey information between two separated entities has always existed. There are many methods in which data can be encoded, transported and decoded. In human society, common ways of communicating include delivering physical packets (mail), speech (acoustic waves), modulating electromagnetic waves at various frequencies (radio waves in air, and optical waves in fibres), and visual observation of physical movements (hand, flag, or smoke signals). Nowadays, the 21st century is likely to see an unprecedented technological shift towards smarter and faster communication styles. Always-on, always-available digital communication has changed the world allowing mankinds to collaborate and share information using handheld devices, in ways unimaginable not long ago. People in various roles are being able to make more informed decisions about their actions, based on on-demand data availability. In order to provide the information, wired or wireless sensors need to communicate data from areas of interest to a data distribution network. This will occur on different levels such as (a) at the microscopic scale, swarms of nano robots with sensors can perform targeted drug delivery and (b) at the macroscopic scale, sensors need to report observations in industrial environments. Yet many of the

physical principles used in everyday digital communication break down as devices approach micro-scale or nano-scale dimensions, for example, the length scale becomes too small for an efficient electromagnetic wave antenna. Tiny devices, with dimensions of microns or less, must use different principles to exchange information. Another perspective to small dimensions is the physical environment (e.g. indoors, subterranean cavities, and tunnels). Points of interest in industry, cities, and military applications often lie in embedded and entrenched areas, accessible only by ventricles at scales too small for conventional radio- and micro-waves, and yet they are located in such a way that directional high frequency systems are ineffective. In detail, conventional wireless communications has been dominated by electromagnetic and acoustic wave-based information carriers. However, the cost and energy of generating high frequency waves can be unrealistic for communications between nano-scale machines. Furthermore, wave propagation obeys a set of laws that can cause severe energy degradation in certain confined environments such as micro-scale cavities, deep shadow, high noise, and other areas where the environment cannot act as a natural wave-guide. Such drawbacks make traditional methods of EM based communications no longer feasible.

However, in the animal kingdom, molecules can be used to convey very simple messages. This molecular signalling can exist on a cellular level, and also in an external environment, which show that information embedded in the property of chemical molecules can be a reliable way to communicate in the aforementioned scenarios. For example, in quorum sensing, bacteria exchange chemical messages to estimate the local population of their species; in signal transduction, cells in the body exchange messages to regulate each other's behaviour; Moths release pheromone to trace and communicate each other and the propagation of pheromone does not require external energy. Such nature inspired communication technique, named as *molecular communication* (MC), in which messages are carried in patterns of molecules [1], is applied on both the micro- and the macro-scale where cells and

animals communicate using a range of chemical molecules.

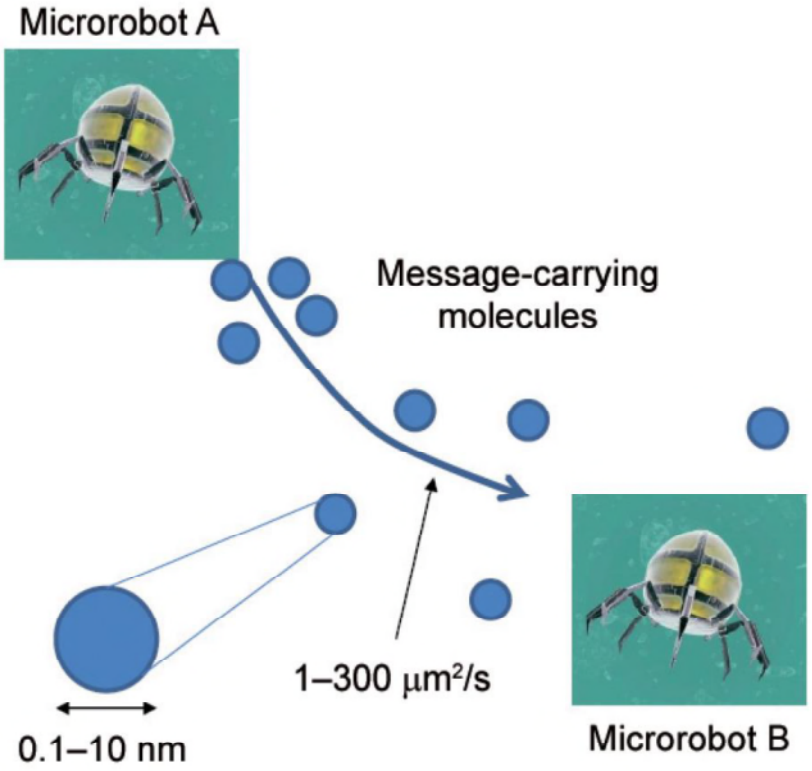

Figure 1.1: Illustration of nanotechnology communications between microsurgery robots.

Based on the existing knowledge of MC, a good question is, why would we devote our time and resources to study *molecular communication*? There is, of course, scientific curiosity: to better understand how organisms or animals signal to each other. Aside from this, to unlock a realm of futuristic possibilities, transforming what are staples of science fiction and technological speculation into reality. *Nanotechnology* is one of the techniques, which benefits from MC. Nanotechnology enables the miniaturization and fabrication of devices in nanometers. At this scale, a nanomachine is considered to be the fundamental unit, made from nanoscale components. With the interconnection of the nanomachines, a network can be re-

alised to execute multiple tasks, including computing, sensing, actuation, and so on. MC is a promising communication paradigm for networks at the nanoscale with nanomachines, where the transmission and reception of information can be achieved through molecules, as it is naturally existing in living organisms. For example, realization of nanotechnology includes, but is not limited to: targeted drug delivery with microscale robotics shown in Fig. 1.1. To accomplish this goal, thousands of blood-cell-sized, tiny robots would be deployed in the body. These robots have to cooperate with each other to autonomously navigate through the body, identify the targeted tumors and then release their carried drug to destroy the tumor. To actually cooperate, these microscale robots must be able to communicate. So the next question is, how to design such communication system in practice? As a result of the tiny size, the robots have few energy reserves, and must operate in the body without disrupting healthy tissues, or being destroyed by immune system before accomplishing drug delivery tasks. These features are consistent with the communication challenge faced by microorganisms, and these have solved the problem by exchanging signals and information composed of molecules, which in another way to say, by molecular communication.

1.2 PhD Project Overview

1.2.1 Project Motivations

This PhD project is concerned with molecular communication, which applies to applications where EM wave communication is not suitable, based on the potential advantages of the molecular diffusion process. However, there are a number of open challenges remaining in this field. First of all, many works have only considered infinite boundary conditions on diffusion based systems, however, a real communication channel normally has finite boundary conditions. Therefore, a channel model based on the real environment should be characterised and further the channel char-

acteristics including effect of inter-symbol interference (ISI), channel performance e.g., bit error rate (BER), throughput and signal to noise ratio (SNR), should be derived. Secondly, the channel environment is normally considered as homogeneous which means the diffusion coefficient is a constant over time. However, the environment can be heterogeneous (e.g., temperature variations in environment, mobile transmitter and receiver) in the real world. The relevant channel models need to be characterised. Finally, the active propagation MC models e.g. bacterial assisted propagation are very few in the literature which requires more attention.

1.2.2 Objectives

The objective of the PhD project is to characterize propagation channel models and understand the communication capacity and reliability for different channels based on a variety of biological and mechanical engineering environments. The PhD project has been separated into following tasks.

(1). Compare the performance of MC and EM wave based communication systems in a confined environment.

(2). Analyze molecular propagation and characterize channel models for static and dynamic environments.

(3). Investigate bacteria based molecular communication and compare the energy efficiency between bacteria based and diffusion based MC.

(4). Apply MC to a realistic problem: underwater search and rescue.

1.2.3 Contributions

The following contributions have been produced during the PhD project with relevant publications and will be explained in detail throughout Chapter 2 to 7.

(1) An extensive overview of recent state-of-the-art molecular communication has been produced [E] [1].

(2) A metal pipe network has been used as a 'confined environment' for comparison tests between MC and EM wave based experimental testbeds. The MC experimental testbed is able to transmit a number of alcohol molecules and detect the concentration of the alcohol. The path loss and delay spread of both EM-wave and MC based experimental testbeds have been compared respectively [H].

(3) A propagation channel model has been proposed for the 1 dimensional straight pipe channel and the theoretical expressions of BER and capacity of the channel have been derived. Based on the empirical results of the channel response of the straight pipe channel, a Nakagami noise model has been proposed for the 1 dimensional pipe channel [D, I].

(4) Two dynamic channel models, namely, a molecular channel fading model due to environmental temperature fluctuations and a mobile molecular communication model where both transmitter and receiver are randomly walking, have been characterised. Particularly, the fading distribution has been analytically derived and validated for the MC fading model, and positional-distance codes have been demonstrated to achieve superior performance over classical Hamming-distance codes for the mobile MC, respectively [B, F].

(5) A bacteria relaying channel model has been characterised and an energy model for this channel has been proposed. Furthermore, the information delivery energy efficiency has been derived and compared to molecular communication via diffusion [A].

(6) Two potential MC solutions applied to an underwater search and rescue application have been proposed, namely, chemical information carrier (CIC) and chem-

[1] See list of publications in Preface.

ical gradient localization (CGL). The performance of both solutions has been investigated by numerical simulations. The energy attenuation and communication latency performance are compared between MC solutions and conventional solutions [C, G].

1.3 Thesis Organisation

Chapter 2 firstly introduces the fundamental concepts of molecular communication and reviews recent state-of-the-art molecular communication advancements. It begins with the communication paradigm and explanation of information particles used in MC. Afterwards, the propagation environment in MC is categorised. Based on the different propagation environments, the relevant channel models, noise models and ISI are discussed. Then the recent modulation techniques of MC are reviewed and presented. Followed by the modulation schemes, the recently developed forward error correction coding schemes for MC are investigated and discussed. Finally, potential applications of MC are discussed and summarised.

Chapter 3 reviews the recent research methods used in MC, including simulation tools developed and experimental platforms created by researchers. Afterwards, this chapter provides the brief introduction of the design of the MC experimental platform, including the information on the design of metal pipes networks and topology, MC experimental system components and EM wave based communication experimental platform in detail. Finally the experimental procedures for testing the channel response of the MC system, the comparison of signal strength for MC and EM wave based system, and the data acquisition procedures for the mobile MC transmitter are presented in detail.

Chapter 4 firstly presents a statistical performance comparison of MC and EM wave based experimental platforms in the metal pipe network which is built in Chapter 3, and then proposes the theoretical channel model for the 1 dimen-

sional straight metal pipe. The channel model has been characterised with relevant boundary conditions and the performance of the channel including capacity and throughput have been derived, and then evaluated by numerical simulations. Then this chapter goes on to characterise the Nakagami noise model found during the channel response experiment of the MC experimental platform. Finally the bit error rate and capacity performance of the noise model have been proposed and evaluated by numerical simulations.

Chapter 5 proposes an analytically derived molecular channel fading model in the 1 dimensional straight pipe environment where the temperature varies approximately according to a Normal distribution. Numerical simulations have been applied to validate the fading distribution. Afterwards, a mobile molecular communication where the transmitter and receiver are mobile in the environment is introduced as well as the transposition error due to the mobility of the transmitter and receiver. Later, potential error correction codes which can be applied to mitigate the transposition errors are discussed and analysed. In order to imitate a large number of transposition errors, a double random walk channel is introduced and proposed for the mobile molecular channel. The performance of positional-distance codes is evaluated and demonstrated by numerical simulations.

Chapter 6 proposes a bacteria relaying channel model where bacteria are used as information molecule carriers and freely walk randomly towards the destination. Particularly, the information delivery energy model and energy efficiency equation are analyzed and derived. The performance including the number of molecules that can be delivered during a specific time period and the energy efficiency of the bacteria relaying model are compared with diffusion based MC by numerical simulations.

Chapter 7 provides two solutions based on MC for a research problem, which is Hidden Transmitter and Absent Receiver (HTAR) problem modelled from the MH370 tragedy in 2014. It begins with the motivations of the overview and drawbacks of conventional underwater communication solutions. Then this chapter pro-

vides the channel model for the underwater environment where the diffusion coefficient is non-isotropic. With understanding of the environment, two solutions for the HTAR problem are proposed and introduced. One is Chemical Information Carrier (CIC) by using information molecules which are embedded with location information. Another is Chemical Gradient Localization (CGL) where the location needs to be traced by the detector according to the gradient of the molecules released at the transmitter. Both solutions are evaluated by numerical simulations, particularly, the signal energy attenuation and latency are compared between CIC, CGL and conventional underwater search and rescue technology.

Chapter 8 concludes this thesis and proposes future work in MC.

Chapter 2

Literature Reivew

2.1 Overview of Molecular Communication

On December 29, 1959, the later (1965) Nobel laureate in physics, Richard Phillips Feynman first envisioned the fabrication of devices at the atomic or molecular level in his speech entitled: 'There's Plenty of Room at the Bottom' [2] delivered at an American Physical Society meeting at Caltech. His talk is to inspire researchers to find the solution to the problem of manipulating and controlling things on a small scale. Over the past decades, new fields of research, such as micro- and nano-electro-mechanical systems (MEMS and NEMS), were spawned for miniaturization. Meanwhile, it has long been recognized that microorganisms such as cells and bacteria, are able to gain information from their environment by gathering information chemicals which are sent by their neighbours. *Quorum Sensing* is an example of the important communication approach found in nature among most species of bacteria as well as some social insects to coordinate gene expression according to the density of their local population shown in Fig. 2.1 [3, 4]. Each bacterium acts as a transmitter as well as a receiver to release and capture specific molecules known as autoinducers in the environment.

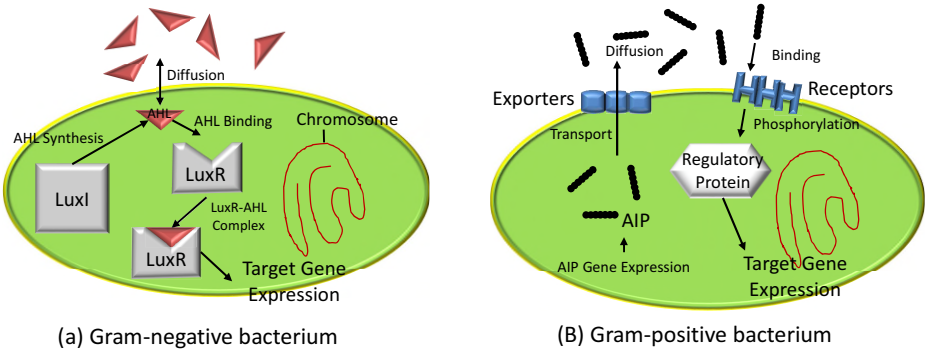

Figure 2.1: Quorum sensing in (a) gram-negative bacteria and (b) gram-positive bacteria.

The engineering aspects of MC, where messages are conveyed in patterns of molecules, was coined in a 2005 paper [5], which was focusing on the diffusion based MC design. Since then, a considerable research has been performed on MC. The work on MC has accelerated in the last 5 years with the contribution of nanonetworks. In order to operate the nanonetwork, multiple nano-sized devices have cooperated, which leads to the need to miniaturize current communication systems. Two approaches can be considered for the miniaturization, namely miniaturizing the traditional communication system on which abundant theory is available over the past century, or mimicking the existing molecular communication systems in nature. The latter approach, MC, has been recognised recently as an enabling technology for nanonetworks.

2.1.1 Communication Paradigm

The objective of a communication system is to transfer the information from one terminal to another terminal over space and time. In order to achieve the communication purpose, a signal is needed to be produced by a transmitter based on the information and then transferred to the receiver. The signal propagates in the communication channel to reach the receiver and then be decoded by the receiver.

Therefore, every communication system has three major components, namely, transmitter, receiver and the communication channel. Fig. 2.2 (a) shows a block diagram of a traditional communication system. In such a system, the information is typically encoded via electromagnetic (EM) waves. Then the signal will be modulated prior to transmission. While the signal is ready, the transmitter will transmit the signal into the channel of a wire or free space. The receiver receives the signal, then this will be demodulated and processed to decode the information. In a communication system, the channel may introduce noise into the system, where the noise is any distortion which results in the degradation of signal power. In the traditional communication system, the source of noise is normally the interference of different EM waves and the fading of EM waves (i.e. due to multipath).

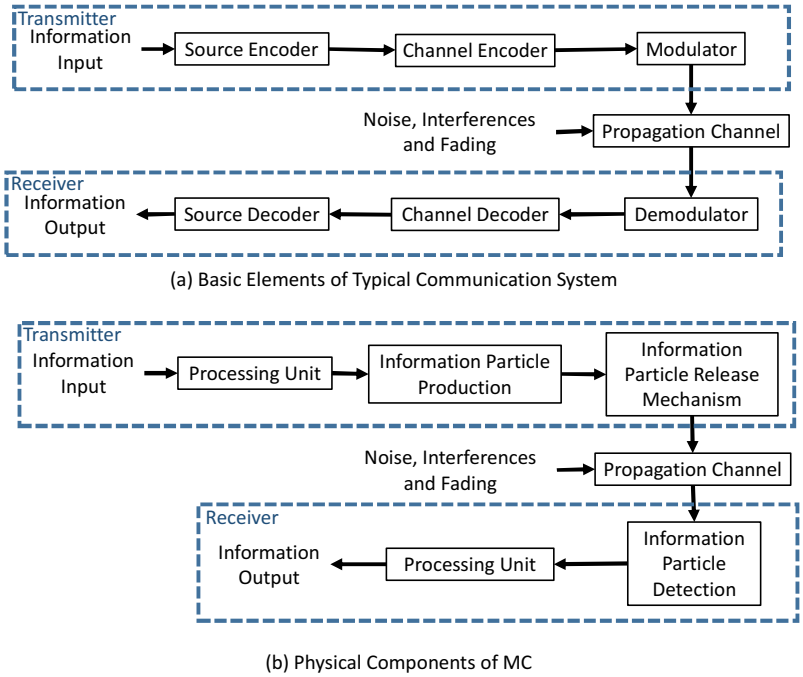

Figure 2.2: The communication paradigm of traditional communication and MC

Similar to the paradigm of traditional communication, Fig. 2.2 (b) shows the physical components required and the communication diagram in molecular

communication (MC). In MC, the information is embedded into the *information particle*, which is typically small biological compounds ranging in a few nanometers to micrometers in size. At the transmitter, a processing unit is needed to control the different processes within the transmitter chemically (chemical pathways) or electrically (microcontroller). The first physical process is required to process the information message into the information particle (i.e., encode the information) and store the information particles for transmission. The second physical process is to encode the information in the variations of chemical strengths (e.g., chemical concentration which can be detected by sensors). The transmitter needs to have a release mechanism to emit the information particles to the environment for propagation. A power source may be needed for the transmitter to function properly. After the information particles are released into the environment for propagation, a propagation mechanism is needed for transporting the particle to the receiver successfully. This mechanism can be free diffusion, flow assisted or an engineered assisting system using particle carrier powered by a molecular motor. At the receiver, a particle receptor or a detector is necessary to measure some properties of the arrival of information particles. For example, the receptor is able to know the presence or absence of the information particle, the type of the information particle, their concentration, time of arrival, etc. Normally the receiver need to decode the information from the information particle, thus a processing unit is necessary to decode and deciphering the received information. Same as the transmitter, a power source may need for the receiver to operation.

In MC, the noise can be introduced into the system from both transmitter, receiver and propagation channel. The sources of noise include transmitter emission noise, receiver counting noise, propagation noise, environment noise (e.g. degradation and chemical reaction) and molecular fading etc. MC is suitable over short-range (nm scale), mid-range (μm to cm scale) and long-range (cm to m scale) communication. For example, inside the neuron cell, neurotransmitters use free

diffusion to communicate with each other on the nm scale; between different cells, motor proteins are used to carry the biological compounds for transporting on the μm scale; hormones are propagated between different organs by flow (e.g. blood flow) over long-ranges.

In this thesis, the short-range and mid-range molecular communication are referred to as the microscale MC, and the long-range as macroscale MC. In the following sections, information particles as well as transmitter and receiver design in MC will first be introduced and reviewed. Afterwards, the propagation channel and noise models, ISI models are presented and reviewed. Then, the recent advancements in modulation schemes are examined. Further, error correction coding schemes are investigated and compared. Finally, the potential applications in MC are discussed.

2.2 Physical Components of MC

2.2.1 Information Input and Output

Molecular communication utilises an *Information Particle* as the information carrier during the communication process. The information particles used in nature include *small molecules* [1] (i.e., hormones, pheromone), peptides or amino acids, deoxyribonucleic acid (DNA) and ribonucleic acid (RNA) molecules and carbohydrates. Small molecules such as hormones [6] or pheromone [7] can be sent at short or long ranges and they are relatively stable in most fluid- and gas-phase channels and can yield up to 10^6 unique chemical combinations. Peptide molecules can transport a higher information content as each amino acid has 20 variables (usually, more in various microbes), yielding a near limitless complexity. There are natural receptors in the form of antibodies one can use to translate the message quickly and possibly bypassing a biological receiver. However, any peptide of > 10 amino acids will likely have secondary and tertiary structures so some parts of the message may get hidden

[1] The Mole mass of *small molecules* are relatively smaller than other biological molecules e.g., peptides and DNA.

on the inside. DNA and RNA molecules are structurally defined as nucleic acids. In cells, two DNA molecules referred to as the DNA strands, typically assemble to form a double-helical structure. RNA molecules are typically single-strand in cells. Both DNA and RNA are rarely sent in nature as a form of information carrier. However, there are small circular DNA molecules called plasmids which transfer themselves between microbes [8]. Carbohydrates are the class of biological macromolecule with probably the greatest potential for complexity and therefore for storing information. Monosaccharides typically contain 3 to 6 carbons, and many can exist as both ringed and straight-chained molecules. Monosaccharides can vary in relatively subtle ways [9], which makes them very difficult to tell apart chemically as well as by mass, but modern technology has made it possible to map their sites and structures [10].

The structure and size of the information particles may affect the way of their propagation in the environment. The information particles should be stable and robust against the noise and interference from other particles in the propagation environment for reliable MC. However, information particles may suffer from degradation in the environment by enzymatic attacks or changes in environmental pH [11]. In nature, in order to overcome the degradation, the transmitter can release a large number of information particles to fulfill the transmission purposes or encapsulate the information particle inside vesicle which is a small container of molecules enclosed by typically spherical lipid membranes. One example of a vesicle is the liposome shown in Fig. 2.3. The membrane of a liposome is made of two layers of phospholipid molecule, commonly referred as a lipid bilayer. Each phospholipid molecule has one hydrophilic head and two hydrophobic tails. The hydrophilic head has a negatively charged phosphate group and is attracted to water molecules. The hydrophobic tail is a fatty acid hydrocarbon chain (e.g., cholesterol) and repelled by water molecules. The lipid bilayer is about 5nm thick and it separates the aqueous environment inside the liposome from the outside environment so that the information particles inside the liposome can be protected by the lipid bilayer.

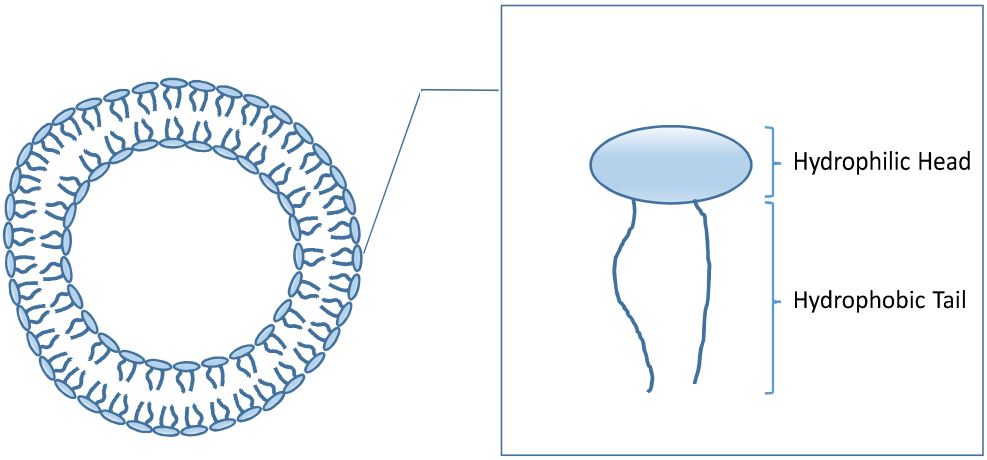

Figure 2.3: The structure of a liposome made of a lipid layer

Besides the biological molecules, any volatile chemicals which are of low toxicity, and safe to society and the environment such as alcohol molecules, carbon dioxide and so on, can be used as information particles for non-biological fields. Modern sensors are capable of detecting the concentration of the volatile chemicals while information signals can be encoded by the variations of the chemical concentration to realise communication purposes [12].

2.2.2 Design of Transmitter and Receiver

Recent research shows that the transmitter and receiver can be realised by artificially creating cells [13, 14, 15], or genetically modifying cells [16, 17, 18, 19] in microscale. Besides modifying the cells, the transmitter and receiver in microscale system can also been artificially created by liposome vesicles which act as the cell membrane and encapsulate different units inside together to form a cell and carry out the communication tasks [20]. In addition, the advancements of designing and manufacturing the components of MC at the macroscale have already been well studied and developed.

- **Processing Unit:** Both transmitter and receiver need a central processing

unit which acts as the brain of the communication system to process the information encoding, giving orders to the information particle generation unit or detection unit etc. In microscale MC, [21] and [22] show that the central processing unit can be achieved by implementing memory and logic gates into the cells. While in macroscale MC, the processing unit of both transmitter and receiver can utilize a computer or micro-controller to achieve the tasks.

- **Information Particle Production:** In order to generate the information particles, references [23, 24, 25] introduce several methods to modify a metabolic pathway of a biological cell which is used to generate information particles, including, transferring via viral vectors, transferring via embryonic stem cell and injecting directly to a germ line. After being modified, the cell metabolic pathway will synthesize and release specific signalling molecules [17, 18]. However, it is easier to obtain the information particles for macroscale MC since the information particles used are typically chemical mixtures (e.g., alcohol) rather than individual molecules in microscale MC.

- **Release Mechanism:** The unit to control the release of the particles in the transmitter can be achieved by a synthetic oscillator [26, 27] with the cooperation of a central processing unit, while in macroscale MC, the chemical mixtures will be released into the environment by an electrical spray.

- **Information Particle Detection:** For microscale MC, the unit to detect and sense the information particle can be realised by synthesising cell surface receptors [28, 29]. These are protein structures which can be seen as an antenna compared to traditional communication. While the receptor detects the information particle, the information particle will then bind to a ligand structure by the intermolecular forces of the receiver, such as hydrogen bonds and ionic bonds [30]. Therefore, in nature, the information particles are captured and removed from the propagation environment during the detection and in

some cases the information particle will be destroyed after dissociation [30]. On the other hand, for macroscale MC, the concentration of chemicals is detected by a sensor to decode the information. An example of macroscale MC communication system was proposed in [12] (see Chapter 3).

2.3 Propagation Channel

There are many different propagation mechanisms for MC to transport information particles, which can be categorized as two modes, namely passive mode and active mode. In passive mode (diffusion channel model), molecules randomly diffuse [31, 32] in all possible directions, making it particular suitable to environments which are unpredictable and dynamic. On the other hand, the active mode (motor protein assisted [33] and bacteria assisted [34], etc.,) provides the mechanism to propagate the information molecule directionally towards the destination. In this section, the propagation channel models will be reviewed in detail over the next subsections.

2.3.1 Diffusion Channel Models

Diffusion is the movement of molecules from a region of higher concentration to a region of lower concentration. The movement of the molecules is known as *Brownian Motion* which is the random motion of particles suspended in a fluid resulting from their collision with other molecules. Through the random motion, the particles do not require external energy for their propagation.

Statistical Channel Model

The propagation of the information particles (e.g., autoinducers) follows Brownian motion, which can be modeled by a *Wiener Process* and be accurately simulated by Monte Carlo simulations [35]. The Wiener process is defined in terms of the Gaussian distribution. Let x_0, y_0, z_0 be the initial position of the information particle at time

$t = 0$, for a discrete time period Δt and any integer $k > 0$, the motion of the particle is given by the sequence of coordinates (x_i, y_i, z_i) for $i = 1, 2, ..., k$ which represents the position of the particle at the time $t_i = i\Delta t$. Thus, (x_i, y_i, z_i) can be found as,

$$(x_i, y_i, z_i) = (x_{i-1}, y_{i-1}, z_{i-1}) + (\Delta x_i, \Delta y_i, \Delta z_i), \tag{2.1}$$

where $\Delta x_i, \Delta y_i, \Delta z_i$ are the random displacement given as,

$$\Delta x_i \sim \mathcal{N}(0, \alpha D \Delta t), \Delta y_i \sim \mathcal{N}(0, \alpha D \Delta t), \Delta z_i \sim \mathcal{N}(0, \alpha D \Delta t), \tag{2.2}$$

where D is the free diffusion coefficient and $\alpha = 2, 4, 6$ if the channel is 1-, 2-, or 3-dimensional, respectively. The value of D is given by [1, 36],

$$D = \frac{k_B T_T}{6\pi\eta R_H}, \tag{2.3}$$

where $k_B = 1.38 \times 10^{-23} JK^{-1}$ is the Boltzman constant, T_T is the temperature in K, η is the dynamic viscosity of the fluid, and R_H is the hydraulic radius of the molecule. In [35], the realistic value of D is considered ranging from $1 - 100\mu\text{m}^2\text{s}^{-1}$ in biotechnological applications.

While considering the information molecule released into the bloodstream, the the Brownian motion would be biased in the direction of the blood flow. Furthermore, it can be very slow for the information particle transporting from transmitter to the destination, thus introducing flow into the environment can be a solution to increase the speed of propagation. Therefore, the Brownian motion with flow needs to be considered. The flow assisted propagation can be investigated using Monte

Carlo simulations by modifying Eq. 2.2, which now given as,

$$\begin{aligned}\Delta x_i &= v_{x,i-1}(x_{i-1}, y_{i-1}, z_{i-1}) + \mathcal{N}(0, \alpha D \Delta t),\\ \Delta y_i &= v_{y,i-1}(x_{i-1}, y_{i-1}, z_{i-1}) + \mathcal{N}(0, \alpha D \Delta t),\\ \Delta z_i &= v_{z,i-1}(x_{i-1}, y_{i-1}, z_{i-1}) + \mathcal{N}(0, \alpha D \Delta t),\end{aligned} \tag{2.4}$$

where $v_{x,i-1}(x_{i-1}, y_{i-1}, z_{i-1}), v_{y,i-1}(x_{i-1}, y_{i-1}, z_{i-1})$ and $v_{z,i-1}(x_{i-1}, y_{i-1}, z_{i-1})$ are the flow speed in x, y, z directions respectively [35] which are a function of time and space as the velocities may not be constant in a real time channel.

First passage time, which is also called first hitting time, is used to describe the amount of time required for a stochastic process, starting from an initial state, to reach a threshold (i.e., barrier, boundary or a state of a system) for the first time. It is important to understand the probability of a first passage time of the information particle in Brownian motion of reaching some position from its start location. It is assumed that information particles diffuse freely in the environment without being absorbed by the medium or transmitter and receivers. Also these particles move independently of each other and will not interact. Based on these assumptions, the diffusion process of information particles in an isotropic fluidic medium is described by Fick's law [31]:

$$\frac{\partial C(x,t)}{\partial t} = D \nabla^2 C(x,t), \tag{2.5}$$

where $C(x,t)$ is the concentration of particles at time $t > 0$ at distance x from the source $\in \mathbb{R}^{\dim}$ with dimension $\dim \in \{1,2,3\}$. D is the diffusion coefficient, and $\nabla^2 = \sum_{\mathrm{i}=1}^{\dim} \partial^2/\partial x^2$ is the Laplacian operator. Therefore, the probability density function (PDF) for a particle to reach the boundary of destination (i.e., receiver) can be found by solving the partial differential equations, given as [37],

$$\phi_{\mathrm{hit}}(x,t) = \frac{1}{(4\pi D t)^{\dim/2}} \exp\left(-\frac{x^2}{4Dt}\right). \tag{2.6}$$

Most receptors in biological molecular communication remove the information particles from the environment through binding, absorbing, chemical reaction, or destruction [30, 38] to make sure all the molecules contribute to the signal only once. Thus, the literature mostly considers an absorbing receiver in 1-dimensional and 3-dimensional environments [32, 39]. By assuming the absorbing radius of the receiver is R_r, the cumulative distribution function (CDF) for capture one molecule is simply given as [40],

$$\begin{aligned} f^{1D}_{\text{capture}}(x,t) &= 1 - \int_{R_r}^{x} \phi_{\text{hit}}(u,t,\dim=1)\mathrm{d}u \\ &= \operatorname{erfc}\left(\frac{x-R_r}{\sqrt{4Dt}}\right), \end{aligned} \tag{2.7}$$

where $\operatorname{erfc}(\cdot)$ is the complementary error function. Therefore, the first passage probability for 1-D environment can be found as [39],

$$\phi^{1D}_{\text{capture}}(x,t) = \frac{\partial f^{1D}_{\text{capture}}(x,t)}{\partial t} = \frac{x-R_r}{\sqrt{4\pi D t^3}} \exp\left(-\frac{(x-R_r)^2}{4Dt}\right). \tag{2.8}$$

Similarly, the first passage probability of a spherical receiver in a 3-D environment is given as [41, 42],

$$\phi^{3D}_{\text{capture}}(x,t) = \frac{R_r}{x+R_r}\frac{x}{\sqrt{4\pi D t^3}} \exp\left(-\frac{(x-R_r)^2}{4Dt}\right). \tag{2.9}$$

Assuming M information particles released at the transmitter, thus the concentration of the information particles at the absorbing receiver in 3-D environment over time t is given by

$$C^{3D}_{\text{capture}}(x,t) = M\phi^{3D}_{\text{capture}}(x,t). \tag{2.10}$$

Additive Noise and ISI Models

In terms of additive noise, most research has focused on utilizing diffusion equations with an additive noise component. In a pulse modulated MC system, noise can arise from many reasons e.g., inconsistent mechanical pulse emissions, physical disturbances, atmospheric influence and receiver design. It is difficult to take all into consideration or argue which dominates. Recent studies on noise models have divided into 2 scenarios, **(1) No Drift:** The noise comes from the random arrival of information particles explained in [43]. For M emitted information particles, the number of arriving molecules follows a Binomial distribution $\sim \mathcal{B}(M, \phi^{3D}_{\text{capture}}(t))$. **(2) With Drift:** Based on the hardware prototype in [12] and further investigation in the performance of the prototype, the authors [44] proposed a Gaussian distributed additive noise model as a reasonable approximation for the flow channel.

ISI is an important issue in MC. One of the propagation mechanisms of the information particle is diffusion where the movement of information particle is random walk, thus it is impossible to predict the accurate arrival time of information particles at the destination. They remain in the environment and will not vanish until they reach the receiver or infinity (only if the boundary and time are infinite). Hence, some information particles may arrive at the receiver in future time slots and cause a form of interference to the detection of that corresponding symbol when they arrive. This interference is known as ISI, which can degrade the channel performance (e.g., capacity, reliability) significantly. Therefore, it is very important that ISI is considered.

An ISI model has been analyzed by [43] for a binary concentration modulated scheme. The number of molecules arriving at the receiver follows $\sim \mathcal{B}(M, \phi^{3D}_{\text{capture}}(t))$, given that M is large enough and the probability $\phi^{3D}_{\text{capture}}(t)$ is neither close to 1 nor 0, the ISI can be approximately modeled as a sum of random variables, each following a Gaussian distribution. In order to use this ISI model, some assumptions are applied: (i) the ISI is dominated by the previous symbol, (ii) the transmission

distance is neither too close nor too far (i.e., $\phi^{3D}_{\text{capture}}(t)$ is neither close to 1 nor 0). The distribution has been used for channel capacity analysis and evaluation of error correction coding scheme performances. Atakan [45] considered a more general ISI model for the binary concentration modulation MC. It showed that the ISI can be represented as an additive noise which could be modeled as Possison- Binomial probability mass function (PMF) and then the maximizing input probability distributions were estimated.

2.3.2 Bacteria Assisted Propagation

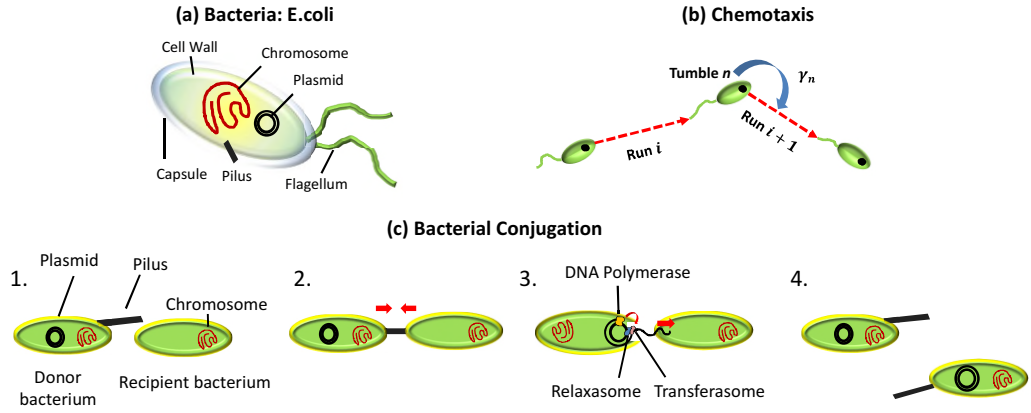

Figure 2.4: Bacteria assisted propagation fundamental: (a) the structure of E.coli, (b) chemotaxis in the environment, and (c) example of bacterial conjugation process.

Despite the passive mode of propagation of the information particle, an active mode is also widely used in nature. One major way to achieve the transportation purpose is using bacteria assisted propagation which is introduced in [46, 47]. Being different from diffusion, in this scheme, the information particles are placed inside bacteria at the transmitter side and the carrier bacteria are released into the environment to propagate to the destination and finally release the information particle to the receiver and finish the communication process. In order to achieve the communication purposes, bacteria have two distinct characteristics suitably acting as the informa-

tion carrier, namely chemotaxis and bacteria conjugation. Fig. 2.4 illustrates the structure of a bacterium, the chemotaxis of bacteria and the process of bacterial conjugation. The bacteria used as information carriers in nature [46, 47] are normally rod-shaped with 2 μm long and 1 μm wide. For example, *E. coli*, which is a flagellated bacterium, is able to self propelling in the environment. The flagellum provides the force of propelling as well as the force to tumble for the bacteria to find a new direction to propel. *E. coli* is able to sense at least 12 different attractants using its chemoreceptor and it has short-term memory (spanning a few seconds [48]) to remember the attractant concentration gradient. It is also able to present no response towards specific attractant [47] so that *E. coli* may be guided to a specific target that emits a given attractant. With the ability of sensing attractants' concentration gradient, the bacteria could swim towards higher concentrations of a preferred attractant. Such a navigation process is known as *Chemotaxis*, and it is possible to simulate the chemotaxis process [49, 50, 51]. As shown in Fig. 2.4 (b), chemotaxis is presented as a modified version of a *Pearson-Rayleigh* random walk [34, 52], which is represented by a repetition of two stages including (i). the bacteria propel over a straight line at constant speed for exponential distributed amount of time and (ii). the bacterium tumbles around uniformly choosing a new direction arbitrarily between 0 and 2π. In stage (i), the displacement is formulated as follows:

$$\Delta r_i = v_i^{\text{prop}} T_i^{\text{prop}}, \tag{2.11}$$

where Δr_i, v_i^{prop}, and T_i^{prop} denote the displacement, propelling velocity and propelling duration for ith run. T_i^{prop} is exponentially distributed random variable with rate λ_{prop}.

Between the ith and $i+1$th propelling, the bacteria tumble and choose a new direction. In the tumble stage (ii), the new angle for the direction of motion is given by,

$$\Theta_{n+1} = \Theta_n + \gamma_n, \tag{2.12}$$

where Θ_{n+1} and γ_n represent the previous angle of motion and the angular variation due to bacteria tumbling; γ_n is assumed to be uniformly distributed on $(0, 2\pi]$.

Fig. 2.4 (c) shows the process of bacteria conjugation, which is the transfer of genetic material between bacterial cells by a bridge-like connection between two bacteria or cells [53]. when two bacteria come closely enough to each other, the bacterium holding the genetic material such as plasmids (i.e., a chemical message encoded as a DNA sequence) will first act as a donor to attach the other bacterium by its pilus, which will retract to get the recipient bacterium in physical contact with the donor. The membranes of both donor and recipient bacteria are now connected and a single strand of DNA will be unwounded from the encoded plasmid and then passed to the recipient bacterium. After this DNA has been transferred, it replicates to a full plasmid in the recipient bacterium while the donor and recipient bacterium separate. As a result, the previous recipient bacterium is transformed into a donor. The single stranded DNA in the previous donor will also replicate to a full plasmid and wait for the next recipient bacterium for transferring the plasmid.

The bacterial channel model was proposed in [46, 47, 51]. The assumption was made that the receiver could release attractant to guide the bacteria in the environment (i.e., chemotaxis). The information particle such as plasmid (i.e., a single strand of DNA) can be encapsulated in the bacterial carrier. With chemotaxis, the information particle can be delivered to the receiver. Particularly, [47] proposed the simulation of the communication process by bacteria and later [54] modeled the process of chemotaxis as a Pearson-Rayleigh random walk and derived the closed form of end-to-end first passage probability of the MC channel via bacteria.

2.3.3 Recent Advancements on MC Channel Characterization

The recent advancements on characterising the channel models of MC can be divided into 3 different categories, namely, discrete diffusion channel model, channel models based on the diffusion equations and time modulation scheme based channel model.

The most widely studied diffusion channel model in MC is based on the binary CSK modulation scheme without flow. Atakan and Akan [55] first proposed the channel model of binary CSK with ligand receptors (i.e., capture receptor). This model can be represented as a binary symmetric channel with some simplified assumptions e.g., ISI was not considered. They then introduced the maximizing input probability distribution for the model in [56] and continued proposing the channel models for the broadcast channel, relay channel, and multiple-access channel in [57] as well as the channel capacity of the proposed channel models in [58]. Reference [59] made a simpler assumption that only the interference from 1 previous symbol affects the current symbol. Under this simplified assumption, the authors derived the data rate and examined this by computer simulations. As explained in the previous section, the molecular degradation and energy consumption of MC are essential and practical issues which are necessary to be considered in the channel model. [60] introduced and modeled the molecular degradation over time (i.e., the number of molecules in the channel) as an exponential probability distribution. With the degradation model, [60] further investigated the channel capacity by different degradation rates. [43] proposed the energy model for the binary-CSK and showed the maximum number of information particles that can be generated and transmitted by the limited energy. It also investigated the data rate and channel capacity for the proposed channel model.

The channel models based on the diffusion equations have also been widely studied. One of the first research works was in [31] where the input signal was defined as $x(t)$, the output signal of the MC channel is $y(t)$ where $y(t)$ is the convolution of impulse response $\phi(t)$ of diffusion equation and input $x(t)$ plus the additive noise $n(t)$

given as $y(t) = \phi(t) * x(t) + n(t)$. In [31], the authors considered an end-to-end model for MC and derived the channel gain and delay function for the continuous model with a capture receiver (i.e., ligand receptors) by using circuit theory to compute the transfer functions of transmission, diffusion and reception processes respectively. Then the authors proposed a closed-form for the lower bound on the channel capacity of continuous MC in [32] which indicated that the channel capacity increased linearly with the bandwidth of the input signal. The authors then proposed a more realistic model which considered the discrete nature of the information particles and the randomness of their propagation during the diffusion in [61]. They modeled the discrete nature and the randomness of propagation as an additive noise which can be directly added to the continuous diffusion equations. Further more, the authors used the same process and provided simplified assumptions and Markov chains to model the randomness of ligand-binding process in the capture receivers (i.e., ligand receptors) as additive noise.

The information can be modulated by the time of releasing the information particles. The first research for modelling such a channel model was proposed in [39] which considered a 1-dimensional channel and proposed a 1-dimensional hitting probability time distribution and derived the channel capacity. It was shown that it is possible to transmit more than 1 bit data per information particle. Later in 2012, the authors further expanded their work to 3-dimensional environment with consideration of flow [62]. They proposed that the arriving time of a single information particle can be modeled by an additive inverse Gaussian noise (AIGN) model and derived the lower and upper bounds for the channel capacity and designed a receiver based on the derived AIGN channel model and maximum likelihood estimator. [62] concluded that the lower and upper bounds were tight when the flow was at low rates and the bounds could separate while the flow rate increased or decreased to zero. Followed by the conclusion, [63] proposed tighter bounds for the capacity of the AIGN model and [64] proposed a more general fundamental framework of

the channel model which considered the information was modulated by both the releasing time (i.e., timing) and the type of particles (i.e., identity).

2.4 Modulation Schemes

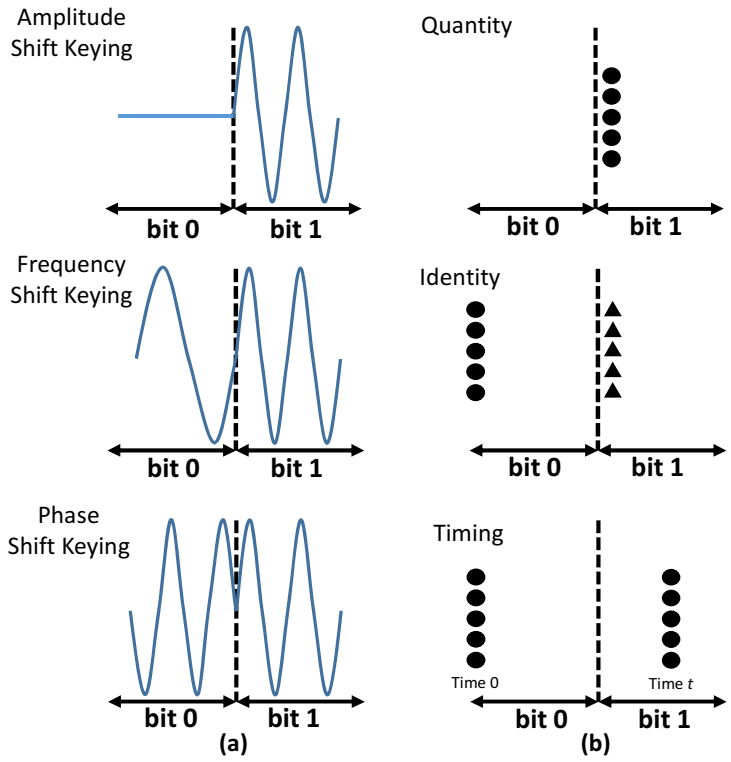

Figure 2.5: Modulation techniques in (a) the traditional communication systems and (b) molecular communication.

A question may be asked, how does MC work? Recalling the traditional communication, in order to achieve communication purposes, the information needs to be modulated onto EM wave carriers. Modulation is the process of varying the properties of a carrier signal according to the transmission symbols. In traditional communication, the carrier signal is EM waves which are sinusoidal signals, characterised by their amplitude, frequency or phase. Information can be modulated on the amplitude (which affects the peak-to-peak value of the sinusoidal signal),

frequency (which affects the number of cycles per second), phase (which affects the amount of shift from the origin) or a combination of these parameters to modulate binary data (0 and 1). Comparing with the traditional communication, in MC, the information is carried by information particles as introduced in Section 2.2.1. In order to convey distinct messages, each possible message is associated with a molecular signal: a unique pattern of molecules for each possible message, which can be distinguished at the receiver. On the other hand, MC is available to transmit digital signals (i.e., binary data), where the information can be modulated based on the properties of information particles, namely, *Quantity*, *Identity* and *Timing* or the combination of theses three parameters.

- **Quantity**: Information can be encoded in the number of particles released from the transmitter. For instance, there are $M > 0$ molecules available at the transmitter, the binary data 0 can be sent by releasing zero molecules, or 1 by releasing M molecules. If the receiver observes 0 molecules, it can decide that a 0 was sent. On the other hand, if it detects at least 1 molecule, it can conclude a 1 was sent. If M is very large (e.g., at macroscale), the concentration (i.e., the number of molecules per unit volume) of the molecules can be used.

- **Identity**: It is possible to encode the information by different type of molecules released. For instance, there are two types of molecule available at the transmitter, namely, Type A and B (which can be distinguished by the receiver). The binary data 0 can be sent by releasing molecule A, or a 1 by releasing B. The receiver would decide data 0 or 1 by observing the type of the received molecules.

- **Timing**: Information can be encoded in the time of releasing the molecules. For instance, a single molecule is available at the transmitter, the binary date 0 can be sent by releasing the molecule right now, or a 1 by waiting $t > 0$

seconds before releasing the molecule. The receiver could decide which binary data was sent by measuring the arrival time the molecule.

Fig. 2.5 demonstrates the comparison between the modulation techniques of traditional communication and MC.

2.4.1 Baseband Modulation

Basic Modulation

The first research on MC modulation schemes was proposed in [65] in 2010 which considered two different modulation schemes for the diffusion based propagation channel of MC. The first modulation scheme was similar to the on-off keying (OOK) modulation scheme in the traditional communication which considered that the binary data of bit 0 was represented by concentration 0 and the bit 1 by concentration C. The other modulation scheme considered the concentration of the information particles is varied by a sinusoidal signal with a specific frequency. It showed that the information can be encoded by the amplitude and frequency of the sinusoidal wave. Furthermore, the researchers in [66, 67] proposed two new modulation schemes for the diffusion based propagation channel. One was based on the quantity of the molecules released by the transmitter and named concentration shift-keying (CSK), and another was based on the identity of the molecules, where the transmission symbols were encoded by two different type of molecules and this modulation scheme was called molecular shift-keying (MoSK). Particularly, [67] considered the interference in the co-channel where two transmitters and two receivers were deployed.

[68] showed that it is possible to encode the information on the pulses of continuous diffusion channel models and proposed using two pulse based techniques, namely, pulse amplitude modulation (PAM) and pulse position modulation (PPM). In PAM, the bit 0 was represented with no pulse sent by the transmitter and bit 1 was represented by a pulse with specific amplitude at the beginning of the symbol

interval. In PPM, the symbol interval was divided into two halves, the bit 0 was considered as a pulse in the first half of the divided interval and the bit 1 was a pulse in the other half of the interval. [69] considered the modulation on the response of the system and further analyzed the maximum value of the peak response, peak's width at half maximum, and the delay to reach the peak value. It concluded that the information can be encoded and decoded by the characteristics of the pulses. [70] introduced a modulation scheme which is hybrid one based on identity and the releasing timing of the information particles. The proposed scheme was asynchronous and was able to achieve higher data rates than identity based or timing based modulation schemes.

ISI Mitigating Modulation

As introduced in Section 2.3.1, ISI can significantly degrade channel performance, therefore, it is important to consider the mitigation of ISI when designing a modulation scheme.

Molecular concentration shift keying [71] is proposed to mitigate the ISI effects. There are two types of information particles used in this scheme, where the transmitter uses type A molecules in odd time slots and type B in even time slots. The difference between MoSK is that the keying is depends on the concentration of the molecules rather than the identity of the molecules so that the receiver would only count the concentration of a specific type of molecules according to the slot number. [72] proposed a molecular transition shift keying (MTSK) scheme by combining CSK and MoSK to realise the mitigation of ISI. Two different types of molecule were prepared and the modulator decided which type of molecule would be sent based on the current symbol and previously transmitted symbol and then released the fixed number of molecules into the channel. For example, the bit-0 instances in the sequence are encoded by the absence of the information particles. The bit-1 instances are encoded by using two different types of molecules, where

the type of the molecules depends on the value of the next symbol. Same authors further proposed a pre-equalization technique at the transmitter side for ISI mitigation [73] and improved the bit error rate (BER) of the molecular communication via diffusion (MCvD) system significantly. As the information particles may remain in the channel, one solution is to remove them by chemical reaction. [74] introduced presenting enzymes in the channel to slowly degrade the information particles while they propose in the environment, which resulted the reduction of ISI and BER. Table. 2.1 compares the modulation techniques of the state of art.

Table 2.1: Comparison of Modulation Techniques

Modulation (Abbr.)	**Based on**	**ISI Mitigation**	**Reference**
Concentration shift keying (CSK)	Quantity	No	[66]
Molecular shift keying (MoSK)	Identity	Yes	[67]
Pulse amplitude modulation (PAM)	Quantity	No	[68]
Pulse position modulation (PPM)	Timing	No	[68]
Molecular concentration shift keying (MCSK)	Quantity and Identity	Yes	[71]
Molecular transition shift keying (MTSK)	Quantity and Identity	Yes	[72]

2.4.2 Receiver Side Signal Processing

Demodulation at the receiver side is also an important research topic in MC. A number of research works consider optimal detection for MC receivers and to reduce the complexity, a sequential estimation strategy is used in practice. For example, maximum the a-posteriori (MAP) criterion is used for designing an optimal receiver for the MoSK modulation scheme [75] to minimize the probability of error. It showed that the diffusion channel was linear and time-invariant and further designed the optimal receiver. The optimal receiver design for the binary concentration scheme was proposed in [76, 77] and for the OOK scheme in [78]. In order to design an optimal receiver, [78] firstly considered the Brownian motion of the information particle as noise which was assumed to be Gaussian noise. By using the continuous diffusion equation as the channel response and solving the equivalent problem of

estimating the state of a finite-state machine, the authors achieved detection based on both the MAP and the maximum likelihood (ML) criteria. Finally, the same authors of [74] proposed the design of an optimal receiver for the MC channels with enzymes deployed as well as with flow and noise in [79]. An ML detector and weighted sum detector was proposed and the expected bit error probability were derived respectively. Another widely used optimal detector is based on the minimum mean square error (MMSE) [78] criterion , which minimises the covariance matrix of the detection errors.

2.5 Forward Error Correction Code

Forward-error-correction (FEC) coding is an important issue of the modern digital communication. This section will review the FEC in MC for two types of errors, namely, additive noise errors for CSK modulation schemes and transposition errors for PPM modulation schemes.

2.5.1 Additive Noise Errors

Considering additive noise, the *Hamming distance* is widely used as a criterion for a code design. Relatively simple block codes use added parity check bits to enable the correction of errors. Hamming codes are described as $n = 2^m - 1$ length codes, where m is the number of parity check bits. The minimum distance of this type of block code is 3, allowing the detection of 2 errors and the correction of 1 error. In order to develop low energy MC systems, minimum energy codes (MEC) were considered in [80]. When considering a BCSK modulation scheme, codewords with a lower weight (more '0' bits) result in a lower energy consumption. Therefore, minimizing the average code weight is necessary to minimizing the energy expenditure. According to the results in [80], this coding scheme is able to achieve significantly lower energy per bit (50% reduction), but will need large codeword lengths to achieve a similar

level of BER performance. A comparison of Euclidean geometry low density parity check (EG-LDPC) and cyclic Reed-Muller (C-RM) codes can be found in [81]. More advanced codes such as Self-Orthogonal Convolution Codes (SOCCs) have also been developed recently and improve on Hamming codes to deliver a superior coding gain and lower energy expenditure [82].

2.5.2 Bit Transposition Errors

There are two sources resulting transposition errors: **(1) Intra-Codeword Errors** due to the permutation of bits position within a codeword, and **(2) Inter-Codeword Errors** due to the late/early arrival of bits which affect other codewords. Hamming distance is particular relevant when dealing with bit distortion due to additive noise, but it may no longer be accurate when dominant errors are due to bit transposition. Thus, in order to tackle the intra-codeword errors, *Hamming Weights* is a sensible choice to achieve the requirements. Distinct Hamming-weight Code (DHW) [83] was introduced which codebook consists of words having distinct Hamming weights. A new criterion named the molecular coding (MoCo) distance function aimed to find the codewords that maximize the minimum pairwise MoCo distance has been recently proposed as criterion for code design that tackles intra- and inter-codeword errors [84]. MoCo is capable of clearly addressing the intra-codeword errors, and the least significant bit '0' in each codeword was believed to serve as a guard band that reduces inter-codeword interference. However, the nature of the exhaustive search for the best codebook and the lack of an analytical expression of the error probability for good MoCo codes make it difficult to assess whether MoCo codes will still be optimal for varying system and channel parameters. Recent research found in [85] has provided a more methodical code construction for molecular communication that addresses both intra-codeword errors and inter-codeword interference. The resulting code is denoted as an (n, k, ℓ) ISI-free code where n is the block length, k is the message length (in bits) and ℓ denotes the correctable

crossover level. The name ISI-free is somewhat misleading, as the codeword does not target the removal of inter-symbol-interference (ISI), and rather it is a positive side effect. The ISI-free code partially uses Hamming weight features, in order to minimize the transposition errors within a codeword. The inter-codeword interference is suppressed by assigning two codewords for each message such that for two contiguous transmitted codewords, the last ℓ bits of the first codeword are identical to the first ℓ bits of the second codeword. Encoding messages $01, 10, 11$ yields codewords $0001, 1100, 1110$. [85] showed that the ISI-free codes improved the performance of MC with lower bit error rates compared to uncoded transmission under the same throughput. Table. 2.2 compares the coding schemes of the state of art.

Table 2.2: Comparison of Coding Schemes

Coding Scheme	**Based on**	**Error Type**	**Reference**
Hamming	Hamming Distance	Additive Noise Errors	[81]
MEC	Hamming Distance	Additive Noise Errors	[80]
SOCCs	Convolution Codes	Additive Noise Errors	[82]
DHW	Hamming Weights	Intra Codeword	[83]
MoCo	Molecular Coding Distance	Intra- and Inter Codeword	[84]
ISI-free	1 to many codewords	Intra- and Inter Codeword	[85]

2.6 Applications and Summary

2.6.1 Applications

There are many potential applications for MC. Although the devices of MC have not been widely devised and manufactured, MC does appear and exist naturally. The application of MC can be categorised into several groups including but not limited to: biomedical, environmental, industrial, military applications and home appliances. The following is the summary of these applications.

- Since MC is a biologically-inspired method of communications, the most direct applications are in the biomedical field, where organs and tissues interact through the use of MC technologies, such as immune system support [86, 87],

bio-hybrid implants [88], drug delivery systems [89, 90], health monitoring [91] and genetic engineering;

- In an industrial context, nano-communications can help with the advances in new materials, manufacturing processes and quality control procedures, such as, food and water quality control [92] and artificial materials and fabrics [93];

- The MC in military scenarios can be widely variable depending on the applications. In large area deployment, the classic application can be nuclear, biological and chemical (NBC) defenses. The MC can be deployed over the battlefield or targeted areas to detect aggressive chemical and biological agents and coordinate the defensive response [94]. Another application similar to consumer goods field but focusing on military equipment is nano-functionalised equipment. Advanced materials containing MC can be used to manufacture equipment which is capable of self-regulating the temperature underneath soldiers clothes and even detecting whether the soldier has been injured [95];

- MC can be applied in environmental fields due to its biological inspiration to achieve some goals which have not been solved with current technologies. These will include the area in biodegradation process, an existing and growing problem with garbage handling throughout the world, which MC can help with by sensing and tagging different materials that can be later located and processed by smart nano-actuator; animals and bio-diversity control, where MC and nanonetworks act to control several species and their presence in particular areas; air pollution control, which is similar to the quality control application, where air pollution level can be monitored and the harmful substances contained in it can be removed by nano-filter to improve the air quality [96].

- Finally, MC can be used as a tool to study animal behaviours e.g., mimic pheromonal communications in insects [97, 98]. Based on the pheromonal

communication, MC can further applied to robotics such as chemical tracking robots and robot communication in harsh environment for search and rescue purposes [99, 100].

2.6.2 Summary

In this chapter, the state of the art in MC and recent advancements are reviewed. It first introduced and reviewed the basic elements of MC namely, information particles as well as transmitter and receiver mechanisms developed in MC. Then the focus was on the channel models including diffusion channel models and the active propagation channel model of bacteria assisted channel models, that were reviewed. Based on the understanding of propagation of information particles, the design of appropriate modulation schemes proposed in recent years has been discovered, particularly, those that targeted on the mitigation of ISI. Afterwards, for error correction codes, two types were analyzed, namely, Hamming codes when in the presence of additive noise and Hamming weights and positional distance codes when in presence of bit transposition errors. Finally, the potential applications and open challenges of MC have been summarized and outlined. Taken together, this chapter has presented a series of literature review of the state of the art of MC which are relevant to this PhD thesis.

Chapter 3

Methodology

As demonstrated in Chapter 2, there are many advancements in theoretical MC in recent years. In order to help verify and evaluate MC, several simulation tools and experimental systems of MC have been developed. In this chapter, the recent developments in both software simulation tools and hardware experimental systems are introduced and reviewed. Inspired by the experimental platform developed in MC, the experiments, which can be carried out in the PhD project are designed and further the experimental platforms used in this PhD thesis are explained and built. Finally, the procedures of a series experiments which were carried out during the PhD project are described in detail.

3.1 Recent Advancements in Simulation Tools and Experimental Platforms of MC

3.1.1 Software Based Simulation Tools

Software based simulation tools for assisting analysing and studying on MC has been developed in recent years. The software simulators are required to precisely track the behaviour of information particles while propagating in the channel. One of the first software based simulators considered was presented in [101]. The simula-

tion was considered by using Monte Carlo schemes in a confined environment where EM waves were not reliable with elastic boundaries while the information particles collided. In the same year, [102] proposed a software simulator platform written in C++ called NanoNS to assist analyzing the channel properties and the arrival time of information particles and the results can be shown in mesh scale. Another software simulator developed later was BINS [103] and the upgraded version BINS2 [104] to model the 3D diffusion process with or without flow. The simulator was capable of supporting abundant features such as the receptor dynamics, all types of information particles, life time of particle, the location of particle and the boundary of the environment. BNsim [105] was introduced in 2013 to model the bacteria assisted MC in a 3D environment. Later in 2014, a distributed simulation tool was proposed in [106] based on high level architecture (HLA) and it was used to analyze the MC in confined space without considering the effect of consecutive symbols. In [107], N3Sim was introduced to analyze the MC with a non-absorbing receiver in 2D and 3D environments (based on specific conditions) and the simulator assumed the transmitter was a point source. While simulating the MC process, the simulator was able to consider the laws of particle collision, inertial forces and electrostatic forces, etc. The problem with N3Sim is that the realistic transmitter in MC probably has a volume and the volume may affect the emitted information particles. Finally, a software simulator based on Matlab was proposed in [108] as MolecUlar CommunitIoN (MUCIN) simulator. This simulator was able to simulate the end-to-end MC by first hitting process from 1D to 3D environment. The simulator was able to consider the effects of sending consecutive symbols, different modulation and filtering schemes, and imperfect receptions.

3.1.2 Experimental Systems

Microscale Experiment

Compared to the theoretical advancements in MC, the practical and experimental works are fewer. One possible reason is that MC needs a strong collaboration across several fields, e.g., biological engineering, chemical engineering, mechanical engineering and communication engineering. Another possible reason is the cost of the experiment (i.e., the expensive nature of wet-lab experiments where performing the practical work is usually time-consuming and laborious) to slow down the development of experimental research.

Despite these issues of experimental research on MC, there are still a number of works focusing on engineering the experimental demonstration of MC. One of the first works was considered and proposed in [109] for microscale MC. With the development of biological technology, artificial cells was used to send a single message to *E. Coli* bacteria and the message was detected and decoded by the receiver artificial cell in [110]. Further, work in [111] performed the experiment by encoded the message sequence into DNA and transmitting the DNA by packaging it inside a bacteriophage.

Macroscale Experiment

In macroscale MC, experimental systems has also been developed. The first tabletop MC system called Kinboshi was introduced in [12]. Kinboshi system was able to transmit short messages over free air and it did not require to access any biological labs which reduced the cost of experiment significantly. Kinboshi had the basic elements of communication systems, namely, transmitter processing unit, molecule releasing mechanism, molecule sensor and receiver processing unit. An Arduino micro controller was used as the transmitter and receiver processing units to encode the short message as binary sequences and decode the received binary sequences.

The molecule used was alcohol so that the detector was an alcohol metal-oxide sensor. While the short message was converted into binary sequences, then the information was transmitted by on-off keying where bit 1 was represented by a spray of alcohol and a bit 0 represent no spray. The released alcohol particles propagated in the channel with assistance of air flow generated by a electrical fan and produced a concentration change in the alcohol sensor. By detecting this and decoding the received pulse, the short message could be reproduced and displayed on an LED screen. The performance of Kinboshi was presented in [12] and the comparison of MC and EM wave based conventional communication system is shown in Table. 3.1.

Table 3.1: Comparison between EM and MC Communication Systems

Parameter	**EM**	**MC**
System	4G LTE	Kinboshi
Resource	Bandwidth (20MHz)	Chemical types
Range	m $\sim$ km	cm $\sim$ m
Reliability	Very high	Medium
Transmitter size limitation	$\propto$ Wavelength (mm-cm)	$>$ Molecule size (nm)
Propagation law	Maxwell	Brownian Motion
Transmission type	Active (Antenna)	Passive or Active
Source of noise	EM fields and signals	Environment, Transmitter and Receiver
Source of ISI	Multi-path	Unpredictable arrival time of molecule

As reviewed in previous sections, the basic laws, diffusion equations and the components of macroscale MC can be applied and shrunk [112] to microscale MC. Thus, the Kinboshi system provided an inexpensive solution to the experimental analysis of MC. Following the Kinboshi system, [113] proposed a robotic communication platform by using persistent chemical tags. As Kinboshi only considered one transmitter and one receiver for MC, later a multiple input multiple output (MIMO) MC platform was proposed recently based on Kinboshi [114, 115]. The prototype was designed with multiple sprays and multiple alcohol sensors and was proved to increase the data rate at least 1.78 times over original Kinboshi system.

3.2 Experimental Systems Design

Based on the University lab conditions, a pipe channel has been selected as the *confined system* and an experimental platform based on Kinboshi [12] has been modified to carry out the analysis. In order to compare the performance, a Zigbee experimental platform has been selected and deployed. This section will introduce the pipe system, the Zigbee platform and the MC experimental platform, respectively.

3.2.1 Propagation Channel Setup

The propagation channel is designed by imitating industrial applications. For example, the transmitter and receiver are deployed in an enclosed tunnel environment and connected by complex pipes (e.g., ventilation pipes). In such an environment, EM waves can barely be used as the pipes cannot act as wave guides and the structures and bends of the pipes may reflect or absorb the EM waves. However, molecules can freely diffuse in the pipe environment which makes molecular communication capable for the pipe environment. Therefore, in order to imitate such an environment, iron pipes are selected as they are inexpensive and suitable under lab conditions for constructing a pipe system with different pipe topology. One issue that needed to be considered is that, if the transmitter and receiver are deployed directly at each end of the pipes, the communication process may be achieved directly through free air rather than the pipe channel, thus metallic boxes are considered to hold the transmitter and receiver to prevent communicating through free space. In such way, both the propagation of EM waves and molecules are guaranteed inside the metallic (confined) environment.

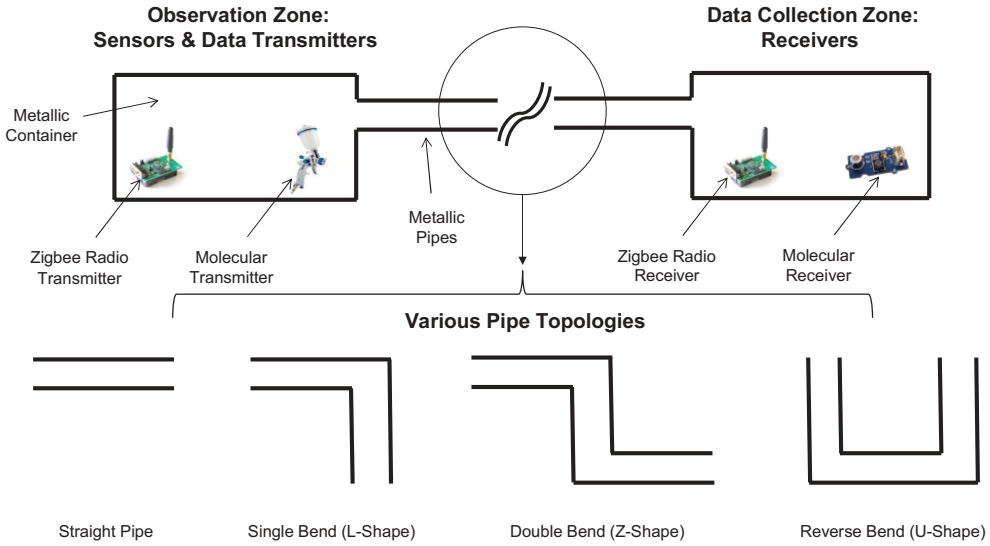

Figure 3.1: Illustration of propagation environment consisting of 2 metallic boxes connected by a metallic pipe with various lengths and bends.

Fig. 3.1 illustrates the topology of the propagation channel between an observation zone and a data collection zone. Each zone consists of a metal tank, interconnected by an iron pipe network. This latter is of a flexible design, whereby the length of individual pipe sections and the number of bends can be adjusted. In order to achieve the pipe topology shown in Fig. 3.1, 4 straight iron pipes are selected and prepared. For each pipe, its thickness is 0.2cm, diameter is 40cm and length is 130cm. The connection between two pipes is by a 90° plastic pipe joint for a right angle shape or by directly interconnected for a straight shape. The topology of a pipe can be categorized as straight, single bend (L-shape), double bend (Z-shape) and reverse bend (U shape). While connecting the pipes by the joints, there are two issues that need to be considered, namely, (i) the connections must be sealed as the molecules may escape from the pipe joint leakage; (ii) the joints must be covered by metal (aluminum) foil while testing the EM wave based system as EM waves may penetrate the plastic joints.

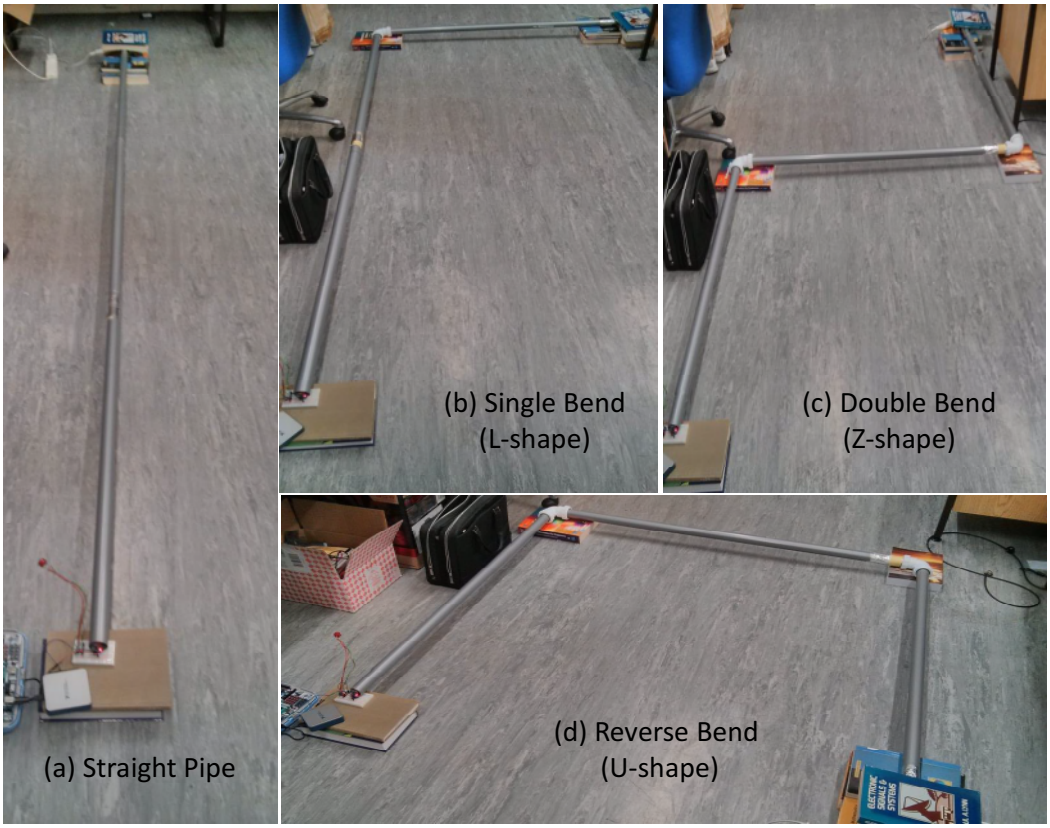

Figure 3.2: Photo of different pipe topology used in the experiment.

Fig. 3.2 shows the different pipe topologies used in the experiment.(a) is straight pipe, interconnected by 3 iron pipes. The total length of straight pipe depends on the number of iron pipes used. (b), (c), and (d) are single bend, double bend, and reverse bend, respectively. With the different combinations of the number of pipes and bends, it is possible to examine the performance of MC and EM based communication systems under different topologies.

3.2.2 Zigbee System

The EM wave based communication system was selected to be based on Telegesis ETRX357 Zigbee modules. Two such modules were used as transmitter and receiver

for EM wave communication. The ETRX357 device is a 2.4GHz Zigbee module based on the third generation Silicon Labs EM357 chipset offering the industry's highest wireless networking performance at lowest power consumption. The transmit power is approximately 1mW and the receiver sensitivity is -99dBm, which can deliver a bit-error-rate below 1%. Telegesis provides a development board for the ETRX357 module where the Zigbee modules can be deployed. Fig. 3.3 shows the ETRX357 module placed in the development board operating by a battery power supply.

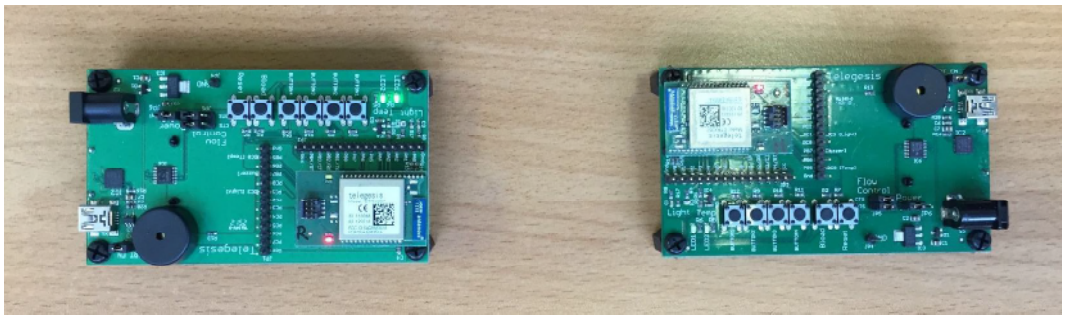

Figure 3.3: ETRX357 module on development board operating by battery power supply

The development board can be then connected to a computer. In order to operate the module, terminal software (e.g., Telegesis Terminal) needs to be installed on the computer. The module has a unique AT-style command line that could be used in the terminal software which enable users to quickly integrate Zigbee technology without complex software engineering. More details of the ETRX357 and the development board can be found in [116].

3.2.3 Experimental Molecular Communication System

Kinboshi, introduced in Section 3.1.2, is inexpensive and suitable for the lab conditions at the University of Warwick. Therefore, the experimental platform in this PhD project was built based on Kinboshi. In this section, the basic components

of the experimental system including the processing unit of both transmitter and receiver, electrical spray of the transmitter and the molecular sensor of the receiver are explained.

Processing Unit

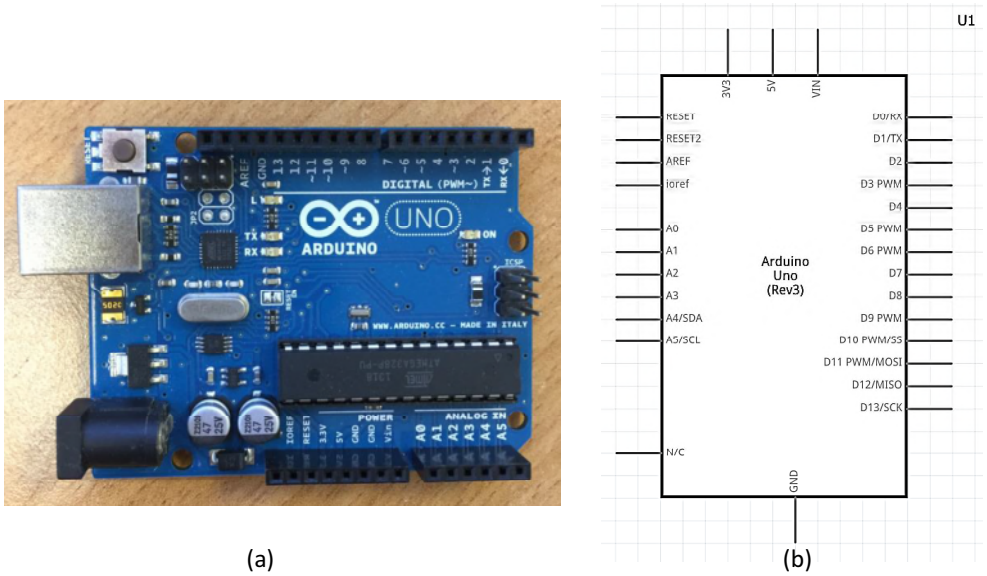

Figure 3.4: (a) Arduino UNO experiment board and its (b) schematic diagram

The central processing unit was selected to be the *Arduino Uno*. This is a microcontroller board based on the ATmega328P [117]. It has 14 digital input/output pins (of which 6 can be used as PWM outputs), 6 analog inputs, a 16 MHz quartz crystal, a USB connection, a power jack, an ICSP header and a reset button. Fig. 3.4 shows the realistic Arduino UNO experiment board and its schematic diagram.

To operating the Arduino board, the Arduino programming language, which is an open-source based on C++, is provided for users to control the microcontroller. On the other hand, MATLAB also provides a toolbox particularly for Arduino hardware, which enables users to read and write sensor data through the Arduino and immediately see the results in MATLAB without having to compile.

Transmitter

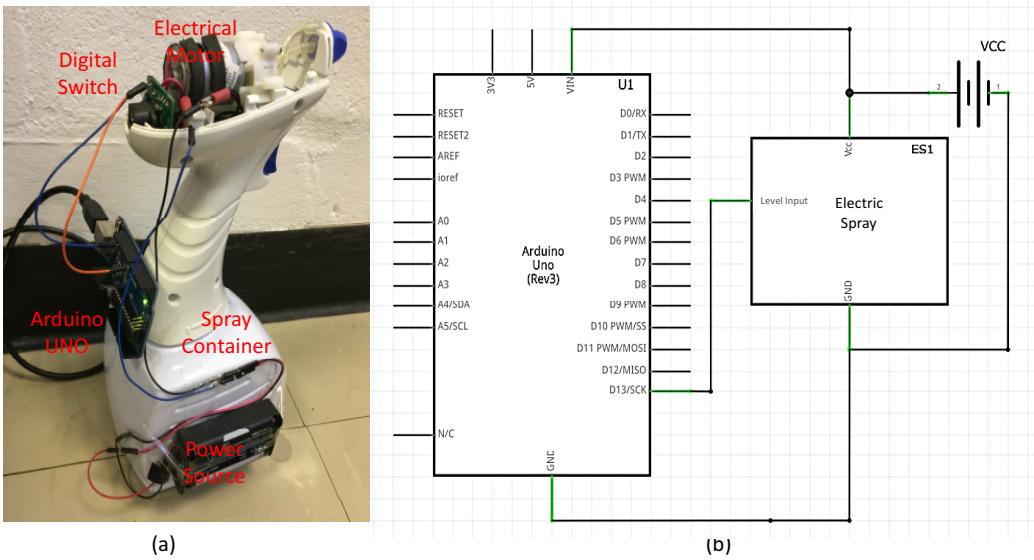

Figure 3.5: (a) Transmitter components and its (b) schematic connection diagram

The transmitter of the platform consisted of three key components, namely, the central processing unit (i.e., Arduino UNO), electric spray with digital switch and power source. Fig. 3.5 (a) shows the hardware of the transmitter and (b) shows the schematic connections between the three components. The electric spray consisted of a container to store the alcohol liquids and a digital switch made with an IRLZ44Z automotive MOSFET to control the release of the alcohol. For example, while the microcontroller gave a high level signal for a time period t, the digital switch would be on and the electrical motor started pumping the alcohol from the container to the spray nozzle to release alcohol for t seconds. Then the microcontroller changed the high level signal to a low level signal to stop the spray releasing.

Receiver

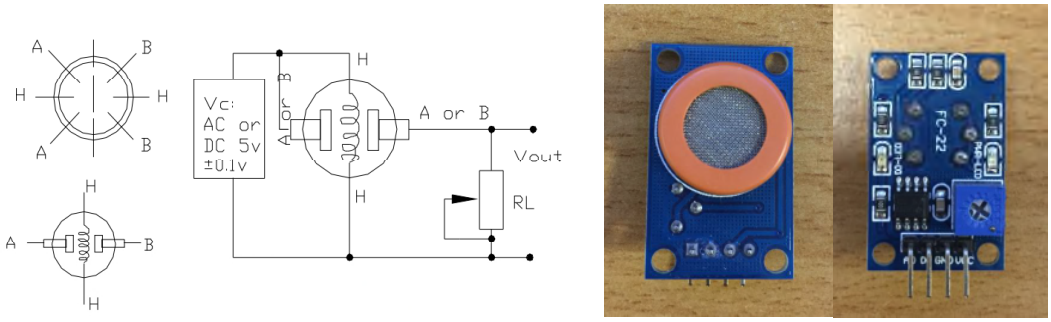

Figure 3.6: (a) The schematic diagram of MQ3 sensor and (b) the MQ3 sensor module.

The receiver contained an alcohol sensor to detect the concentration of the alcohol in the environment and a processing unit to output the received signal to a monitor or computer for further analysis. An MQ3 alcohol sensor was used to detect the alcohol concentration. This is based on tin oxide (SnO_2) semiconducting sensor layer: after heating to 350°C, the SnO_2 semi material presents a drop in electrical resistance in the presence of alcohol gases. According to the sensor structure [118] shown in Fig. 3.6 (a), the MQ3 has 6 pins, both A pins and B pins are used to fetch signals, and other 2 H pins are connected with large resistor to continuously heating the source SnO_2 layer. One example of the application of the MQ3 sensor is also shown in Fig. 3.6 (a), which shows that the change in sensor resistance in the presence of alcohol could be measured using a voltage divider circuit with 5v DC power supply across a load resistor R_L. Assuming that the resistance across the sensor is R_S, the output voltage according to the alcohol level can be calculated as,

$$V_{out} = V_{in} \frac{R_L}{R_S + R_L}. \tag{3.1}$$

For example, it would return a +5V signal as $R_S \to 0$ in the presence of

alcohol saturation, and 0V as $R_S \to \infty$ in clean air. While the rate of $\frac{R_S}{R_L}$ is measured, the concentration of alcohol can be then found from [118]. For convenience, the MQ3 sensor module shown in Fig. 3.6 (b) was used to build the receiver. The module had 4 pins, namely, AO (analogue output), DO (digital output), GND (ground) and VCC (power supply). The module could be directly connected to a 5V power source and ground, then AO pin was capable of producing continuous V_{out} data. DO was able to show whether alcohol was present (output bit 1) or absent (output bit 0).

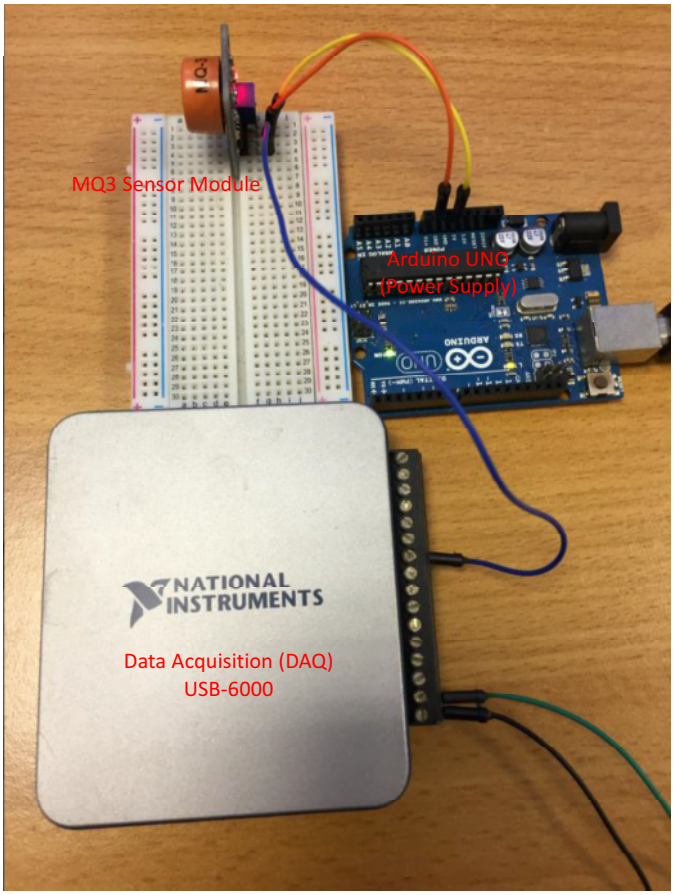

Figure 3.7: The components of receiver.

V_{out} gave an index to the concentration of alcohol molecules. The higher the concentration of alcohol, the higher the value of V_{out}. Therefore, the experiment focused on the value of V_{out}. In order to measure V_{out}, a National Instrument Data

Acquisition (DAQ) system (i.e., NI USB-6000) was used. The USB-6000 is NI's lowest cost USB DAQ device and it provided basic DAQ functionality for applications such as simple data logging, portable measurements, and academic lab experiments. The device had 8 analog inputs and 4 digital I/O lines to measure the electrical output from physical phenomena converted by sensors, such as voltage, current, resistance etc,. Fig. 3.7 shows the component of the receiver including the MQ3 sensor, power supplied from Arduino UNO and DAQ. The analogue output V_{out} from the MQ3 sensor module pin AO was connected to any one of 8 analog inputs of DAQ. By using the NI provided DAQ driver software, V_{out} could be displayed on the monitor and the data can be stored in the computer.

3.3 Experiment Procedures

There are three types of experiment carried out during the PhD project, namely, the performance comparison experiment, straight pipe channel model characterizing experiment and mobile MC experiment. This section explains the procedures of these experiments in detail.

3.3.1 Performance Comparison Experiment

The first experiment was to compare the performance of MC and EM wave based experimental systems and the topology of pipe networks were as shown in Fig. 3.2. The parameter used for the comparison was EM signal strength and the delay spread of pulse modulated MC. The EM signal strength used received signal strength indication (RSSI) as the parameter, and the delay spread was defined as the peak-to-3dB power point of the pulse response of the MC signal. That is to say from the peak of the voltage amplitude to the $1/\sqrt{2}$ of the amplitude.

For the EM wave based system, the RSSI of Zigbee module could be directly measured and read by using the AT command, the value of RSSI for each experiment

could be conveniently displayed on the Telegesis Terminal software interface. For the MC system, the electrical spray was controlled by the Arduino UNO and for each pulse, the digital switch is held a high level for 0.1s to create a pulse, and the pulse response could be stored and displayed in the DAQ driver software. An electrical fan was provided to supply drift from transmitter side towards the receiver to accelerate the diffusion of alcohol with a drift speed of $1ms^{-1}$. In order to have accurate data from the experiment, each test trial was carried out 5 times. The voltage data was analyzed by MATLAB for the delay spread after the end of the entire experiment.

There are two issues that needed to be considered. One is that in each spray of alcohol liquids, a residual amount of the alcohol is probably remain on the inner wall of the pipeline near the spray nozzle. This small amount of alcohol will cause errors in the impulse response. Therefore, after each spray, the pipeline needed to be cleaned and the inner wall was kept dry before the next spray. Another issue is that the MC experiment was undertaken in a sealed environment with insufficient ventilation. The background alcohol molecules would thus affect the pulse response. Therefore, the sealed tank with transmitter and receiver needed to be unsealed and ventilated before next spray.

3.3.2 Straight Pipe Channel Model Experiment

This experiment aimed to empirically find out the additive noise in the pipe system for diffusion based MC. The additive noise is defined as the difference between the measured received signal and the average received signal of the system. Based on the experimental setup in the previous section, without deploying the electric fan in the pipe environment, 3 different length, namely, 0.6m, 1.27m and 2.45m straight pipe pulse responses were measured. There were 10 trials for each length of pipe, each trial waited a sufficient long time (1200s) for the full pulse response. Each pulse response had more than 10000 empirical data points (voltage values). The

voltage values were loaded to MATLAB to calculate the average pulse response for each pipe length. Then the difference between each trial and the relevant average pulse response could be derived. Finally, if the difference can be statistically fitted to a distribution, then the noise model of the straight pipe could be found.

3.3.3 Mobile MC Experiment

The last experiment carried out in the PhD project was to model mobile MC and demonstrate the effects of mobility on bit errors. In order to make the experimental system mobile, a robot chassis with electronic motors was used, which is shown in Fig. 3.8.

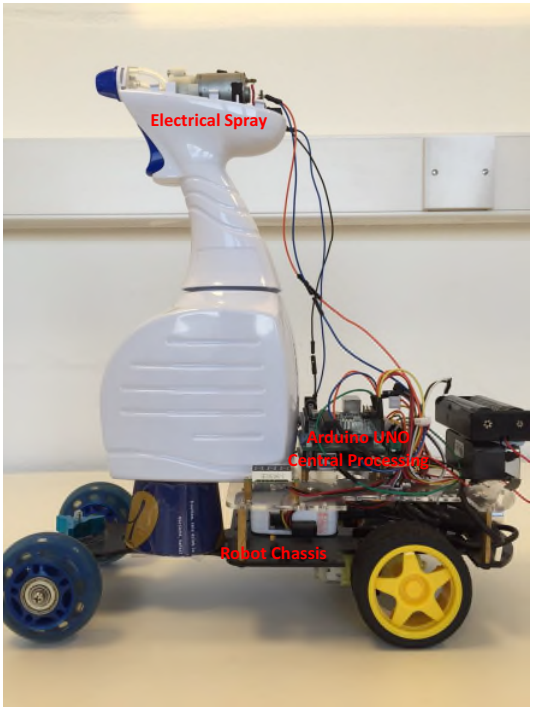

Figure 3.8: Mobile MC transmitter on robot chassis.

In this demonstration, the transmitter and receiver were placed in an open environment, and an electric fan was placed at the transmitter side to generate air drift towards receiver at rate of $2ms^{-1}$. The transmitter was fixed on the robot

chassis and the robot chassis was programmed to move towards the receiver at a constant speed of $1ms^{-1}$. To demonstrate how bit transposition occurred, the robot first remained static and sent an initialization pulse to tell to the receiver that it was ready. After waiting for 5s, the robot then began moving towards the receiver and sent 3 symbols at a fixed interval of 2.5s. DAQ is used to measure the pulse response of the 3 transmitted symbols.

3.4 Summary

In this chapter, recent advancements on the simulation tools and experimental platforms developed for MC have been reviewed. Particularly, the world's first inexpensive tabletop MC experimental platform, Kinboshi, was introduced in detail. Then the research questions which can be answered by experiment were outlined. Based on the research questions, an experimental platform for tackling the research questions was designed based on Kinboshi. The experimental environment and its topology constructed by iron pipes were proposed and explained, and the experimental platform was introduced and presented, including the components of the transmitter and receiver, as well as a Zigbee system for performance comparison. Finally, the objectives and procedures of the experiments operated during the PhD project were presented and explained.

Chapter 4

Static Propagation Channel Model

One motivation for investigating molecular communication is to achieve communication in challenging electromagnetic (EM) environments. As discussed in Chapter 2, MC has been proposed over the past few years and investigated for different environments and Chapter 3 pointed out the lack of channel characterization for the macroscale (a few meters) confined pipe environment. In order to characterise the practical pipe environment constructed in Chapter 3, this chapter firstly proves the availability of MC in pipe networks by analyzing the empirical results of *Performance Comparison Experiment*. Then this chapter focuses on a novel captured molecular concentration equation in Section 4.2.1 and demonstrates the suitability of the equation applied to the pipe environment. Afterwards, with the empirical results from the channel response of *Straight Pipe Channel Model Experiment*, a Nakagami distributed noise model is characterised in Section 4.3 and the bit error rates (BER) and throughput are derived with consideration of both ISI and empirical Nakagami noise, which are achieved by applying the minimum error probability (MEP) criterion of a standard Bayesian detection framework.

4.1 Comparative Testing in Complex Tunnel Environments

4.1.1 Experiment Stages

As explained in Chapter 3, the first experiment *Performance Comparison Experiment* is aim to prove the availability of MC in pipe networks and statistically compares the performance of EM wave based communication system and MC system built for this PhD project. This experiment is divided into 3 stages, namely, *baseline*, *pipeline shape* and *pipeline length*.

Baseline is to compare the performance between EM wave and MC without connecting any pipes. The objective for this experiment is to demonstrate the connectivity of both experimental platform in sealed boxes without connecting pipes.

(1) **Free Space**: Both transmitters and receivers are directly separated 4 meters away and deployed in the environment without any obstacles.

(2) **1 Sealed Tank**: The transmitters of both are placed in a sealed tank separated for 2.5m while the receivers are placed in the open environment, repeat the procedures to measure the RSSI and pulse response.

(3) **2 Sealed Tanks**: Both transmitters and receivers are placed in sealed tanks separated for 1m and repeat measuring RSSI and pulse response.

(4) **2 Open Tanks**: Unseal the tanks in previous step and measure the RSSI and pulse response.

Pipeline Shape is aimed to compare the performance in the pipe environment for different topology. Shown in Fig. 3.1, there are 4 sub-experiments, namely,

(1) **Straight**: Both transmitters and receivers of Zigbee and MC systems are placed in sealed tanks with a hole to connect the iron pipe. The pipe is straight without

fixing any bends. The transmitter and receiver are separated by 3.6m. RSSI and pulse response of alcohol molecules are measured in the same way as Baseline stage.

(2) **L-shape**: Tanks with transmitters and receivers are connected by L-shape pipe where 1 bend is used to create a right angle for the pipe environment (see Fig. 3.2). The displacement of transmitter and receiver are separated by 3.7m and 4.8m respectively.

(3) **Z-shape**: The two tanks holding transmitter and receiver are connected by Z-shape pipe where 2 bends, one right angle to left and another to right, are used and separated by 3.8m.

(4) **U-shape**: The two tanks holding transmitter and receiver are connected by U-shape pipe where 2 bends, both bends are with same direction on right, and separated by 3.9m.

Pipeline Length is to examine the relationship between distance and performance of both systems. Based on the available length to be built in the lab, there are 3 sub-experiment in this stage.

(1) **Short**: The transmitter and receiver are in the sealed tank and connected by a straight pipe with separation of 1.3m without any bends deployed.

(2) **Medium**: The transmitter and receiver are placed by 2.5m away in a straight pipe and 2.6m away in the pipe with 1 bend.

(3) **Long**: The transmitter and receiver are placed by 3.6m away in a straight pipe.

4.1.2 Performance Comparison with EM Wavebased System

The summarized radio and molecular communication results are listed in Table 4.1, which shows the significant propagation results for consideration. The baseline

Table 4.1: Summarized Results Data: mean value from 12 independent test batches with standard deviation in brackets.

Structure Shape	Radio Signal	Delay Spread
Baseline		
Free Space (4.0m)	-70 dBm (1)	17s (3)
1 Sealed Tank (2.5m)	No Signal	No Signal
2 Sealed Tanks (1.0m)	No Signal	No Signal
2 Open Tanks (4.0m)	-90 dBm (1)	65s (11)
Pipeline Shape		
Straight (0 bend, 3.6m)	-79 dBm (1)	3.57s (0.4)
L-Shape (1 bend, 3.7m)	-92 dBm (0)	4.29s (0.3)
L-Shape (1 bend, 4.8m)	No Signal	6.24s (0.5)
Z-Shape (2 bends, 3.8m)	-93 dBm (3)	9.07s (2.0)
U-Shape (2 bends, 3.9m)	No Signal	8.81s (1.1)
Pipeline Length		
Short (0 bend, 1.3m)	-62 dBm (1)	2.20s (0.2)
Medium (0 bend, 2.5m)	-71 dBm (1)	2.91s (0.4)
Medium (1 bend, 2.6m)	-87 dBm (1)	4.45s (0.4)
Long (0 bend, 3.6m)	-80 dBm (1)	3.57s (0.4)
Long (2 bends, 3.9m)	No Signal	8.81s (1.1)
L-Shape (1 bend, 4.8m)	No Signal	6.24s (0.5)

results show that (as expected) neither the radio nor the molecular signal can penetrate sealed metallic tanks. However, communications is possible in both the free-space and open tanks cases. For molecular communications, the delay spread in an open or semi-open environments is very high. Intuitively, this is due to the fact that molecules carrying signals can diffuse anywhere and the arrival process at the receiver is highly stochastic. These numbers can be used a reference point for comparison with more complex structural topologies. The full set of impulse response shapes for different pipe dimensions and configurations can be found in Fig. 4.1. It can be observed that the shape is very much similar, independent of the pipe network, and only the delay spread varies. The variance is also very small across all experimental data.

When the tanks are sealed, but joined by a metallic pipe structure, the results are of more interest. The first observation is that the pipe shape (e.g., U-, or Z-Shape) doesn't strong affect the performance of either the radio or the molecular communication link. That is to say the orientation of the bend is not important. However, the number of bends does strongly affect the molecular communication

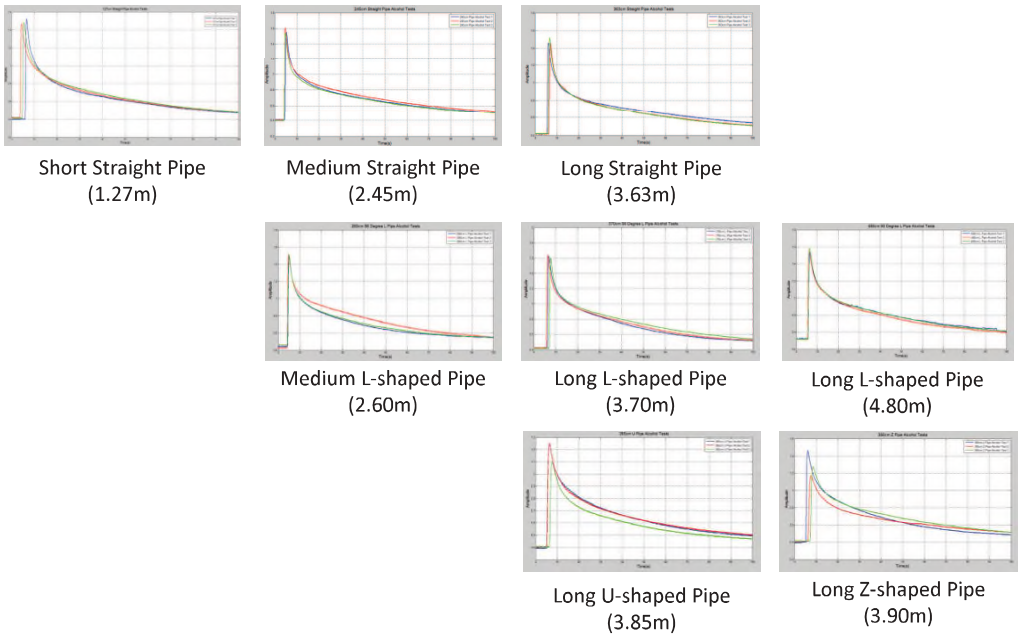

Figure 4.1: Full set of molecular impulse responses for different pipe configurations and dimensions. Each set of result contains 3 independent test data trials.

link. In the second part of Table 4.1, data is presented for 0 to 2 bends for a similar overall distance. The delay spread of the molecular pulse response dramatically increases with each increased bend. In the third part of Table 4.1, data is presented for different pipe lengths. It shows that the radio performance is strongly affected by both the pipe length and the number of bends (especially the first bend), whereas the delay spread of molecular communications is only strongly correlated with the number of bends. It can be seen that the results standard deviation is generally small for the radio experiments (mostly 1 dBm or less), and remain small for most molecular experiments (mostly 1s or less). With greater number of pipe bends and distances, the radio and molecular results' standard deviation can rise rapidly to 3 dBm and 2s respectively.

An approximate propagation loss relationship for EM wave based communications in this proprietary experiment (consisting of 2 metal tanks connected with

iron pipes) is:

$$\mathrm{PL}_{\mathrm{radio}} = \begin{cases} -8 \text{ dB/m} & \text{straight pipe} \\ -10 \text{ dB/bend} & \text{first bend} \end{cases} . \tag{4.1}$$

An approximate delay spread τ_{delay} relationship for molecular communications in this proprietary experiment (consisting of 2 metal tanks connected with iron pipes) is:

$$\tau_{\mathrm{delay}} = \begin{cases} +0.6 \text{ s/m} & \text{straight pipe} \\ +35 \text{ to } 50\% \text{ increase/bend} & \text{pipe network} \end{cases} . \tag{4.2}$$

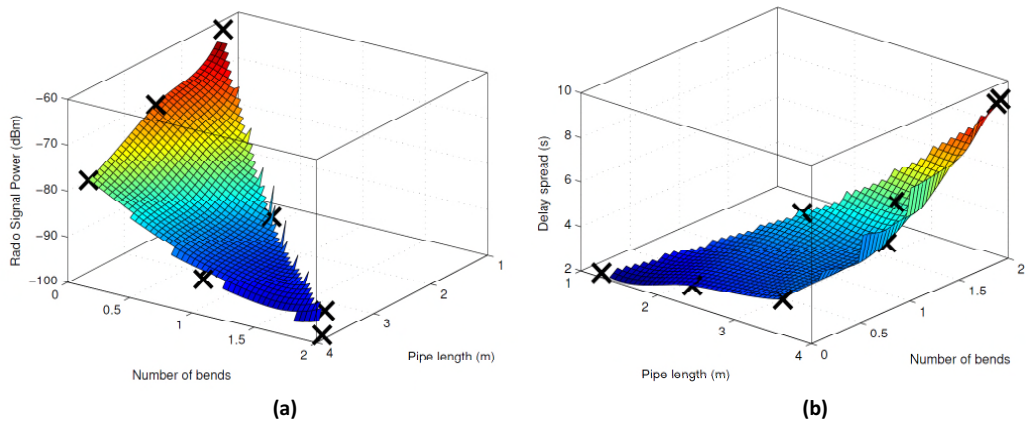

Figure 4.2: (a) Radio signal power loss (dB) vs. different pipe lengths (m) and number of pipe bends, and, (b) Molecular signal delay spread (s) vs. different pipe lengths (m) and number of pipe bends.

This conclusion can be visualized by the 3D plots of radio and molecular performance as a function of the number of pipe bends and the overall pipe length. In Fig. 4.2 (a), the plot shows how the signal power loss (dB) varies with different pipe lengths and number of bends strongly. For the number of bends, it is significant for only the first bend. On the other hand, the results in Fig. 4.2 (b) show that the

delay spread dramatically increases with each bend in a non-linear fashion. The key conclusion are as follows:

- Molecular communications can be established in scenarios where a reliable radio-link can not be established due to propagation losses in complex confined environments. In the experiment case, it was for long pipe lengths (over 4m) and a high number of bends (2 or over);
- EM communications is more sensitive to the pipe length and the first pipe bend, whereas molecular communications is the more sensitive to the number of bends.

4.2 Propagation Channel Model for 1-Dimensional Pipe Environment

4.2.1 Captured Molecular Concentration

Conditions for Impulse Response Capture

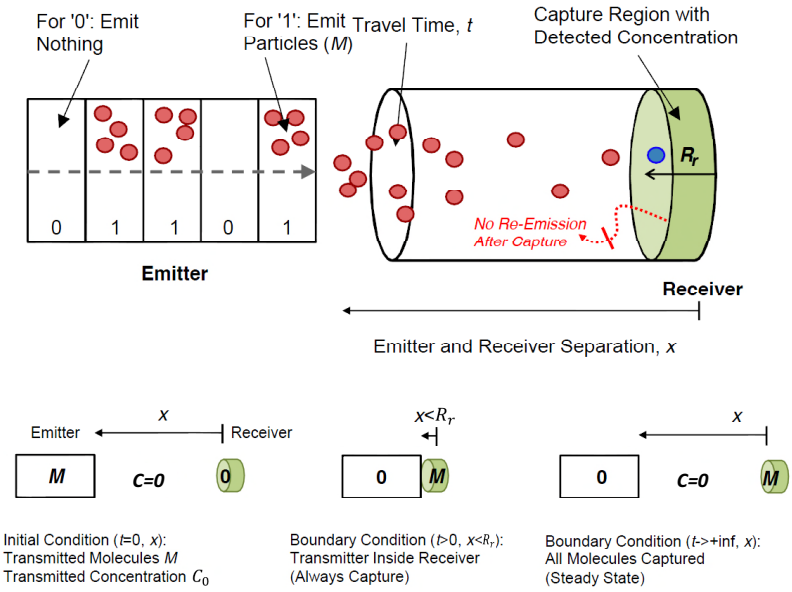

Figure 4.3: Illustration of molecular communication link using On-Off-Keying (OOK) modulation scheme with a receiver that has a capture radius of R_r. Three conditions are presented: i) initial pulse transmission ($t = 0$), ii) always full capture ($x < R_r$), and iii) infinite capture ($t \to +\infty$).

As the environment is considered as pipe networks, which requires specific boundary conditions to diffusion equations that are not commonly used in literature, thus an impulse emission (input), a perfect molecular capturing receiver, and a semi-infinite environment are need to be incorporated. The Fokker-Planck equation [119] predicts

the flux of molecular diffusion as a function of the diffusion coefficient $D(\mathrm{m}^2/\mathrm{s})$:

$$\frac{\partial C(x,t)}{\partial t} = -v\frac{\partial C(x,t)}{\partial x} + D\frac{\partial^2 C(x,t)}{\partial x^2}, \tag{4.3}$$

where $C(x,t)$ is the concentration (melecules/m), t is the time elapsed (s), v is the drift velocity (m/s) and x is the distance from the source (m). The system is shown in Fig. 4.3. In order to solve the ordinary partial differential equation (OPDE), one initial ($t = 0$) and two boundary conditions must be set. The molecular communication link contains a receiver and a transmitter separated by a distance x and the receiver is of size R_r. The concentration C is defined as the molecule concentration at any point outside the capture zone (can include the transmitter). The system has several properties: i) the propagation environment is non-infinite, ii) the information transmitted is modulated by concentration (amplitude), and iii) once the receiver detects a molecule, it is fully absorbed and cannot be recycled. Therefore, 3 key conditions are presented that are necessary to fully describe the communication system:

(1) *Initial Impulse*, $C(x,0) = C_0$: at $t = 0$, a pulse of concentration $C_0 = M$ is emitted at the transmitter which is located at x distance away from receiver;

(2) *Capture Zone and No Re-emission*, $C(R_r,t) = C_0$: if the transmitter is always located at $x \leq R_r$ from the receiver, anything emitted will be captured immediately. At any time $t > 0$, the concentration outside the zone is $C = 0$;

(3) *Long-Term Capture*, $C(x,\infty) = 0$: if a molecule is captured, it cannot be re-emitted. Therefore, over a long time ($t \to +\infty$), the receiver captures all the molecules and the external concentration is $C = 0$.

There are a number of alternative conditions used in other literature, but they are not suitable in this MC system where they assume the infinite source that the transmitter provides a continuous and finite flux of molecules; And the environment is as-

sumed as infinite which is not realistic for the enclosed structural environments that considered in the pipe networks; Finally, the the molecules at sensors are assumed immediately converted to electrical charge and there is zero aggregated chemical interference from previous emissions. However, the gas phase sensors (MQ3) typically have a response time of several seconds and therefore the response can not be arbitrarily fast.

Captured Concentration

The non-capture concentration ($C(x,t)$) equation that satisfies both Fokker-Planck Eq. 4.3 and the three conditions is:

$$C(x,t) = \frac{M}{\sqrt{\pi D t}} \exp\left[-\frac{(x - R_r - vt)^2}{4Dt}\right] \quad \text{for} \quad x > R_r, \tag{4.4}$$

and $C(x,t) = 0$ for $x \leq R_r$. Assuming conservation of molecules, the captured number of molecules is simply $\theta_c = M - \int_{R_r}^{x} C(u,t)\mathrm{d}u$. Given that all molecules will be eventually captured (condition 3), the maximum cumulative captured number of molecules is $\theta_c = M$. Therefore, the *cumulative captured number of molecules* can be defined as the difference between the total emitted number of molecules (M) and the number of molecules outside the capture zone up to any given time t. The resulting number of molecules captured is a monotonically increasing function:

$$\begin{aligned}
\theta_c &= M - \int_{R_r}^{x} \frac{M}{\sqrt{\pi D t}} \exp\left[-\frac{(u - R_r - vt)^2}{4Dt}\right] \mathrm{d}u, \\
&= M\left[\mathrm{erfc}\left(\frac{v}{2}\sqrt{\frac{t}{D}}\right) - \mathrm{erf}\left(\frac{x - R_r - vt}{2\sqrt{Dt}}\right)\right], \\
&= M\left[\mathrm{erfc}\frac{x - R_r}{2\sqrt{Dt}}\right] \quad \text{for} : v = 0.
\end{aligned} \tag{4.5}$$

The concentration inside the capture zone is simply $C_c = \theta_c / R_r$.

Captured Probability Functions

In order for a receiver to sample at the point where there is the greatest flux of molecules, one has to find the flux (captured molecules per second). The number of captured molecules between any two arbitrary points in time is given by $\theta_{\mathrm{c}}(x, t+\Delta t) - \theta_{\mathrm{c}}(x, t)$, which is not a monotonic function. θ_{c} is the average number of captured molecules, which is the product of total number M of molecules transmitted and the probability of capturing one molecule. Thus, the probability of capturing one molecule is given by Eq. 4.5 divided by M. Therefore, the cumulative distribution function (CDF) is: $F_T(t) = \mathrm{erfc}\left(\frac{v}{2}\sqrt{\frac{t}{D}}\right) - \mathrm{erf}\left(\frac{x-R_r-vt}{2\sqrt{Dt}}\right)$. The partial derivative of the cumulative function with respect to time yields the likelihood of capture between any particular time t and $t+\Delta t$ for $\Delta t \to 0$:

$$\begin{aligned} f_T(t) &= \frac{\partial F_T(t)}{\partial t}, \\ &= \frac{(x - R_r + vt)\exp\left[-\frac{(x-R_r-vt)^2}{4Dt}\right] - vt\exp\left(-\frac{v^2 t}{4D}\right)}{2\sqrt{\pi D t^3}}. \end{aligned} \tag{4.6}$$

In the special case of no drift velocity, $v = 0$,

$$f_T(t) = \frac{x - R_r}{2\sqrt{\pi D t^3}}\exp\left[-\frac{(x-R_r)^2}{4Dt}\right], \quad \text{for} : v = 0. \tag{4.7}$$

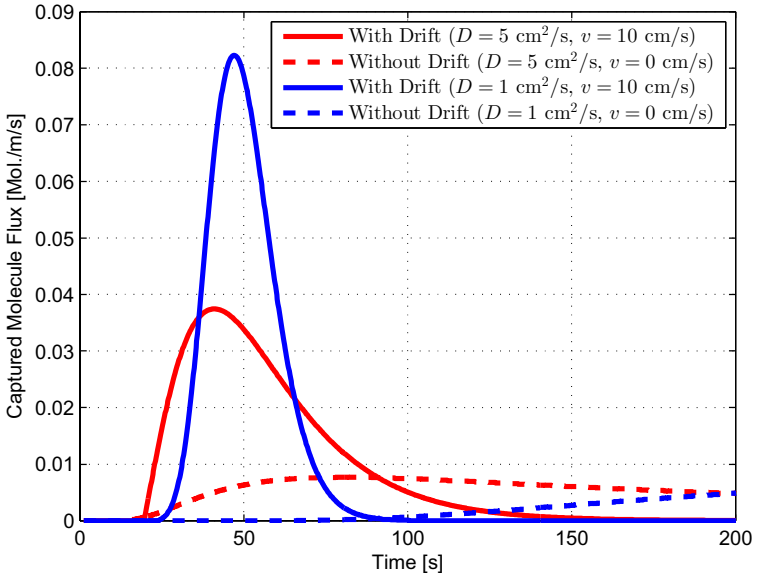

Figure 4.4: Captured molecules flux (molecules/m/s) for zero-drift ($v = 0$) and positive drift ($v = 10$cm/s), for $x = 1$m and $R_r = 1$cm.

This can be interpreted as the flux of captured molecules when scaled by M/R_r. A plot of the captured molecules flux (molecules/m/s) for zero-drift ($v = 0$) and positive drift ($v = 0.1m/s$) is presented in Fig. 4.4. It can be seen that a small drift velocity can significantly shorten the peak arrival time and increase the peak-to-average ratio of the received impulse response.

In *turbulent flow*, increasing the diffusivity D will broaden the width of impulse response pulse, but also shorten the arrival time. Fig. 4.4 demonstrates this by increasing D from 1 to 5 cm^2/s. Therefore, turbulence can be beneficial from the point of view of shortening the communication round trip time, but will cause greater inter-symbol-interference for the same transmit bit duration. As far as it can be aware, both the captured number of molecules and the probability density function (pdf) are novel results. By utilising the flux or pdf, the optimal sampling point and the number of captured molecules can be found.

4.2.2 Performance Parameters

Optimal Sample Point

As shown in Fig. 4.3, the binary digital On-Off-Keying (OOK) modulation scheme is considered without forward error correction coding. The receiver and the transmitter are assumed to be synchronised and that the receiver detects a flux of captured molecules over a Δt period. The maximum flux is given by solving $\partial f_T(t)/\partial t = 0$ for t, yielding:

$$t_{\max} = \frac{(x - R_r)^2}{6D}, \quad \text{for} : v = 0. \tag{4.8}$$

For a positive drift velocity, only a numerical solution can be found. Note, this is a similar result as that arrived with the non-capture diffusion equations in [120].

Assume that the receiver samples over $\Delta t = \tau$ period, where τ is sufficiently small compared to the diffusion process. By substituting the optimal sampling time into the number of molecules captured Eq. 4.5, the peak captured concentration is:

$$\begin{aligned} C_{\max} &= \frac{\theta_{\mathrm{c}}(x, t_{\max}) - \theta_{\mathrm{c}}(x, t_{\max} - \tau)}{R_r}, \\ &= \frac{M}{R_r} \left[\frac{3D\tau}{(x - R_r)^2 \sqrt{\pi/6}} \right] \exp\left(-\frac{3}{2}\right), \quad \text{for} : v = 0. \end{aligned} \tag{4.9}$$

For the zero-drift case, it can be seen that the received signal power (captured molecules flux) is a linear function of the diffusivity D and approximately an inverse square relationship with the transmission range x. The expected delay (or round trip time) of such a system is given by $t_{\mathrm{RTT}} = \frac{(x-R_r)^2}{3D}$ for a reciprocal channel with zero-drift, which can be interpreted as $1/(3D)$ per metre of transmission distance squared.

ISI

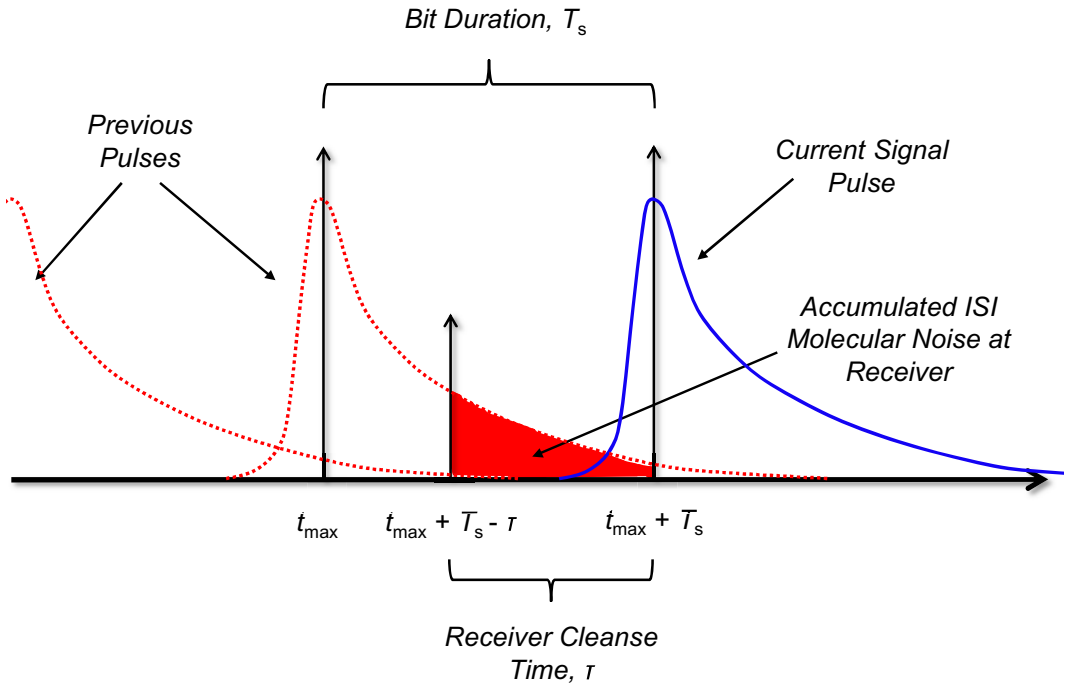

Figure 4.5: Illustration of ISI received at the receiver as a result of molecules captured in the previous τ seconds.

Unlike traditional communications with electromagnetic waves, MC cannot effectively alter the shape of the arrival pulse, such that ISI is avoided. Therefore, the molecules from previously transmitted symbols potentially becomes a dominating source of error. Examining more closely, most molecular receivers aggregate molecules for a period τ , after which the molecules dissipate (cleansed). Therefore, the ISI is not only comprised of the aggregated molecules from previous symbols at the sample time $t_{\max}$, but the aggregated molecules from $t_{\max} - \tau$ to $t_{\max}$.

Referring to Fig. 4.5, an observed signal pulse is considered which is being optimally sampled at its peak concentration point. It receives ISI from $n \to +\infty$ previous symbols. Let T_s denote the transmit bit duration. Using the time reference

of the previous symbol, the aggregated interference is from time $t_{\max} + T_s - \tau$ to $t_{\max} + T_s$. Therefore, the lower-bound to the number of molecules accumulated at the receiver when it is sampling a pulse that is receiving ISI from previous symbols is:

$$\theta_{\text{ISI}} = \sum_{n=1}^{+\infty} \chi_n \left[\theta_{\text{c}}(x, t_{\max} + nT_s) - \theta_{\text{c}}(x, t_{\max} + nT_s - \tau) \right], \tag{4.10}$$

where χ_n represents the emitter transmitting a 1 or 0. The total ISI molecules captured by the receiver over time τ converges absolutely, and more importantly it was found through empirical simulations that it is not dependent on D.

The concentration I in the capture zone is defined by θ_{ISI}/R_r. The maximum value of ISI ($\theta_{\text{ISI,max}}$) occurs when $\chi_n = 1$. Given equal probability of transmitting a 1 or a 0, the mean is $\mu_{\text{ISI}} = \frac{\theta_{\text{ISI,max}}}{2R_r}$. The precise variance of the ISI is challenging to find explicitly, so the upper-bound variance is considered, which is:

$${\sigma_{\text{ISI}}}^2 = \mathbb{E}\left[{\theta_{\text{ISI}}}^2\right] - {\mu_{\text{ISI}}}^2 = \frac{{\theta_{\text{ISI,max}}}^2}{2R_r^2} - \left(\frac{\theta_{\text{ISI,max}}}{2R_r}\right)^2 = {\mu_{\text{ISI}}}^2. \tag{4.11}$$

Bayesian Decision Threshold

There are two forms of noise considered for the pipe channel network, one from the previously mentioned ISI (I) and the other from additive Gaussian noise ($\mathcal{N}$) at the receivers hardware and from background ambient molecules (chemical contamination or interference) [121]. Let ϑ denote the captured concentration including noise:

$$\vartheta = \chi C + I + N. \tag{4.12}$$

Given M is large and $f_T(t)$ is neither close to 1 nor 0, the ISI I can be approximated as normally distributed as $\mathbf{N}\left(\mu_{\text{ISI}}, \sigma^2_{\text{ISI}}\right)$ [43]. The distribution of the AWGN follows a normal distribution $\mathbf{N}\left(\mu_{\text{N}}, \sigma^2_{\text{N}}\right)$. As previously mentioned, the transmis-

sion system is a OOK modulation scheme with ρ_p probability of transmitting a 1. At the optimal sampling time derived previously, the minimum error probability (MEP) criterion of a standard Bayesian detection framework is [122] given by the following with decision threshold η_D:

$$\vartheta \gtrless_0^1 \frac{\sigma_\vartheta^2}{\mu_{\vartheta^1} - \mu_{\vartheta^0}} \log\left(\frac{1-\rho_p}{\rho_p}\right) + \frac{1}{2}\left(\mu_{\vartheta^1} + \mu_{\vartheta^0}\right) \equiv \eta_D, \tag{4.13}$$

where:

$$\begin{aligned} \mu_{\vartheta^0} &= \mathbb{E}[\vartheta \mid \chi = 0] = \mu_{\text{ISI}} + \mu_{\text{N}}, \\ \mu_{\vartheta^1} &= \mathbb{E}[\vartheta \mid \chi = 1] = C_{\max} + \mu_{\text{ISI}} + \mu_{\text{N}}, \\ \sigma_\vartheta^2 &= \mathbf{Var}[\vartheta \mid \chi = 0] = \mathbf{Var}[\vartheta \| \chi = 1] = \sigma_{\text{ISI}}^2 + \sigma_{\text{N}}^2. \end{aligned} \tag{4.14}$$

Bit Error Rate and Throughput

The average error probability is given by [122]:

$$P_e = \rho_p \text{Q}\left(\frac{\mu_{\vartheta^1} - \eta_D}{\sigma_\vartheta}\right) + (1-\rho_p)\text{Q}\left(\frac{\eta_D - \mu_{\vartheta^0}}{\sigma_\vartheta}\right). \tag{4.15}$$

For line-coding with an equal probability of transmitting a 1 and 0 ($\rho_p = 0.5$), the BER is reduced to:

$$P_e = \text{Q}\left(\frac{C_{\max}}{2\sqrt{\sigma_{\text{ISI}}^2 + \sigma_{\text{N}}^2}}\right). \tag{4.16}$$

Note that the probability of error given a 1 transmitted, is equal to the probability of error given a 0 transmitted. Therefore, with $\rho_p = 0.5$, the system is a binary symmetric channel. The achievable throughput of the binary symmetric system is given by [123]:

$$
\begin{aligned}
C_{\mathrm{Th}} &= 1 - H(P_e) \\
&= 1 + P_e \log_2(P_e) + (1 - P_e)\log_2(1 - P_e).
\end{aligned}
\tag{4.17}
$$

4.3 Experimental Nakagami Distributed Noise Model

4.3.1 Noise Model Characterization

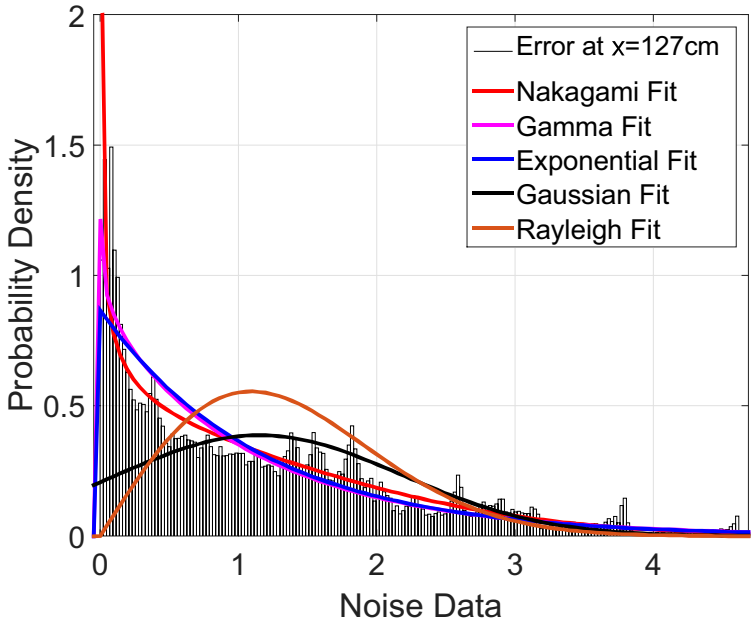

Figure 4.6: The comparison of fitting models on the noise data at $x = 127$cm.

In Section 4.2.2, the noise was assumed as Gaussian noise. However, as mentioned in Chapter 3, the channel response can be empirically analyzed from *Straight Pipe Channel Model Experiment*. The empirical additive noise is defined as the difference between the measured received signal and the average received signal of the system. Given a reliable number of experiments for each of the different channel lengths, Levenberg-Marquardt algorithm is applied to curve fit a probability distribution. Fig. 4.6 shows the comparison of fitting models on the noise data at $x = 127$cm.

According to Fig. 4.6, it can be observed that the *modified Nakagami distribution* fitted the additive noise data. The Nakagami distribution has two parameters: *a shape parameter* k, and *a spread parameter* ω and the probability density function (PDF) of the noise can be expressed as:

$$f_N(z;k,\omega) = \frac{1}{|z|\Gamma(k)}\left(\frac{k}{\omega}z^2\right)^k \exp\left(-\frac{k}{\omega}z^2\right), -\infty < z < +\infty. \tag{4.18}$$

The domain of the traditional Nakagami distribution is $[0, +\infty)$ while in this case, the noise can be negative and the domain is extended to $(-\infty, +\infty)$ to reflect this. By doing so, the pdf had to scale down by 2 from general Nakagami distribution expression otherwise the integral of the unmodified pdf across the whole domain will exceed 1. This PDF captures the fact that the additive noise can be negative mathematically as opposed to the standard Nakagami distribution where the random variable is strictly positive.

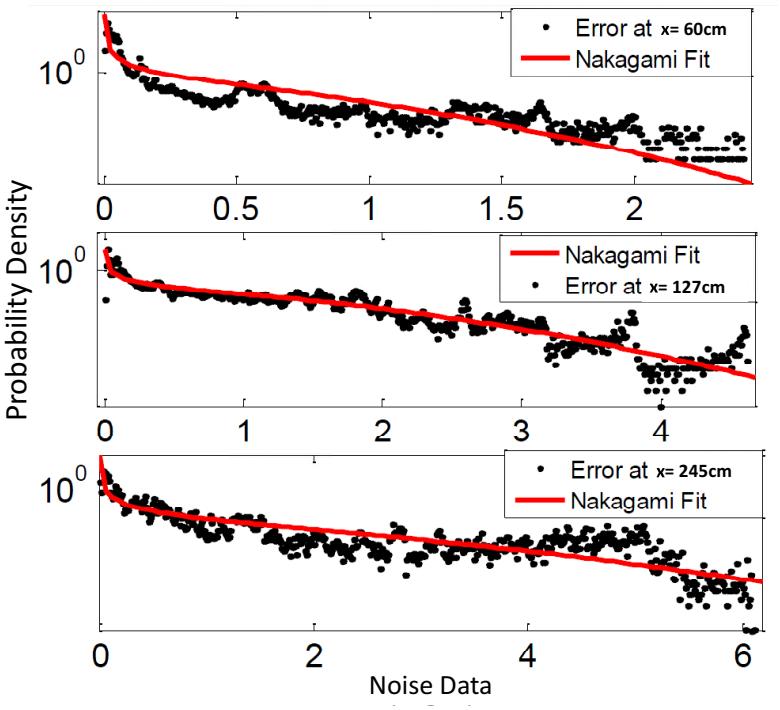

Figure 4.7: Noise (error) PDF with fitted Nakagami distributions (Log Scale.)

Table 4.2: Nakagami Distribution Fitting Parameters

Channel Length, x	**Shape,** k	**Spread,** ω	**Correlation,** R^2
60cm	0.122	0.312	0.59
127cm	0.291	2.510	0.76
245cm or greater	0.310	4.058	0.69

The results in Fig. 4.7 show three examples of the noise (error) measurements given as symbols and the theoretical Nakagami distribution given as the line. In order to examine the match clearly, the noise is displayed on a log-scale. Over 10000 empirical data points were used to generate each noise distribution. An example of the *Nakagami Distribution* parameters are displayed in Table 4.2 for various lengths. It can be seen that with increased pipe length, the shape and the spread parameters of the Nakagami distribution increase. The results saturate at lengths significantly

longer than 2.45m, and the parameters at 2.45m can be used as a stable value for longer distance propagation.

4.3.2 Bit Error Rate and Throughput

Only the additive noise in the system is primarily considered. If the receiver samples at the peak of the captured molecule concentration $C_{\max.}$, the captured concentration including noise is $\vartheta' = C_{\max} + N$. The distribution of the additive noise is now considered that follows the proposed Nakagami distribution (4.18). The transmission system is a OOK modulation scheme with ρ probability of transmitting a 1. At the optimal sampling point, the minimum error probability (MEP) criterion of a standard Bayesian detection framework can be used similar to Eq. 4.13, where $\mu_{\vartheta'0} = \mathbb{E}[\vartheta'|\chi = 0] = \mu_N$, $\mu_{\vartheta'1} = \mathbb{E}[\vartheta'|\chi = 1] = C_{\max.} + \mu_N$, and $\sigma^2_{\vartheta'} = \mathrm{Var}[\vartheta'|\chi = 0] = \mathrm{Var}[\vartheta'|\chi = 1] = \sigma^2_N$. Thus, the average error probability is:

$$P_e = \rho_p \mathcal{F}\left(\frac{\mu_{\vartheta'1} - \eta_D}{\sigma_{\vartheta'}}\right) + (1-\rho_p)\mathcal{F}\left(\frac{\eta_D - \mu_{\vartheta'0}}{\sigma_{\vartheta'}}\right), \tag{4.19}$$

where the $\mathcal{F}$-function represents the complementary cumulative distribution function (CCDF) of the noise distribution. For line-coding with an equal probability of transmitting a 1 and 0 ($\rho_p = 0.5$), the BER is reduced to: $P_e = \mathcal{F}\left(\frac{C_{\max.}}{2\sigma_N}\right)$.

For a Gaussian-distributed noise model, the $\mathcal{Q}$-function is well established. But for the modified Nakagami-distributed noise model, the $\mathcal{F}$-function is:

$$\mathcal{F}(x) = \begin{cases} 1 - \frac{\Gamma(k, \frac{k}{\omega}z^2)}{2\Gamma(k)} & z < 0 \\ \frac{1}{2} - \frac{\gamma(k, \frac{k}{\omega}z^2)}{2\Gamma(k)} & z \geqslant 0, \end{cases} \tag{4.20}$$

where $\Gamma(s,x)$ and $\gamma(s,x)$ are the upper and lower incomplete gamma function, respectively. The associated variance is $\sigma^2_N = \omega(1 - \frac{1}{k}[\frac{\Gamma(k+0.5)}{\Gamma(k)}]^2)$.

Note that the probability of error given a 1 is transmitted is equal to the

probability of error given a 0 is transmitted. Therefore, with $\rho_p = 0.5$, the system is a binary symmetric channel. The achievable throughput of the binary symmetric system is the same as Eq. 4.17.

4.4 Numerical Results

Based on the theoretical analysis in this chapter, a number of macro-scale transmission scenarios are considered and the parameters [120] used for the numerical simulations are given in Table 4.3.

Table 4.3: System Parameters

Parameter	**Values**
M	$10^9 - 10^{10}$ molecules
D	0.3 cm^2/s
x	5-10m
R_r	0.01-1m
v	4-6 cm/s
μ_{N}	$\frac{5\times10^8}{R}$ molecules/m
σ^2_{N}	$0.09\mu^2_{\text{N}}$

4.4.1 Effect of Distance and Capture Zone Size with Gaussian Noise Model

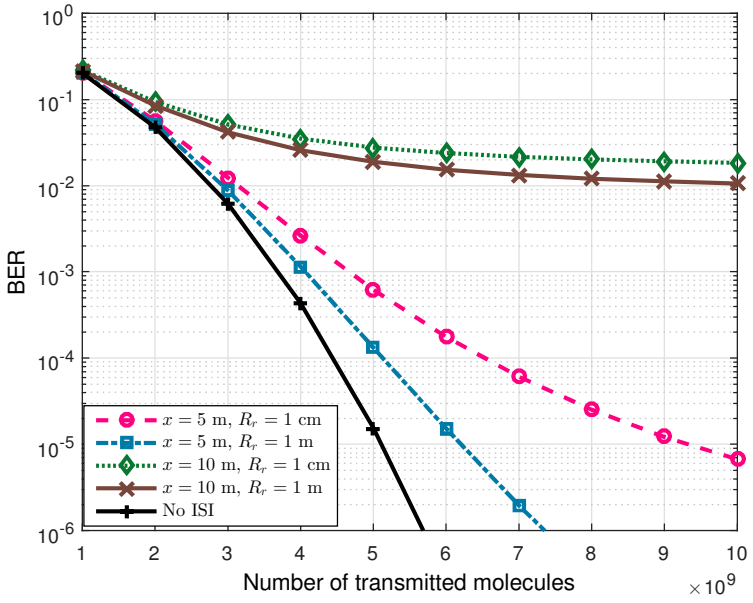

Figure 4.8: BER plot for molecular communications, with Gaussian noise and with or without ISI at different transmission distances x and capture zone sizes R_r. The constant parameters is $T_s = 3$ s, $\tau = 0.5$ s, and $v = 5$ cm/s.

In Fig. 4.8, the BER on a macro-scale ($x = 5$ - 10 m) is demonstrated, as a function of the number of molecules transmitted M, and various capture radius values R_r. It is clear that the BER is small when only Gaussian noise is considered. When ISI is introduced, the BER deteriorates with increased transmission distance and decreasing capture zone sizes. Each BER with ISI will saturate at a high number of molecules transmitted.

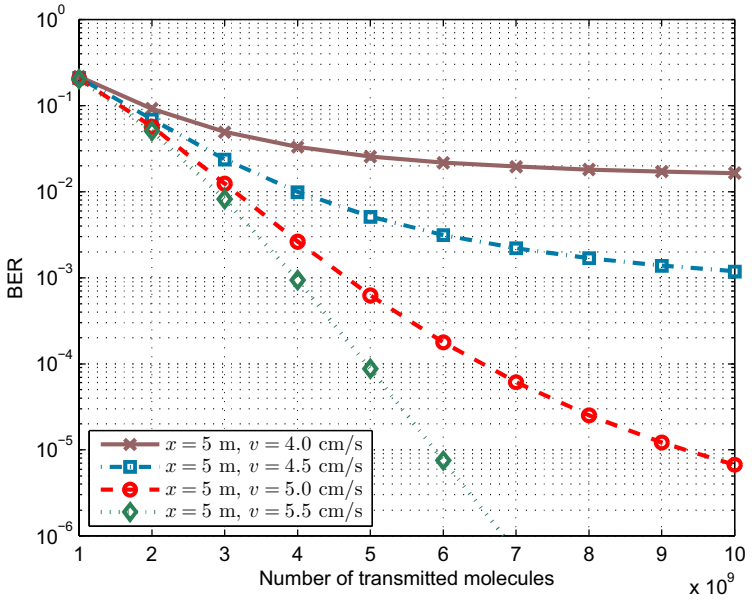

Figure 4.9: BER plot for molecular communications with Gaussian noise and ISI, comparing BER with different positive drift velocities v. The constant parameters is $T_s = 3$ s, $\tau = 0.5$ s, and $R_r = 1$ cm.

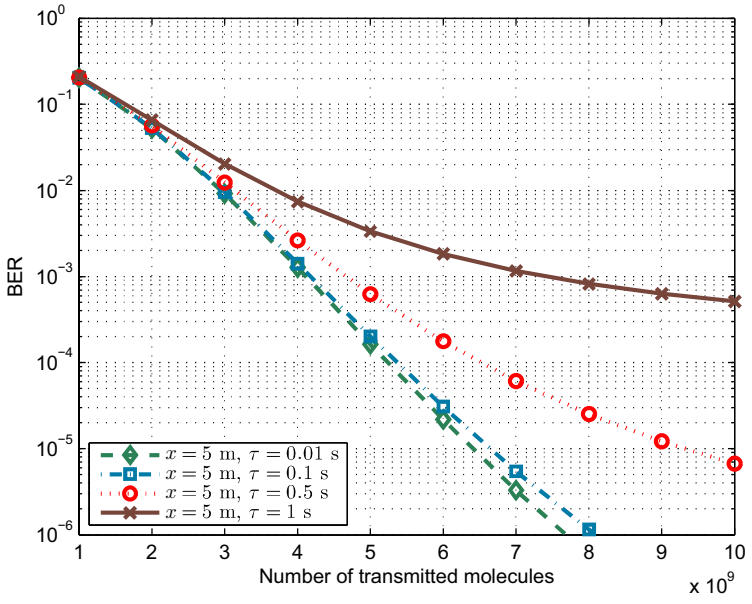

Figure 4.10: BER plot for molecular communications with Gaussian noise and ISI with different sensor cleanse durations τ. The constant parameters are: $T_s = 3$ s, $v = 5$ cm/s, and $R_r = 1$ cm.

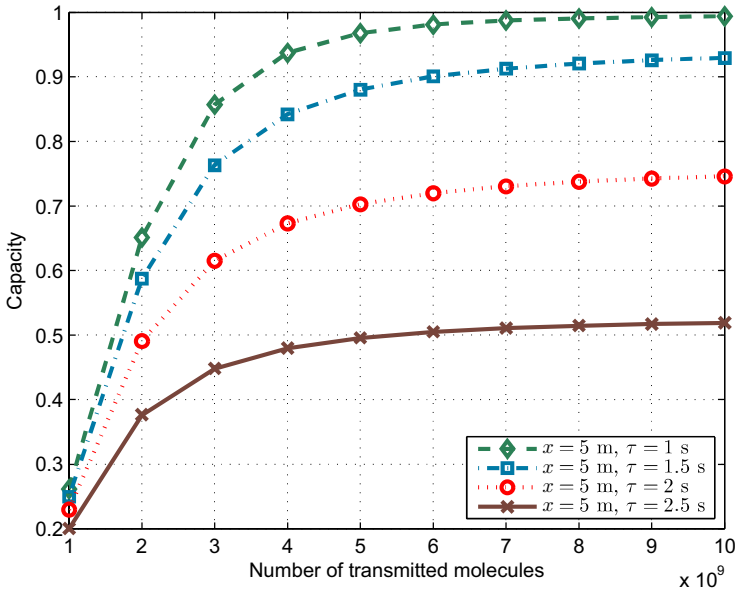

Figure 4.11: Throughput plot for molecular communications with Gaussian noise and ISI with different sensor cleanse durations τ. The constant parameters are: T_s = 3 s, v = 5 cm/s, and R_r = 1 cm.

4.4.2 Effect of Drift Velocity and Sensor Cleanse Time with Gaussian Noise Model

In Fig. 4.9, low drift velocities is considered in the order of a few cm/s. The BER results include both Gaussian noise and ISI. The plot shows that a small drift current can significantly improve the performance, such that increasing the drift from 4.0 to 5.0 cm/s can reduce the BER by orders of magnitude. Therefore, being able to control and maintain a predictable drift velocity is essential to macro-scale communications.

In Fig. 4.10, the effect of the sensor cleanse time τ is demonstrated on the BER in comparison with Gaussian noise. The results show how the BER is very sensitive to the cleanse time, whereby increasing it from 0.1 s to 1 s can increase the BER by several orders of magnitude. Therefore, a rationale conclusion is that the receiver sensor must have a short cleanse time and that the transmission rate must

be designed so that it takes into the cleanse time into account.

In Fig. 4.11, the effect of the sensor cleanse time τ is explored on the throughput. The results show how the throughput converges to 1 bits/s in the best scenario, and is most sensitive to the cleanse time, whereby increasing it from 1 s to 2.5 s can decrease the throughput from 1 bits/s to 0.52 bits/s.

4.4.3 Comparison of BER and Capacity of Empirical Nakagami Noise and Gaussian Noise model

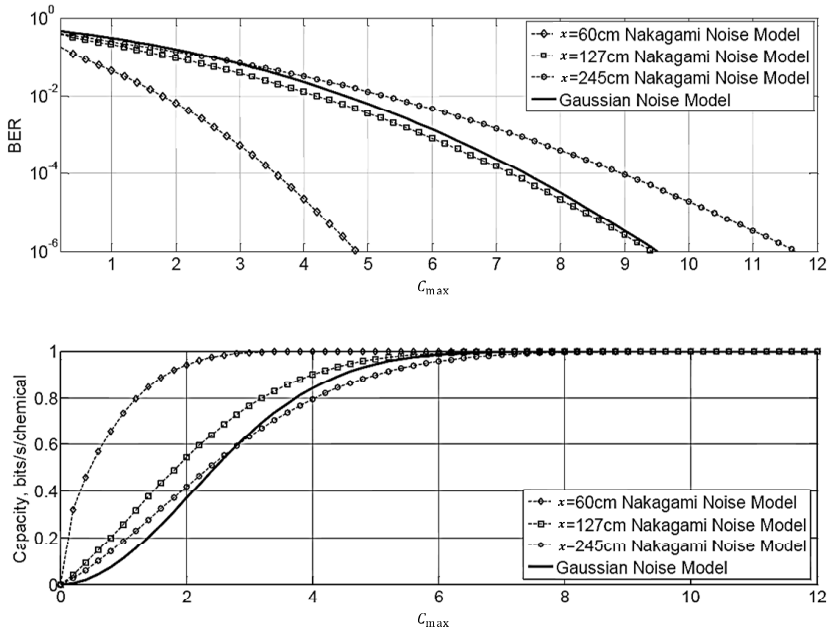

Figure 4.12: Comparison of BER and capacity performance for different noise models at different received peak concentration levels $C_{\max}$.

The results in Fig. 4.12 show that the specific parameters of the noise model can have a dramatic effect on the BER and capacity performance. This is a testament to the importance of employing accurate noise distributions as well as relevant parameters for calculating BER and capacity performances.

4.5 Summary

In this chapter, firstly the performance of EM wave based and MC experimental platform in the pipe channel were statistically compared with a conclusion that MC was more resilient than EM communications in the short ranged complex topologies investigated in the experiment. Then a novel capture probability expression of a finite sized receiver was derived for the 1 dimensional semi-infinite environment in Section 4.2. The semi-infinite environment was modeled by the experimental pipe network built in Chapter 3. Then the concept of time-aggregated molecular noise at the receiver was introduced as a function of the speed at which the sensor can self-cleanse. The resulting ISI was expressed as a function of the cleanse time sensor and its effect on the bit error rates and throughput was derived using a Bayesian decision threshold. Furthermore, with consideration of realistic experiment on the channel response of the pipe channel, a simple and effective Nakagami distributed noise model in a zero velocity pipe channel was developed in Section 4.2. The shape and spread parameters of the model increased monotonically with pipe length until the parameters converge at lengths being greater than a certain value. The proposed noise model could be used as a basis for further molecular communications research. Finally, a number of numerical results on the theoretically derived channel model for both pipe channel and Nakagami noise model showed that the BER and the throughput were very sensitive to the sensor cleanse time, drift velocity and Nakagami distribution parameters, which were depended on the channel itself.

Chapter 5

Dynamic Propagation Channel Model

With the knowledge of the static channel model and the empirical noise model of pipe network characterized in Chapter 4, this chapter focuses on a diffusion based dynamic propagation channel model which is characterised based on the practical situation. There are two scenarios considered for the dynamic propagation channel model, namely, (i) with fluctuated diffusion coefficient due to temperature variations, and (ii) with mobile transmitters or receivers. Molecular channel fading model due to diffusion coefficient fluctuations will firstly be investigated. The derivation of the channel gain will be expressed and validated. Mobile molecular communication model with a mobile transmitter will then be introduced. Particularly, positional distance codes are reviewed and implemented to achieve reliable mobile MC.

5.1 Molecular Channel Fading Due to Diffusion Coefficient Fluctuations

5.1.1 Motivations

Channel models are important in deriving the effective channel capacity, designing effective coding and advancing signal processing algorithms. Based on the analysis in Chapter 4, consider the transmitter emitting M molecules, which undergo diffusion. The receiver at a distance x away samples at a certain time instance t, receives y molecules, such that $y = \phi M + N$, where the channel gain is $\phi(x,t)$, the transmitted signal is M, and the additive noise is N.

Existing research [124] has assumed that the value of ϕ is constant for a fixed time and distance, and variations in the diffusion channel due to random environment changes have been neglected (i.e., channel fading has not been considered in a molecular communication context). Despite the abundance of additive noise based research [69, 61, 80], an examination of how variations in the channel gain itself affect performance has been lacking. Most existing papers assume a synchronized system, whereby each pulse is sampled at its peak response [69]. One recent paper has examined how long term temperature changes affect the MCvD channel performance [125], but did not consider how continuous temporal variations affect bit level performance (e.g., biological systems with short distance communications ($\sim \mu$m - $\sim$mm) suffer from temporal variations due to internal *kinetic energy* transfer or external temperature shift [126]). Whilst it is well established that the mass diffusivity (diffusion coefficient) can vary due to three parameters: (1) the temperature of the medium, (2) the radius of the molecule, and (3) the dynamic viscosity, the resulting impact on communication performance due to continuous and random changes has been neglected.

This section is to show the following: (1) temperature variations in an environment are approximately Normally distributed, which leads to a Normally-

distributed diffusivity, (2) consequentially, the channel gain has closed-form expressions of cumulative distribution function (CDF) and probability density function (PDF), (3) the joint distribution of channel gain and the additive noise, and (4) the impact on the inter-symbol interference (ISI) distribution.

5.1.2 Temperature Fluctuations

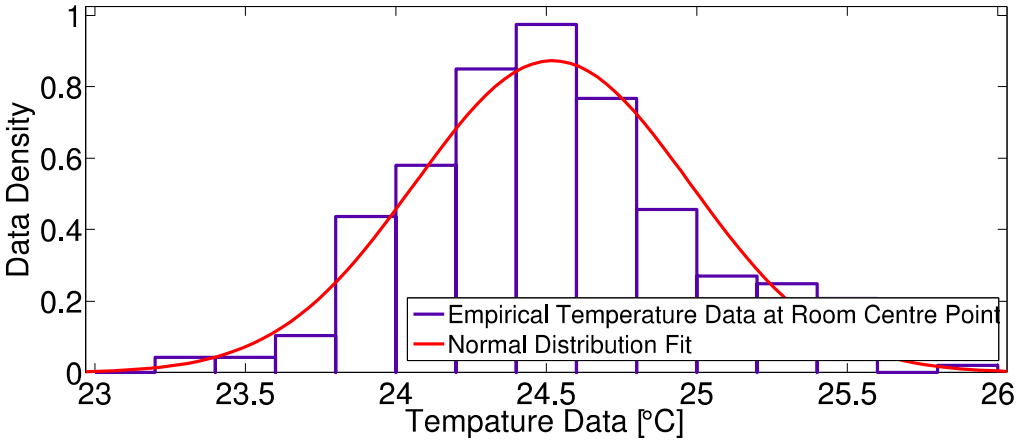

Figure 5.1: Probability density plot of temperature distribution at centre of room fitted with Normal Distribution $\mu = 24.52, \sigma = 0.457$.

The temperature fluctuation is empirically found by experiment in the University Lab. The experiment to measure the temperature variations was setup with a temperature data-logger. A number of temperature data-loggers are deployed around the lab over a continuous period of *24 hours* to record the variations (0.1 degree accuracy) every 30 minutes. The conditions of the lab are uncontrolled in the sense that there is free movement of people and objects. The peak temperature variations varied by up to 2 degrees Celsius which translates to $\approx 8\%$ diffusivity D change. The rate of change is slow (a few minutes) and the distance separation between uncorrelated channels is approximately a few metres. Fig. 5.1 shows an example pdf of temperature distribution at a particular location. The Normal distribution found empirically also conforms to the commonly used Gaussian distribution applied to

model in body temperature fluctuations [127].

5.1.3 Channel Fading Model

Firstly consider that the transmitter utilizes on-off-keying (OOK) to encode and transmit data across 1-dimensional pipe networks (semi-infinite space) and the receiver is passive (i.e., optical molecular counter). The channel gain ϕ is given as,

$$\phi\left(x,t\right)=\frac{e^{-\frac{x^2}{4Dt}}}{\sqrt{\pi Dt}} \tag{5.1}$$

where D is the diffusivity. It is worth noting that the following analysis can be performed more generally for either higher dimensions or molecule capture scenarios or both. The time delay to peak pulse $t_{\max}$ can be found from $\frac{\mathrm{d}\phi}{\mathrm{d}t}=0$ to be:

$$t_{\max}=\frac{x^2}{2D},\quad \text{and}\quad D=\frac{x^2}{2t_{\max}}. \tag{5.2}$$

By inserting the value of $t=t_{\max}$ in (5.2) into (5.1), the peak received gain value $\phi_{\max}$ can be found. Plotting ϕ versus t (for a fixed D) and plotting ϕ versus D (for a given t) will produce a similar trend. Therefore, when t is fixed to $t=t_{\max}$, the relationship of ϕ against D has a similar behavior to that of Fig. 5.2. From here it can be identified that variation of D due to temperature fluctuation will lead to ϕ being randomly distributed over a finite support of $[0,\phi_{\max}]$.

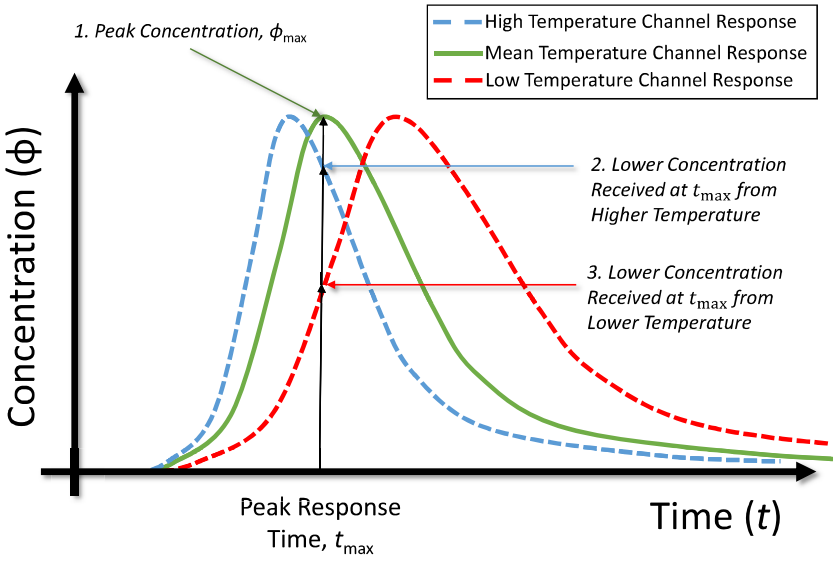

Figure 5.2: Illustration of temperature variations on the peak concentration received at the receiver.

The temperature is assumed following a Normal distribution where $T_T \sim \mathcal{N}(\mu, \sigma^2)$. In vivo environments, the Reynolds number is typically close to zero [1], and hence the *Stokes-Einstein* equation [1] is applied:

$$D = kT_T, \quad \text{where: } k = \frac{k_B}{6\pi\eta R_H}. \tag{5.3}$$

Equation (5.3) implies that D follows a Normal distribution as $D \sim \mathcal{N}(k\mu, k^2\sigma^2)$, where $\overline{D} = k\mu$ and $k^2\sigma^2$ denote the mean and variance of the diffusivity value.

The receiver is assumed that it has the knowledge of the environment average temperature and it can determine the sample time $t_{\max}$, which is fixed based on the average value of D, such that $\bar{t}_{\max} = x^2/2\overline{D}$. Furthermore, the receiver is assumed that it samples at this fixed time interval and observes fluctuations to the peak response value of $\phi_{\max}$. As illustrated in Fig. 5.2, any variations in the diffusivity

[1] Reynolds number is a dimensionless number used in fluid mechanics to indicate whether fluid flow past a body or in a duct is steady or turbulent. When the Reynolds number is close to 0, then the mass velocity in the environment is close to 0.

will cause the peak of the pulses to arrive earlier or later than expected. Given a fixed sampling time of $\bar{t}_{\max}$, the resulting received signal value will fluctuate and always be smaller than $\phi_{\max}$. As shown in Fig. 5.2, the original peak value of $\phi_{\max}$ (labelled 1.) will degrade as a result of either the channel's higher temperature (labelled 2.) or lower temperatures (labelled 3.). Note that it is hard to see how the peak response $\phi_{\max}$ varies as a function of diffusivity D, as the sample time $\bar{t}_{\max}$ will no longer be aligned with the peak response of the shifted pulses. The temperature is assumed that varies consistently across the channel, provided the transmission distance is not too long.

In order to find out the distribution of the generic channel gain Φ, D is firstly expressed in terms of ϕ according to (5.1), i.e.,

$$D(\phi) = -\frac{x^2}{2tW\left[-\frac{(\phi x)^2\pi}{2}\right]}, \tag{5.4}$$

where $W(\cdot)$ is the product log function (*Lambert W* Function).

Note that ϕ is not a monotonously increasing function of D, thus a standard inverse mapping to find the density of function of ϕ cannot be directly applied. In fact, for a given value of ϕ (except for $\phi_{\max}$), there exist two values of D, namely $D = \ell_-$ and $D = \ell_+$, that satisfy (5.1), i.e.,

$$\ell_- = -\frac{x^2}{2tW_{-1}\left[-\frac{(\phi x)^2\pi}{2}\right]}, \quad \ell_+ = -\frac{x^2}{2tW_0\left[-\frac{(\phi x)^2\pi}{2}\right]}, \tag{5.5}$$

such that $\ell_- < \ell_+$, where $W_{-1}[\cdot]$ and $W_0[\cdot]$ are the lower and upper branches of the

Lambert W function. The CDF can then be evaluated as follows.

$$\begin{aligned}
F_\Phi(\phi) &= \Pr\{\Phi < \phi\} \\
&= \Pr\{D < \ell_-\} + \Pr\{D > \ell_+\} \\
&= \frac{1}{2}\left(1 + \operatorname{erf}\left[\frac{\ell_- - k\mu}{k\sigma\sqrt{2}}\right]\right) + \frac{1}{2}\left(1 - \operatorname{erf}\left[\frac{\ell_+ - k\mu}{k\sigma\sqrt{2}}\right]\right) \\
&= 1 + \frac{1}{2}\operatorname{erf}\left[\frac{1}{k\sigma\sqrt{2}}\left(-\frac{x^2}{2tW_{-1}\left[-\frac{(\phi x)^2\pi}{2}\right]} - k\mu\right)\right] \\
&\quad - \frac{1}{2}\operatorname{erf}\left[\frac{1}{k\sigma\sqrt{2}}\left(-\frac{x^2}{2tW_0\left[-\frac{(\phi x)^2\pi}{2}\right]} - k\mu\right)\right],
\end{aligned} \tag{5.6}$$

where $\operatorname{erf}(\cdot)$ is the Gaussian error function. The PDF $f_\Phi(\phi)$ can then be obtained by

$$\begin{aligned}
f_\Phi(\phi) = \frac{\partial F_\Phi(\phi)}{\partial \phi} &= \frac{1}{k\sigma\sqrt{2\pi}} e^{-\frac{(\ell_- - k\mu)^2}{2k^2\sigma^2}} \cdot \frac{\partial \ell_-}{\partial \phi} \\
&\quad - \frac{1}{k\sigma\sqrt{2\pi}} e^{-\frac{(\ell_+ - k\mu)^2}{2k^2\sigma^2}} \cdot \frac{\partial \ell_+}{\partial \phi}
\end{aligned} \tag{5.7}$$

where

$$\frac{\partial \ell_-}{\partial \phi} = \frac{x^2}{\phi t W_{-1}\left[-\frac{(\phi x)^2\pi}{2}\right]\left(1 + W_{-1}\left[-\frac{(\phi x)^2\pi}{2}\right]\right)}, \tag{5.8}$$

$$\frac{\partial \ell_+}{\partial \phi} = \frac{x^2}{\phi t W_0\left[-\frac{(\phi x)^2\pi}{2}\right]\left(1 + W_0\left[-\frac{(\phi x)^2\pi}{2}\right]\right)}. \tag{5.9}$$

For the purposes of evaluating the channel gain ϕ's distribution (both the CDF and PDF), the value of t is taken at the average optimal sample time $\bar{t}_{\max}$.

5.1.4 Validation of Channel Gain

In this subsection, the CDF and PDF that were found are validated by numerical simulations. In the simulation, the temperature is assumed changed at the start of each symbol interval and the simulation repeats 10^6 times to produce sufficient results for each figure.

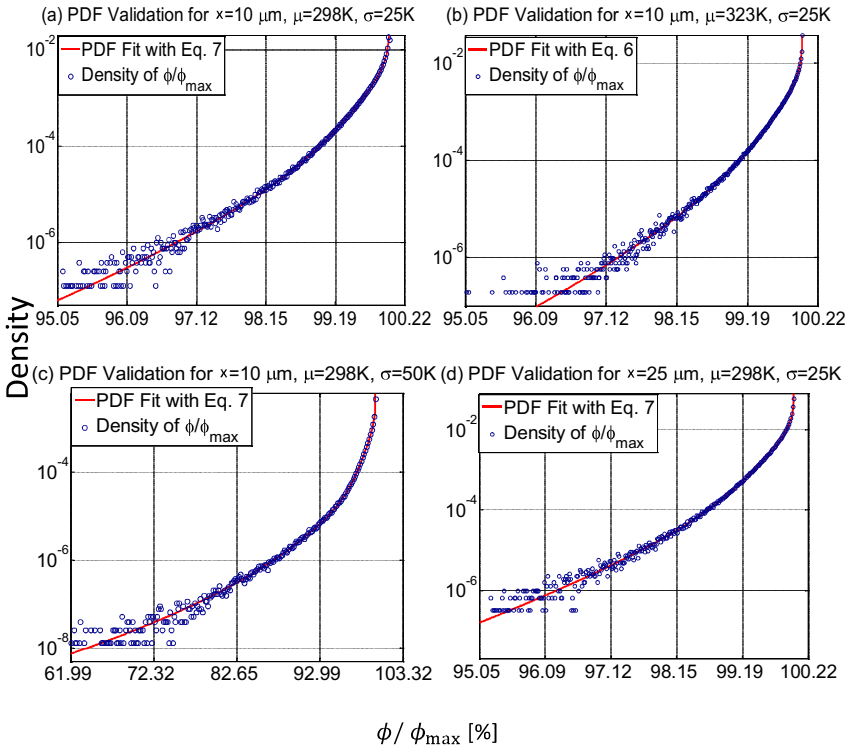

Figure 5.3: Plot of density probability of channel fading gain (percentage of peak response) with comparison of simulation results and theoretical derivation

In Fig. 5.3, the theoretical PDF given in Eq. (5.7) is validated by using numerical simulation for different transmission distances and temperature variance values. The results in Fig. 5.3(a) and (b) show that, with the increase of temperature mean value μ by 25K, the fading gain percentage increases less than 1%. By comparison of (a) and (c), the temperature standard deviation σ dominates the fad-

ing gain percentage(i.e., a +25K increase of σ causes a 30% decrease in the channel gain percentage). Subplots (a) and (d) compares the influence of the distance x. It can be observed that x does not have a significant impact on the normalized fading gain percentage $\phi/\phi_{\max}$ as x only affects the value of $t_{\max}$ (Eq. 5.2) and $\phi_{\max}$.

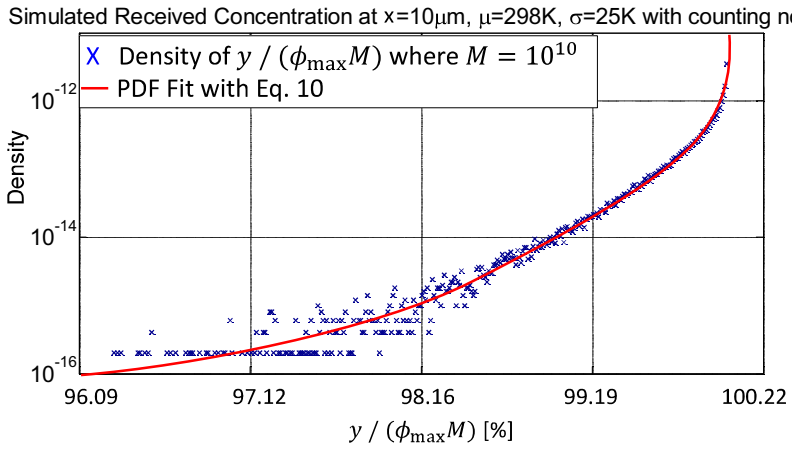

Figure 5.4: Plot of simulation for the PDF of generic received signal with comparison of theoretical derived PDF $f_Y(y)$

In addition, the noise is considered in the model for further validation. The noise is considered as additive counting noise [69] which is Gaussian distributed random variable with zero mean and standard deviation is given as $\sigma_N = \sqrt{\frac{\phi M}{x}}$ in 1-dimension environment. The generic received signal y is a sum of two random variables namely channel gain ϕ and noise N (with a probability density function $f_N(n)$). Therefore, the pdf of y can be given as the integral of both the probability density function of ϕ and N:

$$f_Y(y) = \int_0^\infty f_{\Phi,N}(\phi, y-\phi)\mathrm{d}\phi \tag{5.10}$$

where $f_{\Phi,N}(\phi, y-\phi)$ can be calculated from the derivative of the product of the conditioning probability $P(y-\phi \mid \phi)$ and marginal probability function $P(\phi)$. In Fig. 5.4, the comparison between the simulation results of the generic received signal

and the theoretical derived PDF is given in Eq. (5.10).

5.1.5 Impact on ISI

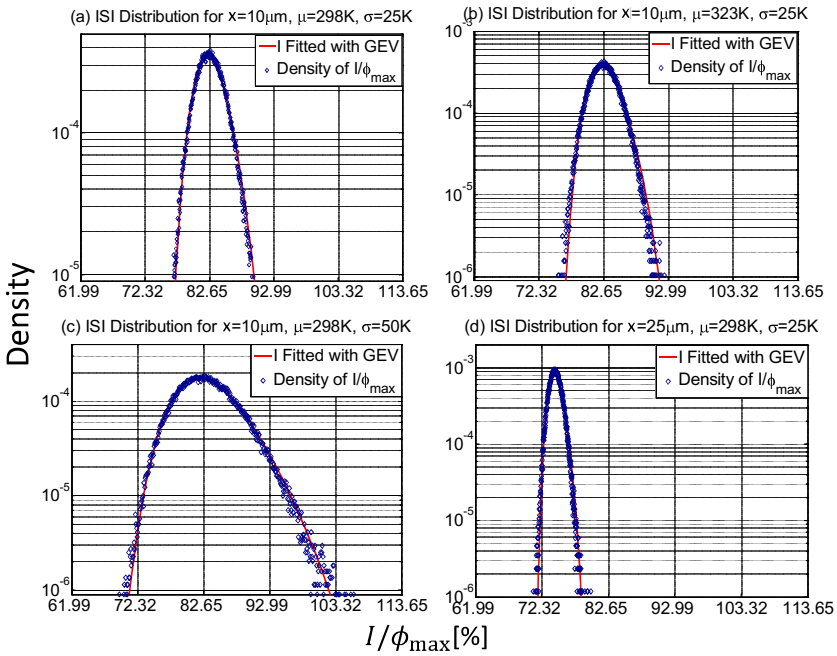

Figure 5.5: Plot of simulated ISI distribution and its Generalized Extreme Value (GEV) fitted distribution with parameters: (a) $k_g = -0.17, \mu_g = 39623.5, \sigma_g = 1069.34$, (b) $k_g = -0.15, \mu_g = 39638.1, \sigma_g = 980.92$, (c) $k_g = -0.02, \mu_g = 39369.5, \sigma_g = 2118.72$ and (d) $k_g = -0.15, \mu_g = 15844.8, \sigma_g = 423.92$.

The ISI can arise from multiple previous symbols (heavy-tail of channel response). With the knowledge of ISI in Chapter 4, assume the probability of transmitting bit 1 and 0 are 0.5, and consider 10 previous symbols for the effect of ISI, the channel response for each interference symbol has a fading distribution that is i.i.d. in accordance to Eq. (5.1) and Eq. (5.3). The ISI for an OOK system with a constant symbol period T_s can generally be expressed as the sum of interference from the 10

considered previous symbols:

$$I(x,t) = \sum_{n=1}^{10} \phi_n(x, \bar{t}_{\max} + nT_s)\chi_n, \tag{5.11}$$

where χ_n is the line-coding output and can take on the value 1 or 0. When we come to consider the effect of channel gain on ISI, we can utilize the generic channel gain ϕ's distribution derived in Eq. (5.7). The ISI PDF with different transmission distances and temperature variation statistics is plotted in Fig. 5.5. It is shown that the ISI density distribution can be fitted by a Generalized Extreme Value (GEV) distribution [128] with parameters k_g, μ_g and σ_g. The results indicate that only the standard deviation of the temperature variations strongly affect the ISI distribution. The detailed results in Fig. 5.5 show that with an increase in mean temperature μ, the distribution in subplots (a) and (b) remains similar. In subplots (a) and (c), as the temperature standard deviation σ increases, the ISI distribution shifts to a higher GEV shape factor k_g, while the range of the ISI stretches significantly. The change of distance does not have obvious effects on the shape of ISI distribution and the percentage of ISI over $\phi_{\max}$ according to subplots (a) and (d) which is similar to the finding in Fig. 5.3.

5.2 Mobile Molecular Communication Model and Positional Distance Codes

5.2.1 Motivation

Another scenario of MC is that the transmitter and receiver may in mobility while transmitting and receiving information patrials. One example is *Quorum Sensing* in bacteria. Recent research on MC focusing on the fixed transmitter and receiver, the channel model for the mobile MC is lacking. In addition, the movement of the transmitters and receivers are likely to cause bits to be disordered due to the slow

propagation rate relative to the their movement speed. Forward-error-correction codes are targeting on the transmission over unreliable or noisy communication channel. However, as reviewed in Chapter 2, traditional forward-error-correction (FEC) codes are inadequate in dealing with the transposition errors. Therefore, in this section, the mobile MC channel will firstly be introduced and characterised, then the cause of transposition errors are demonstrated by the MC experimental robot chassis built in Chapter 3. Finally, the architecture and performance of positional-distance codes is proposed and evaluated with comparison of traditional Hamming-distance approaches.

5.2.2 Mobile MC Channel Model

Firstly recall the channel gain ϕ in 3D environment with a capture receiver reviewed in Chapter 2 is given as [41],

$$\phi_(x,t) = \frac{R_r}{x+R_r}\frac{x}{\sqrt{4\pi D t^3}}\exp\left(-\frac{x^2}{4Dt}\right), \tag{5.12}$$

where x is the transmit distance, and R_r is the radius of receiver. This assumes that each molecule that falls within the radius of the receiver is permanently absorbed and converted into a signal output for detection. The *counting noise* is considered in this scenario. The receiver is commonly designed to detect the peak response or a change in gradient at the peak response, which occurs at the following time and corresponding value:

$$t_{\max} = \frac{x^2}{6D}, \quad \phi_{\max} \propto \frac{DR_{\mathrm{r}}}{x^2(x+R_{\mathrm{r}})}. \tag{5.13}$$

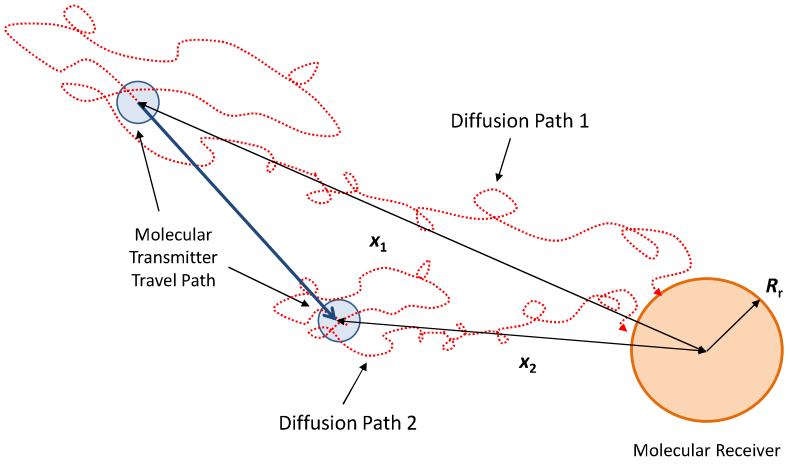

Figure 5.6: Illustration of mobile molecular communications with a transmitter moving towards the receiver.

When one considers a mobile molecular channel, the distance x component in Eq. (5.12) will vary in accordance to time. In the most extreme scenario, the transmitter will be travelling towards the receiver at a velocity that is significantly faster than the rate of diffusion. It is assumed that the movement of the transmitter does not in itself disrupt the diffusion process. Fig. 5.6 illustrated the channel model. Consider 2 symbols transmitted sequentially at distances x_1 and x_2 at times t_1 and t_2 respectively (symbol period of $T_s = t_2 - t_1$). Assume that the receiver uses the received pulse response's peak for detection. For each transmitted pulse, the time to peak value $t_{\max}$ given in Eq. (5.13), will differ such that the second symbol will arrive at a time ΔT_s after the first:

$$\Delta T_s = T_s + \frac{x_2^2 - x_1^2}{6D}. \tag{5.14}$$

For equal distant transmissions, the time difference will simply be the symbol period T. Referring to Eq.(5.14), in order for bit transposition errors not to occur ($\Delta T_s > 0$), the following must hold true: $T_s > \frac{x_1^2 - x_2^2}{6D}$. Certainly, as a simple observation, if the symbol period is larger than the peak response arrival time ($T_s > \frac{x_1^2}{6D}$),

then bit transposition errors cannot occur. However, two caveats exist with adapting the dynamic symbol period in this manner: 1) every subsequent symbol will need to wait a dynamic time period based on the current transmission distance estimated (difficult to achieve), and 2) the resulting data rate can be extremely variable and low. Hence, there is a need to implement new code designs to combat bit transposition errors.

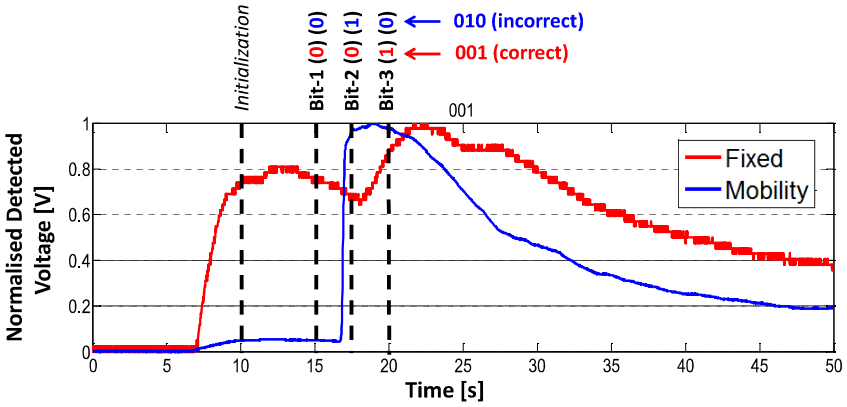

Figure 5.7: Plot of experimental pulse response from 1 trigger symbol and 3 sequential transmitted symbols. The transmitter transmits 001. Each of the time markers show the receiver sampling points. Each bit received is decoded for the (fixed - red) (mobile - blue) channels.

In order to model the effects of mobility on bit errors, a mobile molecular communication system has been developed and tested (see Chapter 3). To demonstrate how bit transposition occurs, the robot first remains static and sends an initialization pulse to signal to the receiver that it is ready. After waiting for 5s, the robot then begins moving towards the receiver and sends 3 symbols at a fixed interval of 2.5s. Referring to Fig. 5.7, 001 is transmitted. For the static case (red), the initialization pulse is received followed by a decrease in gradient at the Bit-1 and Bit-2, indicating a 0 bit for both. This is then followed by an increase in gradient, indicating that Bit-3 is a 1. Hence the data of 001 is correctly received. However, in the mobile case (blue), the receiver will receive a sharp increase in the Bit-2 position

and no change in the Bit-1 and Bit-3 positions, indicating a 010. That is to say, the original Bit-3 has shifted to Bit-2, which is a transposition error. By implementing the $(4, 2, 1)$-ISI-free FEC code (see Algorithms 1 and 2), the robot was able to combat single transposition errors.

5.2.3 Positional-Distance Design

Consider an (n, k)-block-coding strategy that maps k-bit message into n-bit codeword and is implemented in the mobile robot. The movement of the robot causes bit transposition where earlier bits can arrive later than more recent bits, and vice-versa. Therefore, when a stream of k-bit messages are encoded using this strategy, the mobile molecular channel may exchange the bits' positions within a codeword (*Intra-Codeword Errors*) and across codewords (*Inter-Codeword Interference*). Chapter 2 has reviewed several block-coding techniques that are aimed to mitigate errors due to bit transposition. In the following, the rationales behind the development of those techniques is discussed and explored.

Intra-Codeword Errors

Intra-codeword transposition errors that affect (n, k)-block codes to encode 2^k messages is firstly examined. For an n-bit block, the total number of words that can be generated is 2^n. As mentioned in Chapter 2, existing block codes have largely been designed based on maximization of the Hamming distance from the chosen 2^k out of 2^n possible words. This maximization is intuitively useful to correct corrupted bits due to noise/distortion. However, it is likely to be ineffective when the errors are mainly due to permutation of bits' positions.

(1) Back to Repetition Codes: In a trivial example, let us consider block length of $n = 2$ and two possible codebooks, both with the same Hamming distance of 2: $\mathcal{C}_1 = \{01, 10\}$ and $\mathcal{C}_2 = \{00, 11\}$. In the event of a bit transposition error, it is clearly preferable to use codebook $\mathcal{C}_2$. This demonstrates that Hamming distance

alone may not be the only parameter to consider. Codebook $\mathcal{C}_2$ is precisely the repetition code for $n = 2$. Since the structure of a repetition code for any length $n > 0$ is well preserved in the event of bits transposition, the code is effective in combating intra-codeword errors. Yet, repetition codes only achieve a code rate of $R_{\text{Rep.}} = \frac{1}{n}$, whereby a large n will yield a very small coding rate.

(2) Distinct Hamming Weight (DHW) Codes: From a different perspective, it can be observed that the codewords in the above repetition code $\mathcal{C}_2$ have the Hamming weights of 0 and 2, respectively. Further observation is that each of these Hamming weights remains unchanged under permutation of bits within a codeword. Building upon this observation, a coding scheme can be constructed in which each codeword can be identified from its Hamming weight. Such a coding scheme for a length-n block is referred as a *distinct Hamming-weight (DHW) code* of length n. It is worth noting that the DHW code is not unique as the distinct Hamming-weight requirement can be satisfied by more than one set of codewords. A length-n DHW code can achieve the largest rate of:

$$R_{\text{DHW}} = \frac{1}{n} \log_2(n+1), \tag{5.15}$$

which improves on repetition codes by a factor of $\log_2(n)$ for large codewords. A specific instance of length-4 DHW code is given as $\mathcal{C}_{\text{DHW}} = \{0000, 1000, 1100, 1110\}$.

Inter-Codeword Errors

In order to mitigate bit transposition (both within and across codewords), the authors in [84] introduced a new coding parameter, namely molecular coding (MoCo) distance, to replace Hamming distance for code design in molecular communications. Consider two possible binary codewords $\boldsymbol{c}_i$ and $\boldsymbol{c}_j$. Building upon on-off keying modulation with a single molecule for each entry of $\boldsymbol{c}_i$ and $\boldsymbol{c}_j$, the MoCo

distance of $\boldsymbol{c}_i$ and $\boldsymbol{c}_j$ (with its variants for simplification) is defined by

$$d_{\text{MoCo}}(\boldsymbol{c}_i, \boldsymbol{c}_j) \triangleq -\log\left(\Pr\{\boldsymbol{c}_j|\boldsymbol{c}_i\}\right), \tag{5.16}$$

where $\Pr\{\boldsymbol{c}_j|\boldsymbol{c}_i\}$ is the channel transition probability from $\boldsymbol{c}_i$ to $\boldsymbol{c}_j$ that is governed by molecular diffusion. In parallel to Hamming distance approach, the best code is thus given by a codebook that maximizes the minimum pairwise MoCo distance. An example for $n = 4$ is provided in [84], i.e., $\mathcal{C}_{\text{MoCo}} = \{0000, \quad 1000, \quad 0010, \quad 1110\}$. It was argued that from the MoCo distance maximization and the guard band indicator of bit '0' at the end of each codeword in $\mathcal{C}_{\text{MoCo}}$, this coding construction addresses permutation of bits within each codeword and across codewords. This construction, however, has a significant drawback from the fact that it needs to exhaustively search for the best code according to criterion in 5.16, and will be less suitable for practical implementation.

Implementation of Transposition Error Correction Code

Table 5.1: Assigning codewords for the (4,2,1) ISI-free code.

Message bits	Previous codeword has last bit '0'	Previous codeword has last bit '1'
00	0000	1111
01	0001	1000
10	0011	1100
11	0111	1110

The work in [85] recently developed a systematic step-by-step approach to construct a code that attempts to reduce bit transposition errors. The resulting code is denoted as (n, k, ℓ) ISI-free code where n and k follows from the usual coding notations of block length and message length, respectively, and an extra parameter ℓ is the transposition level that can be corrected. The name ISI-free is somewhat mislead-

ing, as the codeword does not target the removal of inter-symbol-interference (ISI), and rather it is a positive side effect. An example of $(4, 2, 1)$ ISI-free code is illustrated in Table 5.1. The ISI-free code partially uses Hamming weight features of that DHW code in order to minimize the transposition errors within a codeword. The bit transposition at level ℓ across codewords can be corrected by ensuring that for two consecutive codewords, the first ℓ bits of the latter are the same as the last ℓ bits of the former. In terms of implementation of the $(4, 2, 1)$-ISI-free FEC code in the mobile robot, the steps are presented in Algorithms 1 and 2, which include both the encoding and decoding techniques.

Algorithm 1 Encoding method using (4,2,1)-ISI-free code

Input: $\boldsymbol{d}$ (vector of N information bits), prev_bit (initialized to 0, indicating last bit of previous codeword)

Output: $\boldsymbol{c}$ (vector of coded bits: length $2N$)

Assume: All vectors start with index 1

if N is odd **then**
  $\boldsymbol{d} \leftarrow [\boldsymbol{d} \quad 0]$
  $N \leftarrow N + 1$
end if
for i from 1 to $N/2$ **do**
  $\boldsymbol{m} \leftarrow \boldsymbol{d}[2i - 1 : 2i]$
  if prev_bit == 0 **then**
    switch $\boldsymbol{m}$ **do**
      case [0 0]
        $\boldsymbol{c}[4i - 3 : 4i] \leftarrow [0\ 0\ 0\ 0]$
      case [0 1]
        $\boldsymbol{c}[4i - 3 : 4i] \leftarrow [0\ 0\ 0\ 1]$
      case [1 0]
        $\boldsymbol{c}[4i - 3 : 4i] \leftarrow [0\ 0\ 1\ 1]$
      case [1 1]
        $\boldsymbol{c}[4i - 3 : 4i] \leftarrow [0\ 1\ 1\ 1]$
  else
    switch $\boldsymbol{m}$ **do**
      case [0 0]
        $\boldsymbol{c}[4i - 3 : 4i] \leftarrow [1\ 1\ 1\ 1]$
      case [0 1]
        $\boldsymbol{c}[4i - 3 : 4i] \leftarrow [1\ 0\ 0\ 0]$
      case [1 0]
        $\boldsymbol{c}[4i - 3 : 4i] \leftarrow [1\ 1\ 0\ 0]$
      case [1 1]
        $\boldsymbol{c}[4i - 3 : 4i] \leftarrow [1\ 1\ 1\ 0]$
  end if
  prev_bit $\leftarrow \boldsymbol{c}[4i]$
end for
return $\boldsymbol{c}$

Algorithm 2 Decoding (4,2,1)-ISI-free codewords

Input: $\boldsymbol{r}$ (vector of N coded bits)

Output: $\boldsymbol{y}$ (vector of decoded bits: length $N/2$)

Assume: N is a multiple of 4, all vectors start with index 1

for i from 1 to $N/4$ **do**
  $\boldsymbol{w} \leftarrow \boldsymbol{r}[4i-3:4i]$
  $hw \leftarrow$ Hamming_Weight($\boldsymbol{w}$)
  switch hw **do**
    case 0
      $\boldsymbol{y}[2i-1:2i] \leftarrow [0\ 0]$
    case 1
      $\boldsymbol{y}[2i-1:2i] \leftarrow [0\ 1]$
    case 2
      $\boldsymbol{y}[2i-1:2i] \leftarrow [1\ 0]$
    case 3
      $\boldsymbol{y}[2i-1:2i] \leftarrow [1\ 1]$
    case 4
      $\boldsymbol{y}[2i-1:2i] \leftarrow [0\ 0]$
end for
return $\boldsymbol{y}$

5.2.4 Performance Comparison

Double Random Walk Mobility Model

In order to create 10^3-10^5 bits with transposition possibilities, a robotic experiment would take an extremely long time, and furthermore, realistic physical boundary conditions will add bias to the results. In order to generate a sufficient number of bit transposition errors and apply a range of FEC codes, a random walk (RW) model for the molecular movement is employed, whereby the distance between the transmitter and the receiver also follows a RW model. The model is called as double RW (double-RW) model. Firstly consider the movement of the transmitter's location as a 1-dimensional Wiener process. Intuitively, the Wiener process is a continuous-time random process with independent Gaussian-distributed increments. Assume

the process starts off at position $x(0) = L$, where L is the initial distance (also mean separation) distance between the transmitter and the receiver. Thereafter, the position $x(t_k)$ at discrete time t_k is a Gaussian random variable (r.v.) with distribution $x(t_k) \sim N\left(L, t_k\sigma^2\right)$. The variance parameter σ^2 is given by $\sigma^2 = 2D_{\mathrm{Tx}}$ where D_{Tx} can be interpreted as the movement speed of the transmitter. Then consider that molecular channel coding using binary alphabets $\{0, 1\}$ to construct the code of length n. Upon encoding a message m, the n-bit codeword $\boldsymbol{c}$ is modulated using a relevant sequence of molecules. For a bit-1 and bit-0, the transmitter emits one single molecule of two different molecule types respectively. Let the expected time of arrival be $t_{\max}$, given in Eq. (5.13). Due to the random motion of the molecule, the random arrival time can be treated as $t_{\max} + N_z$, where N_z is the time noise. The noise N_z is IG distributed [129]:

$$f(N_z) = \sqrt{\frac{\lambda}{2\pi N_z^3}} \exp\left(-\lambda \frac{(N_z - \mu)^2}{2\mu^2 N_z} \right), \quad z > 0, \tag{5.17}$$

where $\mu = x(t_k)/v$ and $\lambda = 2(x(t_k)/D)^2$. The drift velocity v is always towards the receiver. As mentioned earlier, the distance x is a Gaussian r.v. $(x(t_k) \sim \mathcal{N}\left(L, t_k\sigma^2\right))$. By using the double RW model, It is able to simulate a large number of bit transposition errors to yield statistically significant comparative results for different FEC codes.

Numerical Results

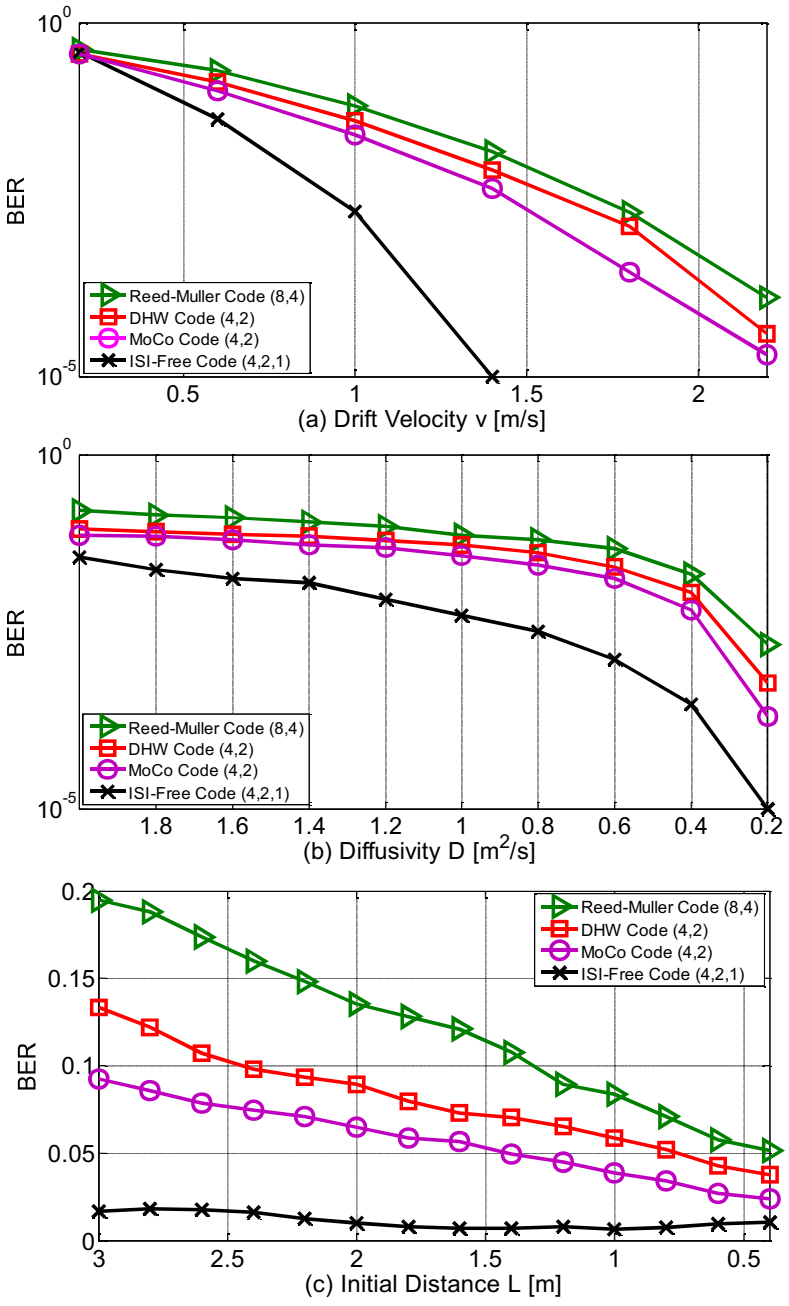

Figure 5.8: BER of various coding schemes as a function of: (top) drift velocity v, (middle) molecular diffusivity D, (bottom) initial distance L. The static parameters used are: $D = 1m^2/s$, $L = 1m$, $D_{\text{Tx}} = 10^{-10} \times Dm^2/s$, and $v = 1m/s$. All the coding schemes have rate of $1/2$.

In Figure 5.8, the bit-error rate (BER) of the various coding techniques is plotted in the presence of bit transposition errors introduced by the double RW model. From the three sub-figures, it can be seen that the initial distance plays a minor role in the BER due to the resulting movement. Then it can be observed that the (8,4) Reed-Muller code (design based on the Hamming distance) has the worst BER performance. It can also be clearly observed that the optimal (4,2) MoCo-distance code has a better performance than the DHW code due to the fact that the MoCo distance (5.16) closely resembles the actual channel transition probability as opposed to the Hamming weight criterion. On the other side of the coin, the main limitation of the MoCo-distance code is the difficulties to generate codewords without resorting a full-scale search to the possible combination of bits. From Figure 5.8, it is identified that the (4,2,1) ISI-free code is superior to other coding techniques in terms of BER. The ability of always meeting the requirement of mitigating $\ell = 1$-level transposition errors and the availability of step-by-step coding mechanism make this code to be attractive for implementation in mobile molecular communications.

Perhaps, a critique to the construction of the (4,2,1) ISI-free code is the idea that two codewords are used to represent a single group of message bits as shown in Table 5.1. This idea leads to the inefficiency in terms of coding rate. From this type of construction, it can be further shown that for a block length of n bits, rate beyond $\frac{n-1}{n}$ is unattainable. In fact, the example above with the (4,2,1) ISI-free code has rate only $\frac{1}{2}$ and increasing rates beyond $\frac{1}{2}$ is challenging. The work in [85] partly addressed this, but further improvement and works are still required to enhance the coding efficiency.

5.3 Summary

In this chapter, the dynamic MC channels were introduced, including a fading channel model due to dynamic temperature variations, and a mobile MC channel due

to dynamic mobile transmitter. In Section 5.1, a statistical distribution of the channel gain, subject to temperature fluctuations was derived. It showed that if the temperature fluctuations followed a Normal distribution, then the channel gain distribution followed a closed form expression. This was important in a communication context, whereby each detected pulse's amplitude would now be subject to variations as a function of the temperature variations in the channel. A joint distribution of the channel gain and the additive noise were further derived, and the temperature variations affecting the ISI, which was conformed to a GEV distribution, was demonstrated. In Section 5.2, the mobile MC was firstly introduced and statistically presented. Afterwards, it was demonstrated by experiments that MC between mobile nodes would yield bit transposition errors, which was a far more damaging source of noise, whilst considering additive noise from random molecules' arrival process. In order to improve the communication performance of mobile MC, a new family of appropriate FEC codes was employed as positional-distance codes and simulated to show a significant improvement over classical Hamming-distance coding strategies.

Chapter 6

Bacterial Relay for Energy Efficient Molecular Communications

As mentioned in Chapter 2, excepted from the passive diffusion propagation mode, another propagation mechanism is the active mode. This chapter focuses on this mode, where bacteria is able to assist information particles delivered to destination. Firstly the motivation of researching on bacterial relay is provided in Section 6.1. Further in Section 6.2, it will present the communication process of the bacteria based MC. Then the information delivery energy model and energy efficiency of bacterial relay will be proposed in Section 6.3. Finally, in Section 6.4, the energy efficiency of both bacterial relay and diffusion based MC is examined and compared.

6.1 Motivation

In conventional wireless communication systems, *mechanical relaying* has been widely studied as an energy efficient delay-tolerant protocol [130, 131, 132]. The advantages of using it includes enhancing the cell coverage, spatial reuse of the scarce wireless re-

sources and enhanced throughput [133]. Moreover, it could potentially achieve order of magnitude reductions in the end-to-end communication energy consumption by the network [134] [1]. Based on the literature review of bacteria in Chapter 2, similar to mechanical relaying, chemotaxis in biological systems perform similar functions in the context of MC by picking up information macro molecules (i.e., plasmids) and delivering them to a receiver [49, 50]. A key advantage of such systems is that the information particles can be protected in bacteria from chemical degradation and predation from the environment [11]. Although the bacteria relaying mechanism has been widely studied in both cell biology and biological physics, the energy efficiency analysis of the information transfer process is still lacking. Therefore, this chapter is aim to establish an information delivery energy model for molecular communication via bacteria relays and analyze the energy efficiency of the process in comparison with conventional MCvD across multiple distances and environmental conditions.

6.2 Molecular Communication via Bacteria

6.2.1 System Fundamentals

The bacteria used is *E. coli* which is reviewed in Chapter 2. The bacteria act as chemotaxis for information delivery process. In order to reverse engineer the chemotaxis process, nanomachines are required. Nanomachines are the artificial devices in nano-scale with potential features including computing, sensing and actuation tasks. It is able to manufacture bio-hybrid nanomachines ranging from 5 to 100μm in diameter [135]. Such machines can contain: 1) *DNA Processing Unit* (DPU) to embed artificial information through the synthesis of DNA (forms a plasmid) [136], 2) *Bio-Compartment* to store the produced plasmid, and 3) *Bionic Pilus*[2] to transfer the plasmid to bacteria carrier. In terms of assisting the navigation of the previously

[1] Note the mobility energy of mechanical relays are not considered as the information packets are piggy-backing existing mobility systems.

[2] A pilus is a hair like appendage found on the surface of many bacteria for direct contact of two bacteria [137].

mentioned bacterial carrier, the nanomachine can further emit chemical attractant to guide the bacteria. The transmitter distinguishes itself by emitting *transmission attractant* (TA) at a constant rate to creating a concentration gradient in the channel. This serves the purpose of luring empty bacteria carrier to pick up the information. Likewise, the receiver nanomachine transmits *reception attractant* (RA), which serves the purpose of luring information bearing bacteria to the receiver.

6.2.2 Communication Mechanism

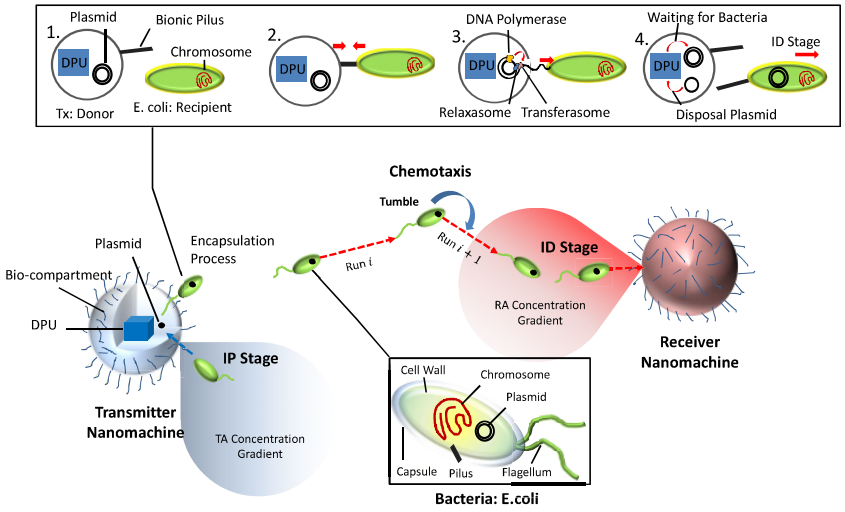

Figure 6.1: Communication Steps of Molecular Communication via Bacteria Relaying.

The communication mechanism is illustrated in Fig. 6.1. The communication mechanism has 5 steps namely *Encoding, Encapsulation, Propagation, Decapsulation,* and *Decoding.*

Encoding

At the beginning of the communication, the DPU starts encoding the message by transferring in a double-stranded DNA molecule. This molecule will then be formed as a plasmid which is a circular DNA strand with capability of self-replication

and self-transfer by the DPU. The plasmids are stored in the transmitter *bio-compartment* and at the mean time the transmitter starts releasing the TA in order to attract the empty bacteria carriers in the vicinity.

Encapsulation

Encapsulation process is an biological technology which is used to transfer genetic materials from man-made nanomachines to another nanomachines or bio-organism. *Encapsulation* is inspired by *bacterial conjugation* [3] in nature. In Fig. 6.1, *Encapsulation* happens when the bacterial carrier comes closely enough to the transmitter nanomachine. The transmitter will first act as a donor to attach the bacteria by the *bionic pilus*, which will retract to get the carrier in physical contact with the transmitter. The membranes of both transmitter and bacterium is now connected and a single stranded DNA will be unwounded from the encoded plasmid and then passed to the bacterial carrier. After the single stranded DNA has been transferred, it replicates to a full plasmid in the bacterial carrier while the transmitter and carrier separate. In this case, the remaining part of plasmid in the transmitter is assumed to be discarded.

Propagation

The *propagation* of the bacteria in the environment guided by attractants is *chemotaxis*, its movement modeled by a modified version of *Pearson-Rayleigh* random walk, which is represented repeating of two stages. In stage a), the bacteria propels over a straight line at constant speed for exponential distributed amount of time. In stage b), the bacterium tumbles around uniformly choosing a new direction arbitrarily between 0 and 2π (see Chapter 2). The propagation process from bacteria's original position to transmitter and from transmitter to receiver after *encaspulation*

[3] *Bacterial conjugation* is the transfer of genetic material between bacterial cells by direct cell-to-cell contact or a bridge-like connection between two cells [53].

is defined as the *Information Pick-up* (IP) and the *Information Delivery* (ID) stages respectively. IP and ID stages are two independent random walk processes.

Decapsulation and Decoding

Once the information bearing bacteria arrives at the receiver and connects by the *bionic pilus*, the receiver decapsulates the plasmid and release the empty bacteria back to the environment for the IP stage. In the decoding step, the DPU of the receiver determines the structure of the plasmid by sequencing it and then extract the information from the message region of the plasmid. The receiver finally processes the message and ends the communication.

6.3 Propagation and Energy Model

6.3.1 Propagation Channel Model

A 3-dimension (3-D) aqueous environment represented by a cubic area with $X\mu$m side length is considered. In order to simplify the simulation process, there are several assumptions are applied:

1. The environment is assumed to be free from biased flow currents and free diffusion takes place and the bacteria will bounce back at the boundary;

2. A multiple transmission system is considered, where there are M pairs of transmitters and receivers, and a population of Q bacteria units are used as mobile relays. All the transmitters, receivers and bacteria are assumed to be deployed uniformly in the environment. The size of bacteria is assumed to be significantly smaller than transmitter and receiver;

3. The transmitters have capture radius R_{t}, where inside the radius we assume the bacteria will be successfully connected, and the receivers have reception

radius R_{r} where we assume the plasmid is received once the bacteria move in the reception radius;

4. The receivers are assumed to be able to count the number of received plasmid in any given time interval and duplicate messages are able to be deleted by the receiver [4].

5. We assume the communication process happened during the bacterial *lag-phase*, where the the bacteria adapt themselves to growth conditions, and they are maturing themselves and not yet able to divide. Therefore, bacteria death is also not considered.

6. The distance between one of the pairs of transmitter and receiver is denoted as x.

We now consider a single bacterium and we assume the bacterium swims at a constant speed v^{prop} and can change direction instantaneously [54]. We define the time it takes the bacterium arrive at the the destination (Tx in IP stage and Rx in ID stage respectively) as their respective *First Passage Times* (FPT). While M is large, it is reasonable to assume that despite the purposeful movement of bacteria, they are nonetheless i.i.d., and the overall distribution of bacteria is therefore random and uniform throughout the aqueous medium. Thus, consider the bacteria's location in steady-state, which is expressed as $f(x, y, z)$, and the spatial position of the bacteria is uniform over X^3 in 3D environment, given as,

$$f(X) = \frac{1}{X^3}. \tag{6.1}$$

Since the size of the bacteria is assumed to be significantly smaller than transmitter and receiver, for the IP stage, the FPT can be approximated by the probability to

[4] This can be accomplished if the messages are encoded as DNA/RNA barcodes for example, which can achieve sufficiently low error rate [138]

'cover' a point (bacteria) uniformly distributed in the X^3 by the transmitter, which is an exponential distribution with a rate given by [54]:

$$\lambda_{\mathrm{P}} \approx \frac{2\pi R_{\mathrm{t}}^2 Q v}{X^3}. \tag{6.2}$$

Similarly, the FPT rate λ_{D} of ID stage is given as:

$$\lambda_{\mathrm{D}} \approx \frac{2\pi R_{\mathrm{r}}^2 v^{\mathrm{prop}}}{Y^3}, \tag{6.3}$$

where Y is the side length of the cubic area from the transmitter to the receiver with diagonal of x, therefore, $\lambda_{\mathrm{D}} \approx \frac{2\pi R_{\mathrm{r}}^2 v^{\mathrm{prop}}}{\sqrt{\frac{x^2}{3}}^3} = \frac{6\sqrt{3}\pi R_{\mathrm{r}}^2 v^{\mathrm{prop}}}{x^3}$.

Since the IP and ID stages are independent processes, the overall delivery time for a plasmid been successfully picked up and delivered follows a generalized *Erlang* distribution that is presented as a sum of two exponential phases with rate λ_P and λ_D [54], respectively. Therefore, the PDF of overall delivery time can be calculated as the convolution of the PDF of the aforementioned FPTs:

$$\begin{aligned} f_{\mathrm{T}}(t) &= \int_0^\infty f_{\mathrm{P}}(u) f_{\mathrm{D}}(t-u)\mathrm{d}u \\ &= \frac{\lambda_{\mathrm{P}}\lambda_{\mathrm{D}}}{\lambda_{\mathrm{P}} - \lambda_{\mathrm{D}}} \left(e^{-\lambda_{\mathrm{D}} t} - e^{-\lambda_{\mathrm{P}} t} \right), \end{aligned} \tag{6.4}$$

where $f_{\mathrm{P}}(u)$ and $f_{\mathrm{D}}(u)$ are the exponential distribution with rate in Eq. 6.2 and Eq. 6.3 respectively.

We assume each transmitter produce one plasmid. Therefore, the number I_N of plasmid being picked up by bacteria during a finite time period T_p is given as,

$$\begin{aligned} I_N &= \int_0^{T_p} M f_{\mathrm{P}}(t)\mathrm{d}t \\ &= M\left[1 - \exp(-\lambda_{\mathrm{P}} T_p)\right] \end{aligned} \tag{6.5}$$

The number N_N of plasmid been successfully picked and delivered in T_p is given as,

$$\begin{aligned} N_N &= \int_0^{T_p} M f_{\mathrm{T}}(t)\mathrm{d}t \\ &= M\frac{\lambda_{\mathrm{P}}\left(-e^{-\lambda_{\mathrm{D}}T_p}\right)+\lambda_{\mathrm{D}}\left(e^{-\lambda_{\mathrm{P}}T_p}-1\right)+\lambda_{\mathrm{P}}}{\lambda_{\mathrm{P}}-\lambda_{\mathrm{D}}}. \end{aligned} \tag{6.6}$$

6.3.2 Attractant Gradient

The process of *chemotaxis* requires the existence of attractant gradient. We model both the transmission attractant (TA) and reception attractant (RA) of different receivers as a continuously released process with the same diffusion coefficient D_{A} at the same rate of N_{A} [mol/s]. Thus, the process of the releasing attractants can be considered as a step function. According to Fick's second law of diffusion, the impulse response of a diffusion channel $\phi(x,y,z,t)$ at a location of (x,y,z) from the source in 3D medium is given as [139],

$$\phi(x,y,z) = \frac{2\exp\left[-\frac{(x^2+y^2+z^2)}{4D_{\mathrm{A}}t}\right]}{(4\pi D_{\mathrm{A}}t)^{3/2}} = \frac{2\exp\left[-\frac{L^2}{4D_{\mathrm{A}}t}\right]}{(4\pi D_{\mathrm{A}}t)^{3/2}}, \tag{6.7}$$

where L is the distance away from the attractant origin. Thus, the step response $S(L,t)$, which represents the concentration of the attractants at distance L over time t is given as [139],

$$S(L,t) = \frac{N_{\mathrm{A}}}{2\pi D_{\mathrm{A}}L}\mathrm{erfc}\left(\frac{L}{2\sqrt{D_{\mathrm{A}}t}}\right). \tag{6.8}$$

Therefore, the concentration gradient at distance L can be found via the derivative of distance, given as,

$$\frac{\partial}{\partial L}\left(\frac{N_{\mathrm{A}}}{2\pi D_{\mathrm{A}} L}\mathrm{erfc}\left(\frac{L}{2\sqrt{D_{\mathrm{A}} t}}\right)\right) = \frac{N_{\mathrm{A}}\left(-\sqrt{\pi}\mathrm{erfc}\left(\frac{L}{2\sqrt{D_{\mathrm{A}} t}}\right) - \frac{L e^{-\frac{L^2}{4D_{\mathrm{A}} t}}}{\sqrt{D_{\mathrm{A}} t}}\right)}{2\pi^{3/2} D_{\mathrm{A}} L^2}. \tag{6.9}$$

6.3.3 Energy Efficiency

In the molecular communication via bacteria system, the energy is spent for the production of messenger molecules (*plasmid*), their release to the bacteria, propagation to the target and extraction cost for the receiver. Previously, the 5 energy consuming communication steps were introduced as: *Encoding, Encapsulation, Propagation, Decapsulation* and *Decoding*.

Encoding: In order for the DPU to produce such plasmid, every single plasmid has a fixed energy cost of 202.88 zJ [5] [53]. The energy cost of encoding and synthesising of a single *plasmid* is defined as $E_{\mathrm{P}} = 202.88$ zJ, and producing M plasmids needs $M \times E_{\mathrm{P}}$ zJ.

Encapsulation: The energy cost of passing a plasmid to the single bacterium carrier is 2 units of ATP [6], which in turn equals 2×83 zJ [137, 20]. The energy cost of passing one *plasmid* to one bacterium via the is defined as $E_{\mathrm{B}} = 166$ zJ, and I_N number of plasmids are picked up according to Eq. 6.5, which requires $I_N \times E_{\mathrm{B}}$ zJ energy.

Propagation: We consider the energy cost for the bacterial motility as EC_{M}, which is defined as the sum of energy cost of propulsion EC_{s} and tumbling EC_{t}. [140] proposed the expression of EC_{M}, given as,

$$EC_{\mathrm{M}} = EC_{\mathrm{s}} + EC_{\mathrm{t}} \approx \frac{k_B T_a D_m}{{r_b}^2} + 3{r_b}^3, \tag{6.10}$$

[5] The zeptojoule (zJ) is equal to one sextillionth (10^{-21}) of one joule.

[6] Adenosine triphosphate (ATP) is a small molecule used in cells as a coenzyme for energy transfer.

where k_B is the Boltzmann's constant, T_a is absolute temperature, D_m is translation molecular diffusion coefficient of bacteria and r_b is the radius of the bacteria. The constant 3 is in the centimeter-gram-second unit system. By assuming the radius r_b of E.coli. in our model is 1 μm and $D_m = 5.19 \times 10^{-6}\text{cm}^2/\text{s}$ at 25°C [141]. Therefore, EC_{M} is calculated to be $EC_{\text{M}} \approx 2165.4$ [zJ/s] and the total energy cost for the bacterial motility during time T_p is $EC_{\text{M}} \times T_p$ [zJ].

Decapsulation and Decoding: Reverse of the *encapsulation* process and as such the energy cost is defined as $E_{\text{D}} = E_{\text{B}}$. Finally, after the Rx collect the plasmid, the DPU needs to extract the information from the plasmid and decode the information. The extraction and decoding cost from plasmid is defined as E_{E} which consumes roughly 10 ATP of energy [43, 20] which gives $E_{\text{E}} = 830$zJ. Thus, the energy cost of decapsulation and decoding is based on the number of delivered plasmids N_N in Eq. 6.6 given as $N_N \times (E_{\text{D}} + E_{\text{E}})$.

Total Energy: Therefore, the total energy cost E_{Total} for the communication process is given as,

$$E_{\text{Total}} = M \times E_{\text{P}} + I_N \times E_{\text{B}} + Q \times EC_{\text{M}} \times T_p + N_N \times (E_{\text{D}} + E_{\text{E}}). \tag{6.11}$$

Each plasmid is regraded as an information packet containing 60 bits [142], thus the energy efficiency ρ is defined as the total energy usage per delivered information bits, given as,

$$\rho = \frac{E_{\text{Total}}}{60 \times N_N}. \tag{6.12}$$

6.4 Energy Model for Diffusion Based MC

In order to compare the energy efficiency of molecular communication via bacteria with molecular communication via diffusion (MCvD), the energy model of MCvD should be firstly obtained. The communication system of MCvD is considered as the same except the transmitter of the MCvD is a point source of a size equal to

zero. The information molecules are assembled into vesicle [43] (instead of bacteria) and the vesicle diffuse to the receiver. In MCvD, the first passage probability $\phi(t)$ to a spherical absorber is given as [41, 121],

$$\phi(t) = \frac{R_{\mathrm{r}}}{x}\frac{x - R_{\mathrm{r}}}{\sqrt{4\pi D_v t^3}}\exp\left[-\frac{(x - R_{\mathrm{r}})^2}{4D_v t}\right], \tag{6.13}$$

where D_v is the diffusion coefficient of the vesicle in the specific environment.

The vesicles is considered to suffer from the molecular degradation [143, 144] which is modelled as an exponential distribution $\exp(-\lambda t)$, where: $\lambda = \frac{\ln(2)}{\Lambda_{1/2}}$ and λ is the rate of degradation and $\Lambda_{1/2}$ is the corresponding half-life of the vesicle molecule. Therefore, the average number R_N of information molecules can be received of MCvD is given as,

$$\begin{aligned} R_N &= \int_0^{T_p} M\phi(t)\exp(-\lambda t)\mathrm{d}t \\ &= \frac{MR_{\mathrm{r}}}{x}\exp\left[-\sqrt{\frac{\lambda}{D_v}}(x - R_{\mathrm{r}})\right] \\ &- \frac{MR_{\mathrm{r}}}{2x}\exp\left[-\sqrt{\frac{\lambda}{D_v}}(x - R_{\mathrm{r}})\right] \\ &\times \left\{\mathrm{erf}\left(\frac{x - R_{\mathrm{r}}}{\sqrt{4D_v T_p}} - \sqrt{\lambda T_p}\right) + \exp\left(2\sqrt{\frac{\lambda}{D_v}}(x - R_{\mathrm{r}})\right)\right. \\ &\times \left.\left[\mathrm{erf}\left(\frac{x - R_{\mathrm{r}}}{\sqrt{4D_v T_p}} + \sqrt{\lambda T_p}\right) - 1\right] + 1\right\}. \end{aligned} \tag{6.14}$$

The energy cost of MCvD is similar to the molecular communication via bacteria, but the mobility energy cost for vesicles is 0 as the vesicle is freely diffusing in the environment which will not cost any energy for the propagation. We assume the vesicle contains the same length of bits information for the purpose of comparison. Thus, the energy efficiency expression of MCvD is given as,

$$\rho = \frac{E_{\text{Total}}}{60 \times R_N} = \frac{M \times (E_{\text{P}} + E_{\text{B}}) + R_N \times (E_{\text{D}} + E_{\text{E}})}{60 \times R_N}. \tag{6.15}$$

6.5 Numerical Analysis

6.5.1 Determination of Communication Range Based on the Attractant Gradient

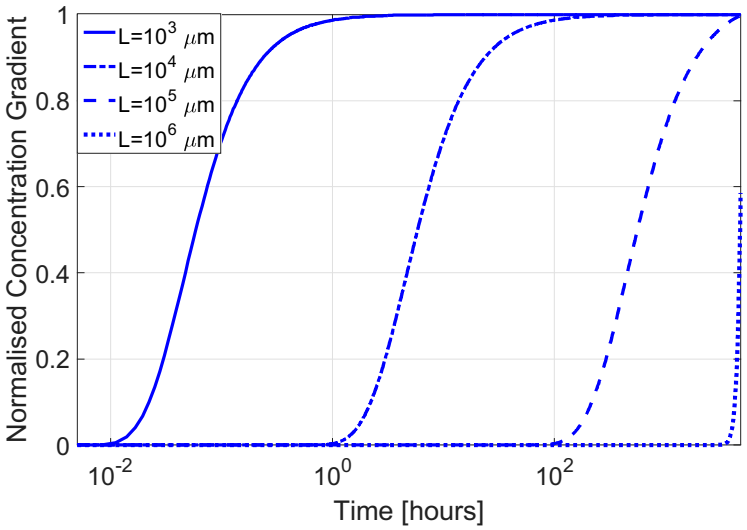

Figure 6.2: Normalized concentration gradient as a function of time, where $D_{\text{A}} = 1000\mu\text{m}^2/\text{s}$, and $N_{\text{A}} = 10^{-11}\text{mol/s}$.

We first discuss the communication range for the molecular communication via bacteria. According to Eq. 6.9, we show the normalized attractant gradient as a function of time in Fig. 6.2. It can be observed that the bacteria need to wait 0.01, 1, 100 and approximately 3000 hours for the existence of attractant gradient at a distance of 10^3, 10^4, 10^5, and 10^6 μm respectively. We consider the bacterial communication happened during the bacterial *lag-phase*, which can be maintained

up to 48 hours [145, 146] without considering bacterial division and death. Thus, the maximum range of the communication model is in the order of 10^4 μm and the total time is considered up to 10 hours for the rest of the simulation.

6.5.2 First Passage Probability

Table 6.1 shows the symbols used in the model and their values from references, which considered the same aqueous environment in the numerical analysis.

Table 6.1: Symbols and Common Values

Parameter	Definition	Values
X	Side of cubic area	$10^4\mu$m
R_{t}	Tx radius	10μm [43]
R_{r}	Rx radius	50μm [47, 54]
x	Distance between Tx and Rx	up to $10^4\mu$m
Q	No. of bacteria	up to 500 [147]
r_b	Bacterial radius	1μm [140]
v^{prop}	Bacteria speed	20μm/s [147]
D_{m}	Bacterial translation diffusivity	$5.19 \times 10^{-10}\mathrm{m}^2/\mathrm{s}$ [140]
M	No. of Tx-Rx pair	up to 1000
N_{A}	Attractant releasing rate	10^{-11} mol/s [47]
D_{A}	Attractant diffusion coeffcient	$10^{-9}\mathrm{m}^2/\mathrm{s}$ [47]

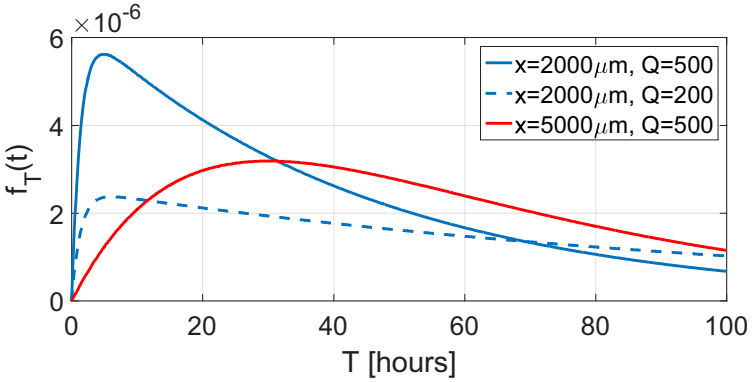

Figure 6.3: The probability density function of successfully deliver a plasmid to the receiver where $X = 5000\mu m$

We then analysed first passage probability $f_T(t)$ in Fig. 6.3. It can be seen that: for a fixed distance between transmitter and receiver, the higher number Q of deployed bacteria, the higher peak value of $f_T(t)$. On the other hand, if the Q is fixed, when the distance x increases, the peak value of $f_T(t)$ will decrease and the time to reach the peak value will shift to right which makes the peak $f_T(t)$ point longer to reach. In summary, increasing the number of bacteria and decreasing the communication distance greatly affect the probability of successful delivery.

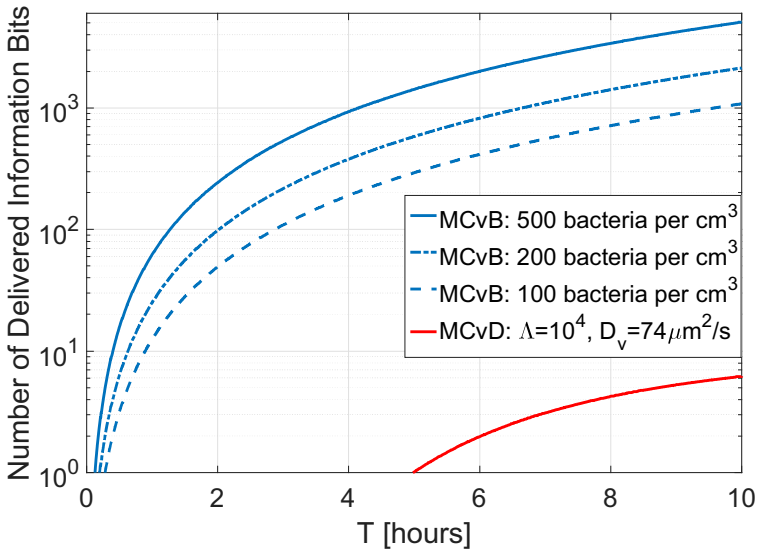

Figure 6.4: The plot of the number of information bits been successfully delivered as function of time period T_p where $x = 2000\mu m, M = 1000, X = 10^4\mu m$.

We now consider the number of information bits being successfully delivered within a specific time period T_p and compare the performance with molecular communication via diffusion. In Fig. 6.4, the blue lines compare the difference between 500, 200, and 100 bacteria relays deployed in the environment. With fixed side length X, changing the number of bacteria varies the density of the bacteria in the environment ($\frac{Q}{X^3}$ in Eq. 6.2). We can observe that with a the higher bacterial density, the higher number of information bits can be delivered in the same time

period (e.g. at a fixed T_p). Moreover, higher bacterial density can also advance the time for the first information bit delivered. Compared with the MCvD in Eq. 6.14, we can see the MCvD needs significantly longer time to deliver the first bit and the total number of information bits delivered is also orders of magnitude less.

6.5.3 Energy Efficiency

Effect of Time

We now discuss the energy efficiency (EE) as a function of time for both MCvB and MCvD. In Fig. 6.5, we can see the EE of MCvB dramatically decreases at the beginning and then continuously decrease slightly after 1 hour. While changing the number of bacteria deployed in the environment, the EE has little difference. With comparison to the MCvD (red line), the energy efficiency is orders of magnitudes higher than MCvB before $T_p \approx 2.5$ hours, after then, the EE of MCvD continuously decreases below EE of MCvB. As EE is defined as [zJ/s], which means the energy consumption for each information bit successfully delivered, we hope the EE is the smaller the better. Thus, based on Fig. 6.5, it can be summarized that MCvB is suitable for *delay-sensitive* molecular communication.

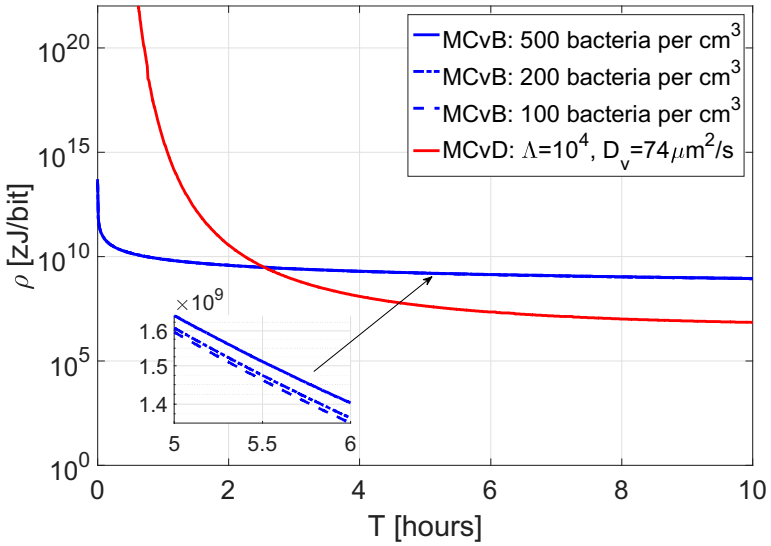

Figure 6.5: The comparison of the energy efficiency between molecular communication via bacteria and diffusion over time period T_p where x is fixed at $x = 5000\mu$m, $X = 10^4 \mu m$

Effect of Distance

In Fig. 6.6, the EE is compared over distance. We can observe that, the EE of both MCvB and MCvD will increase over distance. But the increasing rate of MCvD is higher than the rate of MCvB, which indicates that EE of MCvD is more sensitive than EE of MCvB on distance. Again, the lower of the bacterial density will reduce the EE, but the overall difference is little. Furthermore, in Fig. 6.6(a), the EE of MCvB is lower than MCvD after $x \approx 3200\mu$m at T_p=1 hour. Afterwards, the EE of MCvB will be always higher than MCvD. In Fig. 6.6 (b), (c), it can be observed that the difference between EE of MCvB (blue lines) and MCvD (red line) is decreasing over distance. Therefore, it can be concludes that MCvB is further suitable for *long-distance* molecular communication.

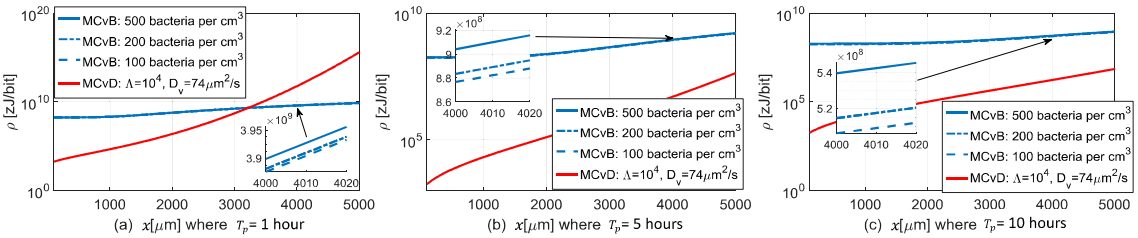

Figure 6.6: The comparison of the energy efficiency between molecular communication via bacteria and diffusion over distance x where $D_v = 74\mu\text{m}^2/\text{s}$, $\Lambda_{1/2} = 10^4\text{s}$, $M = 1000$, $X = 10^4\mu m$.

Effect of Bacterial Density

Finally, we show the effect of bacterial density in Fig. 6.7. The results are straight forward that the bacterial density has little effects on the EE, where the black lines tends to be flat, which conforms the findings in Fig. 6.5 and Fig. 6.6 on bacterial density. With the conclusion of the bacterial density on EE, we concludes that increasing the bacterial density is able to increase the probability of successfully delivering plasmid and the total number of information bits. However, the higher bacterial density does not result a better EE. This fact is of special importance in practical applications, where the population of bacteria deployed cannot be infinitely increased for better EE and without harmful effects on bio-organisms.

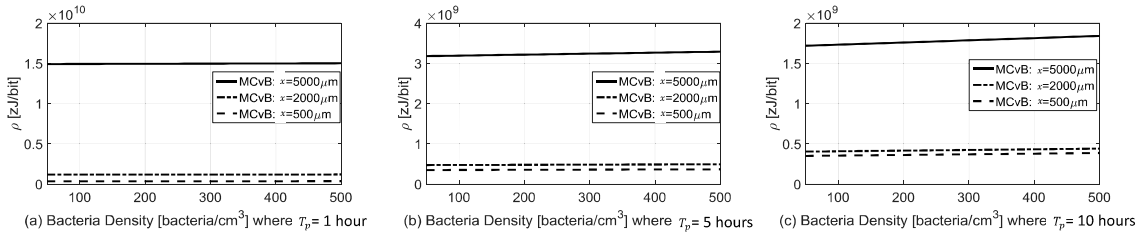

Figure 6.7: The plot of energy efficiency as a function of bacterial density $\frac{Q}{X^3}$ where x is fixed at $2000\mu m$.

6.6 Summary

In this chapter, a communication model of molecular communication via bacteria (MCvB) was introduced and an energy efficiency model for cross-comparison between different communication systems was proposed. In particular, the energy efficient performance for both MCvB and molecular communications via diffusion (MCvD) was compared. It showed that MCvB had better first passage time profile and larger total number of information bits being delivered than MCvD. The energy efficiency of MCvB was superior for long distance or delay-sensitive communications (i.e., bacteria swimmers were more efficient than free diffusion), but inferior over short distances and delay-tolerant communications.

Chapter 7

Underwater Molecular Signalling

This chapter focuses on underwater molecular signalling for a potential application of MC. Firstly in Section 7.1, the motivation of researching on underwater molecular signaling will be presented as well as an overview of conventional underwater signalling methodologies. Afterwards, in Section 7.2, a underwater molecular signalling propagation model will be introduced and examined. Then it will propose two molecular schemes for underwater signalling in Section 7.3, namely, chemical information carrier (CIC) and chemical gradient localization (CGL). Particularly, the communication system for CIC and the computation algorithm for CGL will be proposed. Finally, Section 7.4 will analyse the performance of both schemes and compare it with conventional underwater signalling schemes including acoustic and underwater optical wireless systems.

7.1 Motivation

Terrestrial long-range wireless communication systems have operated successfully on land, offering a variety of broadcast and multi-cast services. Reliable wireless

communication systems usually have knowledge of (i) the distance or location area of the receiver, and (ii) the channel for successful radio planning. However, challenges remain in scenarios where the transmitters and receivers have no knowledge of each others' location areas, and little knowledge is available about the propagation channel. This is especially the case in search and rescue services (e.g. for locating an underwater crashed object such as a submarine or an aircraft. The location area of the object is unknown and the search radius can be up to 1000km, as is the case for theAF447 (2009) and the MH370 (2014) air crashes). Such a localization problem has two distinctive characteristics: (i) a hidden transmitter (the crashed object), and (ii) absence of receivers in the vicinity of the transmitter. Such problem is defined as the hidden transmitter and absent receiver (HTAR) problem. The transmitter blindly broadcasts a distress signal, in the hope that receivers can detect it. Knowledge of either where the transmitter is, or presence of the receiver in the vicinity of the transmitter within a set time frame would solve the localization problem. The time frame constraint arises from the finite energy of the transmitter.

7.1.1 Overview of Underwater Systems

In underwater environments, current conventional *black box* and other underwater communications utilize acoustic waves to transmit information in the form of 10ms sharp pulses on a 37.5 kHz carrier frequency. A typical battery supply can last up to 30 days with proposals for 90 days for future systems. The current receiver technologies (180dB and 1μPa) can reliably detect the signal at a range of 5km (normal conditions) and 7km (good conditions) [148]. The fundamental problem with all wave-based communications is that once the signal pulse is transmitted, the pulse's energy decays with propagation distance over time. There is both a finite distance (approx. 10 to 30km) and time (approx. a few seconds after the last transmission), beyond which the receiver cannot reliably receive the signal. Therefore, the absence of receivers in the reception zone during the short transmission time period will lead

to the loss of transmitters' location. In order to solve this time-constrained HTAR problem, the transmitter must send messages that can persist for a long period and over long distances.

7.1.2 Overview of Related Work

On the other hand, another localization method is inspired by animals and insects using olfaction to trace the location of the odour source for foraging or reproductive activities. The problem of finding the source of the odour plumes is known as Chemical Plume Tracing (CPT). Odour plumes are created when odour molecules are released from their source and taken away by a combination of diffusion and random turbulent flow caused by temperature gradients. This combined process can be modeled on a macroscopic scale as diffusion with empirical diffusivity parameters that reflect the random turbulent flow [149, 150]. The basic approach for CPT is to calculate a concentration gradient with subsequent plume tracing based on gradient ascent. However, gradient-based algorithms are only feasible in environments where flow can be approximated by diffusion (low Reynolds numbers), resulting in a chemical concentration field that is reasonably well defined by a continuous function with a peak near the source [151, 152]. Existing researches on localization based on chemical gradients have largely considered a homogeneous diffusion environment where the diffusivity D is a constant and the search space is a plane [153, 154]. This assumption is valid for small volumes of search space or on a single plane (constant depth). However, the diffusivity will vary significantly in a vast ocean [149], creating potential **zones of zero gradient**.

7.2 System Model

7.2.1 Underwater Diffusion Channel

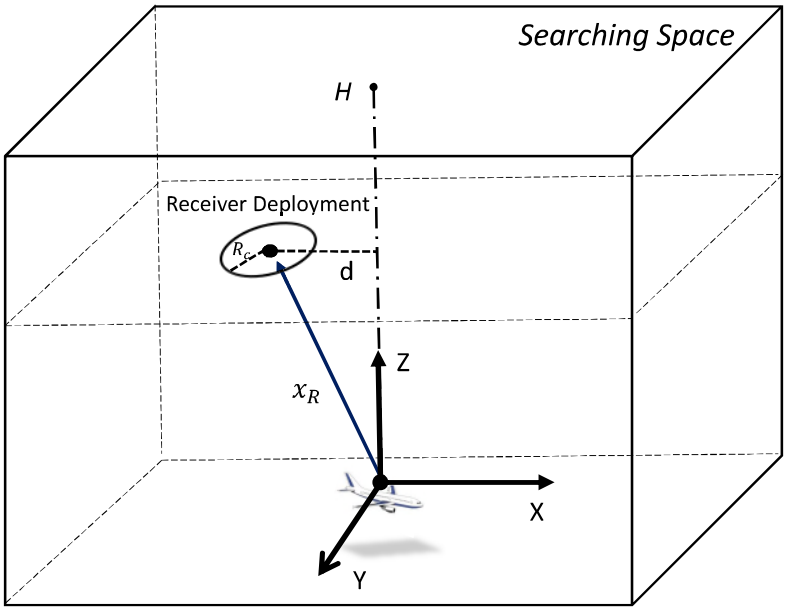

Figure 7.1: Illustration of underwater diffusion model.

In this section, the underwater diffusion channel and the receiver sensitivity definition are presented. Consider underwater diffusion in the context of oceans for the HTAR problem, e.g., an aircraft or a submarine has crashed into the ocean and sunk to a certain depth. The underwater diffusion propagation model is shown in Fig.7.1. It is assumed that the molecules used are of the same density as water and the vertical forces exerted to the molecules are entirely related to diffusion and ocean currents. The propagation process of molecules released at the origin can be modeled by solving Fick's laws of diffusion. In oceans, the rate of diffusion is not isotropic. If the molecules are released at the time instant $t = 0$, the impulse response (hitting

probability density function) ϕ at a given point (x, y, z) of a hemisphere is:

$$\phi\left(x, y, z, t\right) = \frac{2\exp\left(-\frac{x^2}{4D_x t} - \frac{y^2}{4D_y t} - \frac{z^2}{4D_z t}\right)}{\left(4\pi t\right)^{3/2}\sqrt{D_x D_y D_z}}, \tag{7.1}$$

where D_x, D_y and D_z are the diffusion coefficients of x, y, z directions respectively. Since the diffusivity is **non-isotropic** in oceans, the specific ocean diffusion coefficient values found in [149] is considered. For a depth of 3-5km, the diffusion coefficient is constant for the horizontal and vertical directions, i.e., $D_x = D_y$ and D_z are approximately constants.

Assume the crashed object has a transmitter that releases molecules continuously for a time period T at a constant magnitude M and consider the input molecular signal $x(t)$ can be modelled as a rectangular pulse with magnitude M and pulse width T given as: $x(t) = M[u(t) - u(t-T)]$, where $u(t)$ is the Heaviside function. The channel output $p(t)$ without noise can be calculated as the convolution of the input signal $x(t)$ and the channel response in Eq.7.1. Therefore, in order to find out the $p(t)$, firstly, consider the Laplace transform of the channel impulse response $\phi(x_{\mathrm{R}}, D, t)$ is,

$$\mathcal{L}_t\left[\frac{2}{\left(4\pi D t\right)^{3/2}}\exp\left(-\frac{{x_{\mathrm{R}}}^2}{4Dt}\right)\right] = \frac{e^{-x_{\mathrm{R}}\sqrt{\frac{s}{D}}}}{2\pi D x_{\mathrm{R}}}, \tag{7.2}$$

where D is the equivalent diffusion coefficient given as $D = \left(D_x D_y D_z\right)^{\frac{1}{3}}$, parameter x_{R} is the equivalent molecular propagation distance given as $x_{\mathrm{R}} = \frac{1}{D}(D_x D_y z^2 + D_x D_z y^2 + D_y D_z x^2)^{1/2}$ and erfc () is the complementary error function.

Therefore, a step response with delay τ is an inverse Laplace transform of $\exp(-\tau s)/s \times$ Eq. 7.2:

$$S\left(x_{\mathrm{R}}, t, \tau\right) = \frac{M}{2\pi D x_{\mathrm{R}}}\mathrm{erfc}\left(\frac{x_{\mathrm{R}}}{2\sqrt{D(t-\tau)}}\right). \tag{7.3}$$

Thus, $p(t)$ can be calculated as,

$$\begin{aligned} p\left(x_{\mathrm{R}}, t, \tau\right) &= x(t) * \phi(x, y, z, t) \\ &= \frac{M}{2\pi D x_{\mathrm{R}}}\left[\operatorname{erfc}\left(\frac{x_{\mathrm{R}}}{2\sqrt{Dt}}\right) - \operatorname{erfc}\left(\frac{x_{\mathrm{R}}}{2\sqrt{D(t-T)}}\right)\right], \end{aligned} \tag{7.4}$$

7.2.2 Detection and Noise

The information particles released in the environment should be sensing its chemical concentrations, thus the receiver's concentration sensitivity is necessary to be considered. The receiver sensitivity is determined by the Limit of Detection (LOD) value, which is defined as the quantity of compound that gives a signal intensity that is a factor of 3 greater than the standard deviation of the background signal [155]. The unit of LOD is *parts-per notion* which is a set of pseudo units to describe small values of miscellaneous dimensionless quantities. For a given receiver sensitivity (LOD), LOD is set as the threshold. Thus the *Arrival Time for Detection* is defined as the total time which the molecule needs to diffuse in the environment until the molecule concentration reaches above the threshold.

In terms of noise, existing communication research has focused on counting noise effects [61], which is Gaussian distributed. However, when considering molecule motion in an ocean, it is more interested in the LOD and the background chemical noise. It has been shown that the background chemical noise is Gaussian distributed [156] with a standard deviation of $\sigma = \frac{\mathrm{LOD}}{3}$ in sea water environment, giving rise to a noise model $\sim \mathcal{N}\left(0, (\frac{\mathrm{LOD}}{3})^2\right)$. By transferring the units in parts-per notation [ppq] to concentration [molecules/m^3]

$$\mathrm{SNR} = \frac{P_{\mathrm{signal}}}{P_{\mathrm{noise}}} = \frac{|p(t)|^2}{\sigma^2} = \frac{9|p(t)|^2}{\mathrm{LOD}^2}, \tag{7.5}$$

where P_{signal} and P_{noise} are the power of signal and noise respectively.

7.3 Underwater Molecular Signalling Schemes

7.3.1 Chemical Information Carriers (CIC)

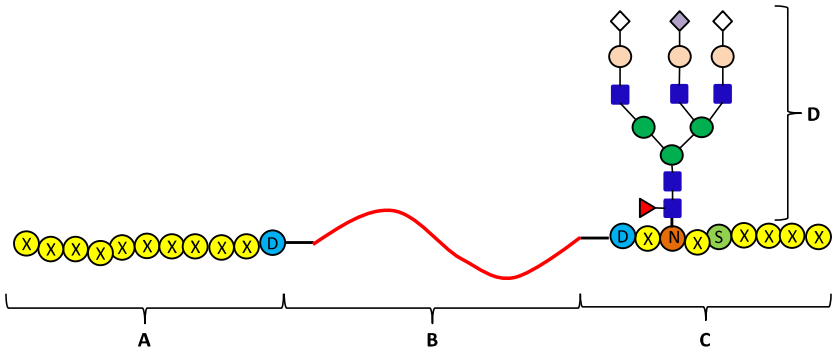

Figure 7.2: An example of a possible chemical message, comprised of peptides, non-biological molecules, and a N-linked glycan.

As reviewed in Chapter 2, the possible information particles can be used includes *small molecules, peptides or amino acids, DNA,* and *carbohydrate.* It may be useful to use a combination of biological and non-biological molecules to assemble a chemical message. Although biological molecules hold greater potential for complexity, it is usually faster and more reliable to synthesise non-biological polymers. Modern biochemical engineering can use a range of techniques for modifying biomolecules with a range of chemical groups (such as with dehydroalanine [157]) which can be bonded with any number of non-biological molecules. Therefore each system can have its own unique peptide sequence, ending in a functionalised dehydroalanine, which can be assembled with 3 different polymers in sequence each giving a different dimension of the coordinates. A second peptide containing a glycosylation site could then be added with a customised carbohydrate using different glucosyl transferases and hydrolases to create a personalised message. In Fig. 7.2, an example of a possible chemical message is illustrated, with the following components:

- A: peptide epitope signature specific to the system that can be easily recognised by a specific antibody. X = any amino acid, D = dehydroalanine, used to connect the peptide to non-biological molecules.
- B: non-biological components of different chemical makeups of specific mass to give accurate location data.
- C: peptide with N-glycosylation recognition motif Asn-X-Ser to allow glycosylation.
- D: A typical mammalian N-linked glycan with each different colour and shaped object representing a different type of monosaccharide. Glycans can vary in size, structure and make up and can be customized using different monosaccharides and enzymes during synthesis, making it a good candidate molecule for personalized messages.

The whole message would then be wrapped in a non-biodegradable polymer by a bubble machine, and propelled into the environment.

Thus, the transmitter and receiver design for CIC are as follows. An envisaged chemical message transmitter would have 3 sections. Section 1 would be connected to the navigational equipment of the vehicle. Section 2 would be the message synthesis system, which would use the information from section 1 to create the chemical message. This section would need to have a numerous of compartments to house the various different possible components of a message, the catalysts for assembling the message, and reaction chambers for the messages to be synthesised. Numerous reaction chambers are probably necessary for speedy synthesis of different components of a message before final assembly. Section 3 would be the message delivery system which would package the message in a shell and propel it out of the vehicle. A micro-bubble machine is envisaged that can produce bubbles which acts to both protect the chemical information carriers and can be detected by a receiver. A receiver would first have to identify and unwrap a message; it would

then reverse the assembling mechanism to dissect the message into its component parts. The peptide identification components may be quickly identified by antibody based techniques. Glycosylated peptide and polymers could both be interpreted using LC-MS. In this scheme, if at least one information carrier is captured by the receiver, the communication process is successful and the location of the transmitter can be discovered.

7.3.2 Chemical Gradient Localization (CGL)

Inspired by animal's method of locating objects (e.g., prey) using smell,a search-and-rescue robot (i.e., receiver) is proposed that homes in on the chemical emitted by a crashed object (i.e, transmitter). Existing localization methods using chemical concentration gradients have largely considered a homogeneous diffusion environment where the diffusion coefficient D is a constant in all directions. This assumption is valid for small volumes of search space or on a single plane but not for a vast ocean where the diffusivity in different directions will vary significantly [149] creating potential zones of **near zero gradient**. For example, in Fig. 7.3, an emitter located at $[0, 0, 0]$ emits a rectangular pulse with magnitude M of chemicals and after a certain time the diffusion varies at various depths and distances. The rate of diffusion on a plane is much faster than across planes [149], and hence the robot may find a viable gradient at a deeper depth (smaller z value) but not enough gradient at lower regions. Thus, in this section, a multi-stage gradient algorithm that can recover from zones of zero gradient is proposed to improve over previous under water gradient localization methods.

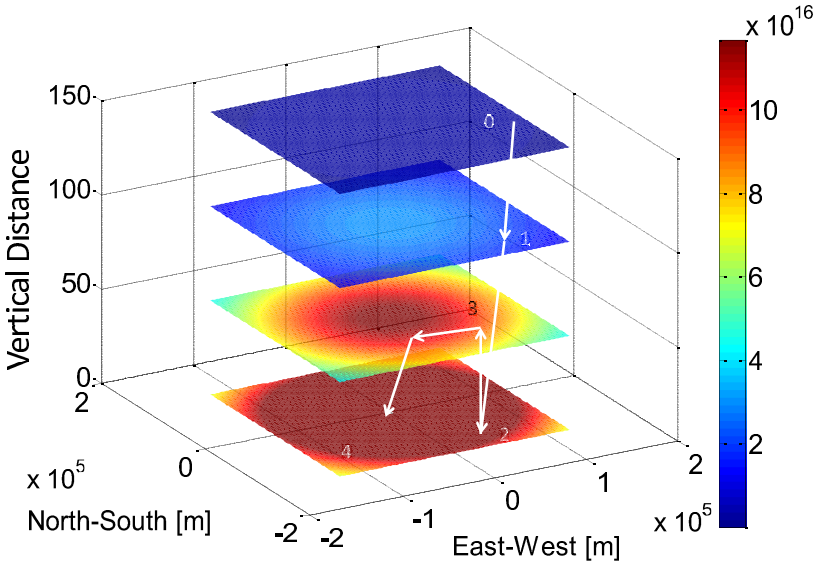

Figure 7.3: Plot of chemical concentration (molecules per m^3) at various distances away from source for $t = 347$days

To operate in a heterogeneous diffusion environment and without an explicit function of the gradient, Rosenbrock gradient based search method [158] as detailed in Algorithm 3 is proposed and described below as a two-stage process. Each stage is a general process that comprises of multiple robot steps.

- **1. blind search stage:** In this initialization stage, it is necessary to find a feasible searching area where there is sufficient chemical gradient to initiate the correct start direction. The robot begins at position $\boldsymbol{P}_0$.

- **2. repetitive search stage:** the robot searches in the sea according to the Rosenbrock method. The robot waits a certain time period (stays stationary) before it re-calculates a new search direction vector. If the new search vector is in agreement with previous vector, the robot increases the waiting period by α-fold. If not, it increases the waiting period by β-fold. The starting waiting period is given by $\boldsymbol{e}$. Each step will remember the location of previous

calculation $\boldsymbol{P}_s$ and update it with the new location $\boldsymbol{P}_e$. Once the Rosenbrock searching process stops: 1) it stops in the vicinity of the transmitter and the robot surfaces to report its location and the whole searching process terminates successfully; or 2) it is still far away but can not find a gradient to action upon. In this case, the robot stops and it is set to a new start point $(x_n, y_n, z_n + h)$ and start another Rosenbrock searching process with the blind search stage detailed above. This step is repeated until the robot reaches the crashed object.

The reason that using the Rosenbrock algorithm is that, in the considered scenario the location of the transmitter is unknown so that it is not possible to obtain the analytic function of the molecular concentration varying along the locations. Therefore, although the target location problem is formulated as an optimization problem, the analytic objective function cannot be obtained. Other gradient based schemes e.g. the conjugate gradient algorithm and the Newton algorithm which are all premised on the analytic gradient function, cannot be applied in our scenario. Therefore, the numerical search scheme to obtain the optimum point on the objective function has to be used. Rosenbrock algorithm is specially designed for such a realistic problem. For example, in the numerical simulation (see Section 7.4), the robot will obtain various molecular concentration values from the hidden objective function during both blind search step and repeat search step. Based on the receipted concentration values, the proposed Rosenbrock search algorithm can construct their approximate gradient so that to trace the hidden object.

Algorithm 3 Rosenbrock gradient search algorithm.

function SEARCHINGTRANSMITTER($\boldsymbol{P}_0$)

Initialise $\alpha \leftarrow 2$; $\beta \leftarrow -0.5$; $\boldsymbol{e} \leftarrow \mathbf{1}$;

$\boldsymbol{\xi}_1 \leftarrow \begin{bmatrix} 1 \\ 0 \\ 0 \end{bmatrix}$; $\boldsymbol{\xi}_2 \leftarrow \begin{bmatrix} 0 \\ 1 \\ 0 \end{bmatrix}$; $\boldsymbol{\xi}_3 \leftarrow \begin{bmatrix} 0 \\ 0 \\ 1 \end{bmatrix}$;

Blind Search $\boldsymbol{\xi}_s \leftarrow$ INITIALDIRECTION($\boldsymbol{P}_0$);

$\boldsymbol{P}_s \leftarrow \boldsymbol{P}_0$;

repeat ▷ Start searching

$\boldsymbol{P}_e \leftarrow$ ROSENBROCKSEARCHING($\boldsymbol{P}_s$, α, β, $\boldsymbol{e}$, $\boldsymbol{\xi}_s$);

$\boldsymbol{P}_s \leftarrow \boldsymbol{P}_e + \begin{bmatrix} 0 & 0 & h \end{bmatrix}$;

$\boldsymbol{\xi}_s \leftarrow \begin{bmatrix} \boldsymbol{\xi}_1 & \boldsymbol{\xi}_2 & -\boldsymbol{\xi}_3 \end{bmatrix}$;

until Receiver robot stops in vicinity of the transmitter, i.e., $\boldsymbol{P}_e \in \mathcal{P}$

return $\boldsymbol{P}_e$;

end function

Fig. 7.3 shows an example of the robot movement path in finding the transmitter. Each numbered point represents the algorithm re-calculating a new movement vector. At point 0, the algorithm performs blind search to find the correct initial vector and travels along it for a period of $\boldsymbol{e}$. Then it reaches point 1, whereby the algorithm has verified that the new direction agrees with the previous one and increases the travel duration by a factor of α. Upon reaching point 2, the algorithm discovers that no viable gradient can be found and the algorithm performs a reset. At the reset, it surfaces $h = 50$m upwards to find a gradient (slower rate of diffusion) at point 3, whereby it proceeds to find the crash object at point 4. The reason why the robot moves upwards is because the horizontal planar diffusion is less progressive (likelihood of sharper gradient) at lower depths of the ocean. The *number of search iterations* is defined as the number of distinctive stages it took for the robot to find the transmitter (4 in the case of Fig. 7.3). A *repeat stage* is defined as the robot losing the gradient and repeating the first part of the algorithm to regain the

Table 7.1: The Definition of Parameters with the Simulation Values

Parameters	**Values**
Released Molecule Magnitude (M)	1 [mol/s]
Transmission Period (T)	30 [days]
Sea Depth (H)	5 [km]
Reception Zone Radius (R_{r})	1 [m]
Limit of Detection (LOD)	1 [ppq]
Repeat Stage Surface Distance (h)	50 [m]
Horizontal Distance (x, y)	$0 - 1000$ [km]
Vertical Distance (z)	$0 - 2000$ [m]
Horizontal Diffusivity (D_x, D_y)	250 [m^2/s]
Vertical Diffusivity (D_z)	4.5×10^{-5} [m^2/s]

gradient (1 occurrence in the case of Fig. 7.3). The *total trace distance* is defined as the total distance travelled by the search robot (including any repeat stages).

7.4 Numerical Results

In this section, a number of scenarios for underwater molecular signalling will be considered and examined, as well as comparison for communication performance (e.g., energy attenuation and latency) of acoustic communication (AC) and MC systems by numerical simulations. The parameters used to for the following results can be found in Table.7.1.

7.4.1 Performance Results for CIC and CGL

CIC Performance

In order to present the performance of CIC, the molecular energy is considered as the main metric, which is defined as the total number of molecules received over an infinite time [69]. However, in reality, the receiver can not sample from $t = 0$ to $t = +\infty$. Thus, a finite period energy is defined, which is $E_p = \int_{T_1}^{T_2} p\left(x_{\mathrm{R}}, t, \tau\right) \mathrm{d}t = E_s(x_{\mathrm{R}}, t, \tau = 0) - E_s(x_{\mathrm{R}}, t, \tau = T)$, where T_1 and T_2 are defined as the receiver start searching time and receiver finish searching time, respectively, and E_s is the energy of the step response in Eq. 7.3 over a finite time period, given as,

$$E_s(x_{\mathrm{R}},t,\tau)=\int_{T_1}^{T_2} S\left(x_{\mathrm{R}},t,\tau\right)\mathrm{d}t=\frac{M}{2\pi D x_{\mathrm{R}}}\times$$
$$\left[t'\{\mathrm{erfc}(\frac{x_{\mathrm{R}}}{2\sqrt{Dt'}})-\frac{x_{\mathrm{R}}e^{-\frac{{x_{\mathrm{R}}}^2}{4Dt'}}}{\sqrt{\pi Dt'}}\}-\frac{{x_{\mathrm{R}}}^2\mathrm{erf}(\frac{x_{\mathrm{R}}}{2\sqrt{Dt'}})}{2D}\right]\Bigg|_{T_1}^{T_2},\quad \text{for}:\quad t'=t-\tau, \tag{7.6}$$

In addition, consider that the receivers for CIC are distributed in a circular field of radius R_c at a distance x_R from ocean surface of the crash site. Two kinds of receiver deployment spatial distributions are considered, namely:

1. Normal Random Deployment (NRD)

2. Uniform Random Deployment (URD)

Within the circular receiver region, the random distance between the centre to a receiver i is defined as δ_i, which follows a distribution $f_D(\delta)$:

$$f_{\mathrm{D}}\left(\delta\right)=\begin{cases}\frac{1}{2R_c} & \mathrm{URD}\\ \frac{1}{\sigma\sqrt{2\pi}}e^{-\frac{\delta^2}{2\sigma^2}} & \mathrm{NRD}\end{cases}, \tag{7.7}$$

where σ is the standard deviation of NRD.

It is assumed that there are N_R molecular receivers deployed in the deployment area and the location of each receiver (x_i, y_i, z_i) is specified which follows the distribution of the aforementioned deployment methods. Therefore, the total molecular received energy $E_{p,\mathrm{total}}$ from N_R molecular receivers can be expressed as the sum of individual receivers' energy $E_{p,i}$:

$$E_{p,\mathrm{total}}=\sum_{i=1}^{N_R}E_{p,i}(x_{\mathrm{R}},t)=\frac{N_R}{2\pi R_c}\int_0^{R_c}\int_0^{2\pi}E_{p,i}f_{\mathrm{D}}(\delta)\,\mathrm{d}\theta\delta, \tag{7.8}$$

where θ is the angle that the receiver makes to d.

1. Long Endurance: In Fig.7.4, the received energy over a finite time is demonstrated, for the both AC and CIC system, both transmitting for the same duration

of 1 month and at the same propagation distance of $x_{\mathrm{R}} = 20$km. From the results, it can be seen that the received energy of the AC system is restricted significantly by the transmission period, whereas the CIC chemical messages will persist in the ocean for significantly longer, rising in energy over time (at least up to a few years).

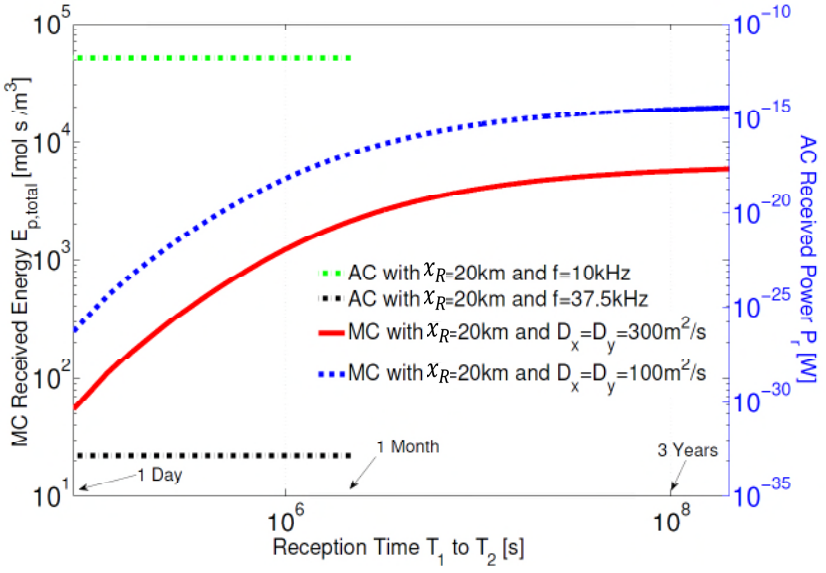

Figure 7.4: The comparison between AC and MC systems at a set receiver location over a finite reception time of 1 day to a few years. Parameters: $R_c = 18$km, $h = 0.5$m, $d = 20$km, $x_{\mathrm{R}} = 20$km, $D_z = 5 \times 10^{-5}\mathrm{m}^2/\mathrm{s}$, $\sigma = R_c/100$, $T_1 = 40000$s (12 hours), and $T_2 = 80000$s (1 day) to 2×10^8s (6 years).

2. Deployment Formation: In Fig.7.5, the effect of the two deployment methods is demonstrated on MC's received energy. The results show that for a medium or longer distance away from the crash site ($d > 30$km), the deployment formation is not important. For smaller distances of a few km, the NRD formation with a small standard deviation of $\sigma < 11$km will perform significantly better than URD formation. However, a high standard deviation of $\sigma > 11$km will perform worse. For example, NRD with a standard deviation of $\sigma < 180$m will yield a 35% increase

in energy received; whilst NRD with a standard deviation of $\sigma = 18$km will yield a 17% decrease in energy received. This is intuitive, as the closer the receivers are to the crash site, the more focused their formation needs to be towards the centre of the search area.

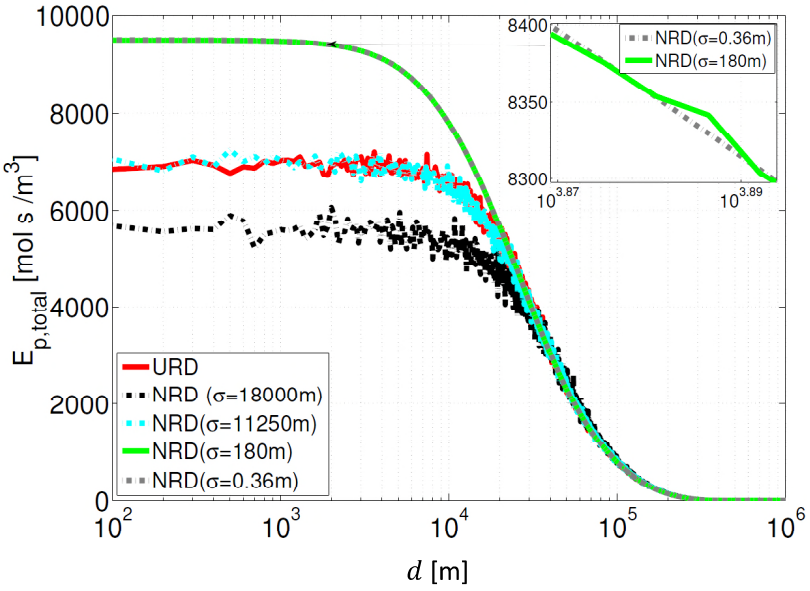

Figure 7.5: The comparison between NRD with different σ and URD over an increased d. Parameters: $R_c = 18$km, $N_R = 100$, $h = 0.5$m, $D_x = D_y = 300\text{m}^2/\text{s}$, $D_z = 5 \times 10^{-5}\text{m}^2/\text{s}$, $T_1 = 40000$s (12 hours) and $T_2 = 10^8$s (3 years).

3. Receiver Deployment Area: In Fig. 7.6(a), the effect of receivers' deployment radius r on energy is demonstrated. The results show the received energy is independent of the deployment distribution when $R_c < 10$km. The parameters used are: $N_R = 100$, $h = 0.5$m, $d = 100$km, $D_x = D_y = 300\text{m}^2/\text{s}$, $D_z = 5 \times 10^{-5}\text{m}^2/\text{s}$, $T_1 = 40000$s, $T_2 = 10^8$s. The results show that for larger deployment radius, NRD with a large variance is preferred, which is intuitive given that this increases the probability that a given receiver is closer the unknown crash site.

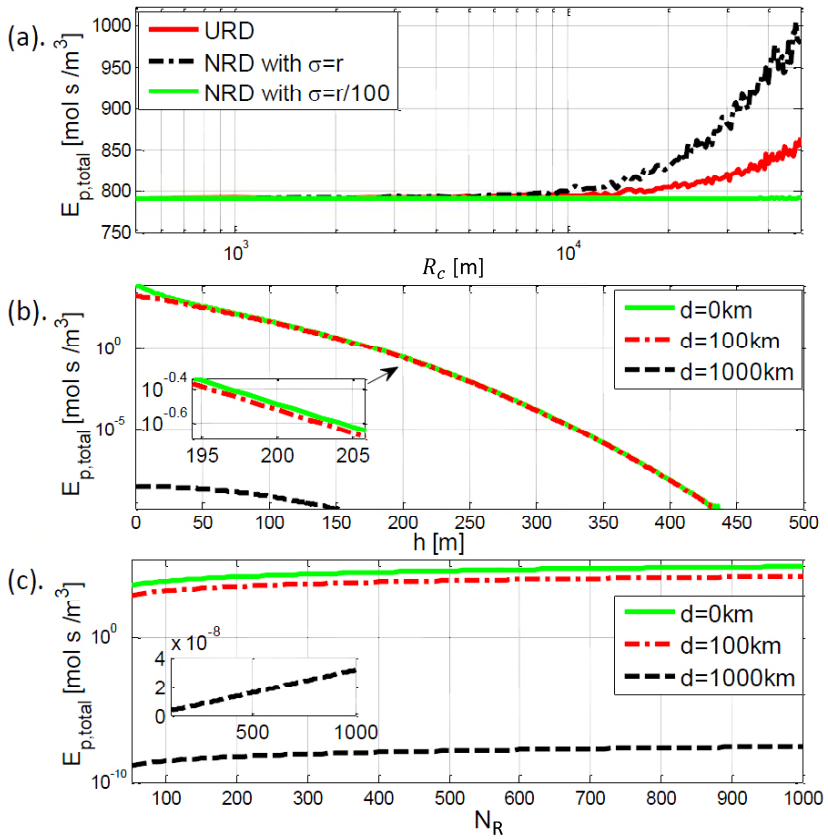

Figure 7.6: Plots of the relationship between energy $E_{p,\text{total}}$ and the parameters R_c, h, N_R respectively.

4. Search Depth: In Fig. 7.6(b), the effect of the searching depth distance h on the received energy in comparison with d is demonstrated. The parameters used are: $R_c = 18\text{km}$, $N_R = 100$, $D_x = D_y = 300\text{m}^2/\text{s}$, $D_z = 5 \times 10^{-5}\text{m}^2/\text{s}$, $T_1 = 40000\text{s}$, $T_2 = 10^8\text{s}$ and deployment formation: NRD with $\sigma = R_c/100$. The results show that the receiving energy is very sensitive to h, whereby increasing every 100m can reduce $E_{p,\text{total}}$ by several orders of magnitude. Therefore, a rationale conclusion is that h must be small which means the molecular receivers must be deployed as deep as possible.

5. Effect of Number of Deployed Receivers: In Fig. 7.6(c), the effect of the number N_R of receivers on the received energy is demonstrated. The parameters

used are: $h = 0.5$m, $R_c = 18$km, $D_x = D_y = 300\text{m}^2/\text{s}$, $D_z = 5 \times 10^{-5}\text{m}^2/\text{s}$, $T_1 = 40000$s, $T_2 = 10^8$s and deployment formation: NRD with $\sigma = R_c/100$. It is clear that received energy has a linear growth with N_R from the results and from Eq. 7.8.

CGL Performance

CGL performance is evaluated in three areas: (i) the effect that the transmission duration has on the concentration gradient, (ii) the amount of ambient chemical noise in the ocean, and (iii) the starting location of the robot. The parameters used in the analysis and numerical simulations are found in Table.7.1.

1. Robust Concentration Gradient: Firstly, unlike wave-based communications, the gradient of molecular concentration is not strongly affected by the transmission period. In acoustic wave communications, the power of the acoustic signal will decay to below noise level after less than 1 minute of propagation. As shown in Fig. 7.7, not only will there be a significant gradient ($\frac{\partial p(t)}{\partial x_{\text{R}}}$ [molecules per m^4]) after several years, but also the shape of the gradient doesn't vary between a transmission period of T =15 days, and T=360 days.

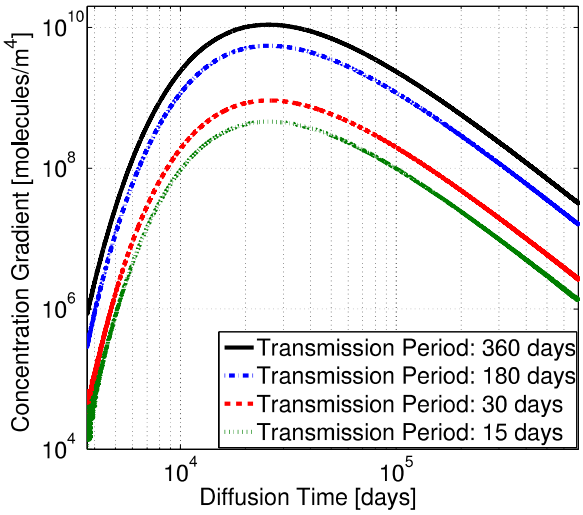

Figure 7.7: Plot of chemical concentration gradient (molecules per m^4) for various transmission durations at the transmitter. The receiver is at x =100km, y =100km, z =1000m away from the transmitter.

2. SNR Threshold: In Section 7.2.2, the macroscopic ocean noise as a function of the LOD was defined, and the SNR is given in Eq. (7.5). The main effect of noise is to cause false gradients and causing incorrect search direction decisions. Fig. 7.8 shows the simulation for total number of search iterations as a function of the SNR. Monte-Carlo simulations were performed for each SNR value ranging from 140dB to 240dB, for different transmission durations T. It is found that if the SNR falls below a threshold value of 140dB, the number of search iterations required grows rapidly. For an SNR value of 200 or over, the algorithm is robust enough to always find the hidden object with approximately 24 search iterations. The results also reinforce the earlier claim that increasing the transmission duration doesn't significantly affect the number of search iterations' sensitivity to noise.

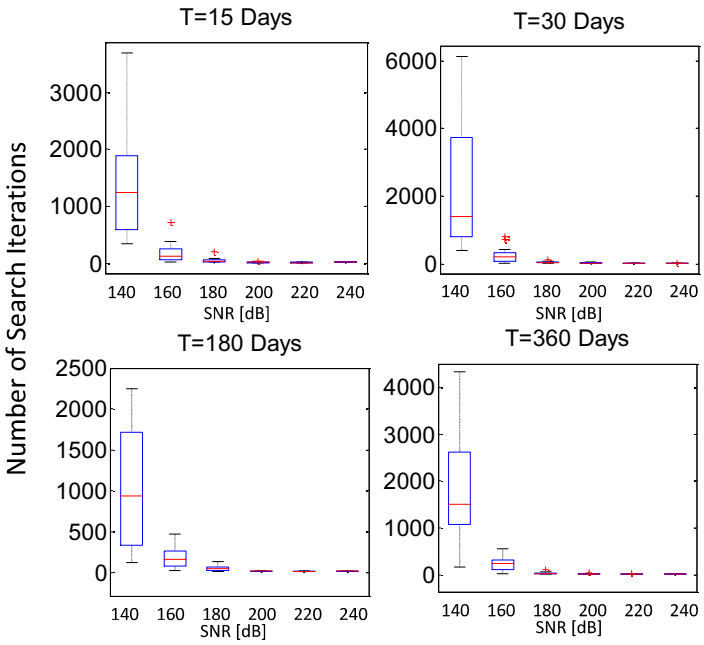

Figure 7.8: Plot of search iterations as a function SNR. The receiver starts at x =100km, y =100km, z =1000m away from the transmitter.

3. Starting Location: In terms of where the robot initially starts, how the number of search iterations vary in according to the horizontal distance x, y and the vertical distance z is considered. In Fig. 7.9(a) and (b), the total number of search iterations (steps) for different (a) horizontal distance (where vertical distance fixed at 1000m) and (b) vertical distance range (where horizontal distance fixed at 100km) are demonstrated. The results show that the number of search iterations is largely uncorrelated with the horizontal distance, but rises significantly for a vertical distance of over 1300m. In Fig. 7.9(c) and (d), the number of search iterations (steps) for different number of repeat stages (as a result of different horizontal and vertical distances) are demonstrated. The results show that the search iterations are positively correlated with the repeat stages at both distances. A repeat stage can significantly increase the search distance of the robot.

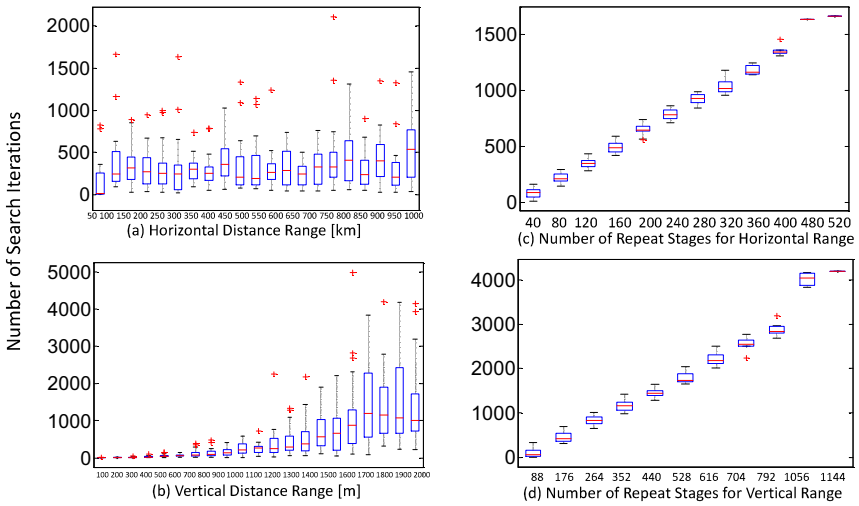

Figure 7.9: Box plot of number of search iterations as a function of the: (a) horizontal distance, (b) vertical distance. Box plot of search iterations as a function of the number of repeat stages for: (c) horizontal distance range, (d) vertical distance range.

In Fig. 7.10, the total trace distance as a function of the horizontal and vertical distance is demonstrated. The results show that the total trace distance is positively correlated with both the vertical and horizontal distance. In terms of the outliers, they are more exasperated for the vertical distance due to the existence of a high number of repeat stages described above.

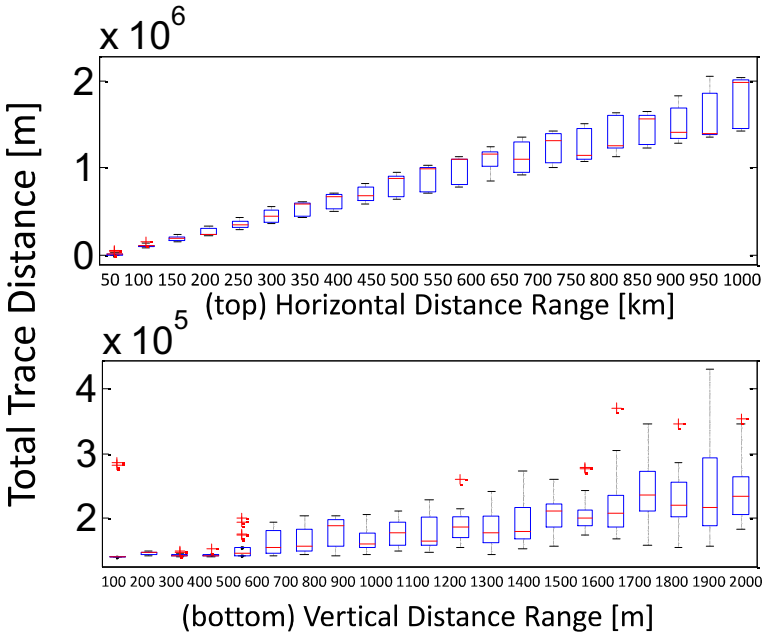

Figure 7.10: Boxplot of total trace distance travelled by the robot as a function of (top) horizontal distance range and (bottom) vertical distance range.

7.4.2 Performance Comparison

This subsection compares the energy and latency performance of the CIC, CGL and conventional communication systems, namely, acoustic (AC) and underwater wireless optical (UWOC). In order to simplify the comparison, the molecular energy is calculated with integral of MC impulse response from time $t = 0$ to $t = +\infty$. Particularly, the information particles of CIC may suffer from molecular degradation during its propagation in the ocean, thus while calculate the energy of CIC, degradation is taken into consideration.

Received Impulse Energy

1. CIC:

In the CIC method, biological components (peptides and N-linked glycan), which are employed as sufficiently complex chemical information carriers, will be

detected as food by the bacteria in the oceans. Thus, the information components can be damaged during the propagation in the ocean. Accordingly, CIC molecules is considered having a life expectancy with a *molecule degradation*, which can be modelled as an exponential distribution [41], and the concentration with degradation $\phi(t)$ is modeled as $\phi(t) = \phi_0 \exp(-\lambda t)$, where: $\lambda = \frac{\ln(2)}{\Lambda_{1/2}}$. ϕ_0 is the non-degraded concentration found in Eq. (7.1), λ is the rate of degradation, and $\Lambda_{1/2}$ is the corresponding half-life of the message molecule. Therefore, the energy of CIC is given as

$$\begin{aligned} E_{\mathrm{CIC}} &= \int_0^{\infty} \phi(x_{\mathrm{R}}, t) \exp(-\lambda t)\, \mathrm{d}t \\ &= \frac{M}{4\pi D x_{\mathrm{R}}} \left[1.84 \exp(-x_{\mathrm{R}} \sqrt{\frac{\lambda}{D}}) + 0.16 \exp(x_{\mathrm{R}} \sqrt{\frac{\lambda}{D}}) \right]. \end{aligned} \tag{7.9}$$

The time delay to peak amplitude is $\propto x_{\mathrm{R}}^2$.

2. CGL:

CGL is based on a gradient ascend localization method using the chemical gradient in oceans. The received molecular energy can be expressed by integrating Eq.7.1 over time:

$$E_{\mathrm{CGL}} = \int_0^{\infty} \phi(x_{\mathrm{R}}, t) \mathrm{d}t = \frac{M}{2\pi D x_{\mathrm{R}}} \tag{7.10}$$

Therefore, using Eq. 7.10, the energy attenuation for chemical gradient localization is $\propto \frac{1}{x_{\mathrm{R}}}$, and the time delay to peak amplitude is $\propto x_{\mathrm{R}}^2$.

3. AC:

In an underwater acoustic channel over a propagation distance x_{R} [km], the propagation channel's energy attenuation A [dB] is statistically characterised by [159]:

$$A_{\mathrm{AC}}(x_{\mathrm{R}}, f_a) = k 10 \log_{10}(x_{\mathrm{R}}) + x_{\mathrm{R}}(a(f_a)) + 10 \log_{10}(A_0), \tag{7.11}$$

where A_0 is a constant, and k is an acoustic spreading factor (typically 2). The func-

tion $a(f_a)$ characterizes the absorption coefficient which is a function of frequency f_a [kHz]. The time delay to peak amplitude's arrival is $\propto x_{\mathrm{R}}$.

4. UWOC:

In an underwater wireless optical channel over a propagation distance x_{R} [km], the attenuation of the light beam in water can be quantified with beam light attenuation coefficient $c(v/f_o)$ in [160]:

$$A_{\mathrm{UWOC}}(f_o, x_{\mathrm{R}}) = \exp\left(-c\left(\frac{v_o}{f_o}\right)x_{\mathrm{R}}\right), \tag{7.12}$$

where f_o is the frequency of the light beam, v_o is the speed of light in sea water. The time delay to peak amplitude's arrival is $\propto x_{\mathrm{R}}$.

Energy Attenuation and Latency Comparison

Fig. 7.11 shows the results of chemical concentration as a function of diffusion time for the two methods under consideration at an equivalent distance $x_{\mathrm{R}} = 20$km. It is found that the concentration of CIC is very sensitive to molecule half-life time $\Lambda_{1/2}$, but the receiver will immediately know the location after decoding the chemical message. On the other hand, CGL does not suffer from molecular degradation because no information needs to be encoded in bio-molecules. The detection period is sufficient long (above LOD threshold), but the search robot has to wait a long time before the concentration reaches above receiver sensitivity, and wait a further longer time before the robot can locate the transmitter after many search iterations. In summary, CIC provide the exact location information for the receiver so that once one information carrier is captured and decoded, the location can be found. However, the complexities of assembling the carriers and the carrier life expectancy need to be carefully considered. CGL, on the other hand, doesn't suffer from the complexity and degradation issues, but is sensitive to the noise in the ocean environment and the need for waiting a longer period in order to initialize the search start.

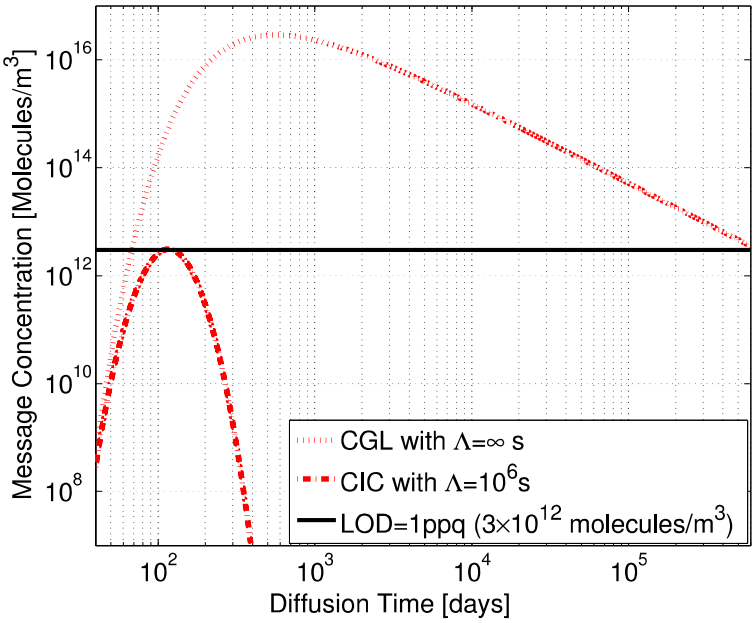

Figure 7.11: Plot of chemical concentration for: (1) chemical gradient localization (CGL) method with receiver LOD and (2) chemical information carrier (CIC) method with molecular decay rates.

In Fig. 7.12, the energy attenuation and latency as a function of propagation distance for both molecular and conventional systems are demonstrated. Fig. 7.12 (top) show that conventional systems suffer faster energy attenuation than molecular communications. This means rescue nodes are far more likely to detect molecular messages at long distances than either acoustic or optic signals. Fig. 7.12 (bottom) shows the latency (the peak pulse's arrival time) increases quadratically for molecular communications, whereas acoustic and optical waves' latency increase linearly. This means the nodes that expect molecular signals need to wait significantly longer.

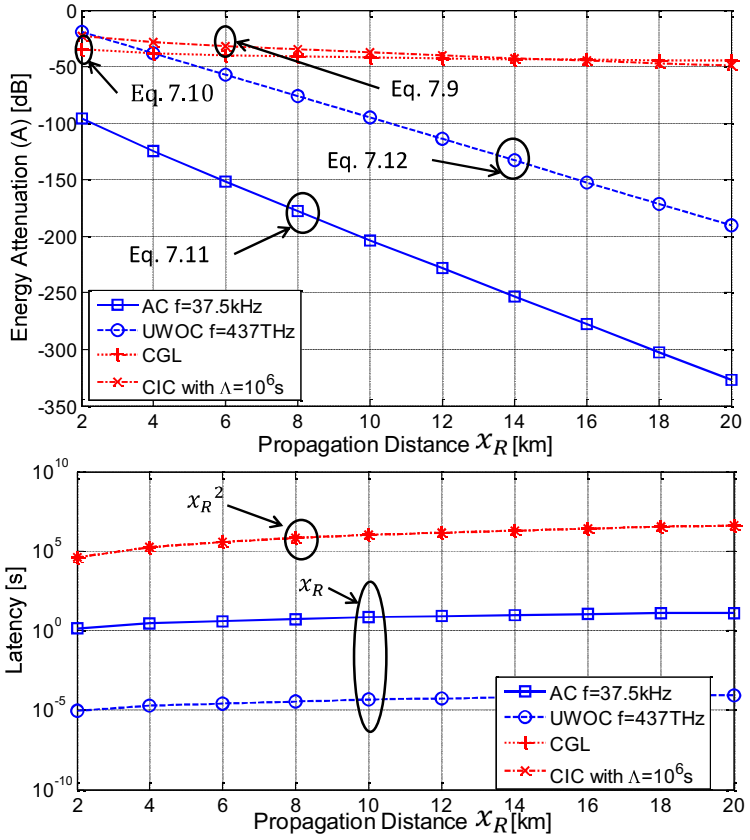

Figure 7.12: Plot of energy attenuation as function of propagation distance (top) and plot of latency as function of propagation distance (bottom) for acoustic, wireless optical, chemical gradient localization and chemical information carrier

It can be summarized that the difference between the 4 underwater communication metrics as follows: optical wireless has a high data rate (Mbits/s), but the free-space transmission distance is strictly limited to a few metres underwater. Acoustic systems are widely used for search and rescue nowadays due to its low complexity and reasonable detection distance (10-30km). However, when the search space is large and the search duration is prolonged, acoustic systems can not reliably allow the rescuers to find the hidden crashed object (as it is in the MH370 case). The persistence time of the signal after transmission is a few seconds, indicating

that the search time is limited by the battery life of the system. Compared to the aforementioned conventional systems, both of the chemical methods have the advantages of higher signal persistence time (months to years) and longer propagation distance (1000km or more).

7.5 Summary

In this chapter, an underwater searching problem of trying to locate a single hidden object was tackled with consideration of underwater molecular signalling. Typically, such problem might have a size of environmental radius up to 500km and the searching duration could take several months to years, but current state-of-the-art acoustic systems solutions restricted receiving signal up to 30km away and each signal pulse persisted for only a few seconds to a minute after transmission. In addition, the rapid energy attenuation of acoustic waves in under-water channels led to expensive and lengthy long range searching and recovery missions. Unlike the acoustic communication, MC presented advancements on longer endurance and less energy attenuations. There are two MC approaches proposed in this chapter, one was that the location information was inside the chemical composition of bio-molecules. The drawbacks for this approach were degradation and system complexity. The alternative approach was therefore proposed, whereby no information was embedded in the chemical molecules. Instead, the molecules served as a chemical concentration gradient to aid a receiver robot to find the transmitter through gradient ascent. An adapted Rosenbrock algorithm was implemented to achieve the process. Finally, the performance energy attenuation and latency of both MC approaches and conventional underwater system were compared by simulation results.

Chapter 8

Conclusions and Future Work

8.1 Conclusions

A major motivation for this work was to understand the physical properties that govern the information capacity of molecular communications (MC) across different distance scales. In particular, MC offers advantages when the environment is hostile to EM waves either through propagation loss or interference.

The thesis initially demonstrated that MC can reliably transport data across complex confined environments, where conventional EM communication technology may falter. Based on empirical data, the capture probability expression of a finite sized receiver with drift was derived and a novel Nakagami distributed noise model was developed. The performance metrics of BER, delay and throughput were shown to be very sensitive to the sensor cleanse time, drift velocity and transmission length. The thesis went on to propose a molecular channel fading model due to temperature fluctuations in Chapter 5. The fading distribution was analytically derived based on the Normal distributed temperature and validated using numerical simulations. After understanding the static channel, mobile diffusion channels were examined. In such a situation, bit transposition errors were likely to be the dominant noise source. A proof-of-concept robot was constructed to demonstrate how transposition

errors form and positional-distance codes could be applied to achieve a superior performance over classical Hamming-distance codes. In Chapter 6, mobile relays were proposed to assist in the diffusion process. A bacteria based MC channel model was characterised and related energy model was derived. Based on the energy model, the energy efficiency of the bacteria based MC channel model was examined and compared to diffusion based MC. It was shown that bacteria based MC is superior for long distance or delay-intolerant communications. Finally, the problem of how to locate a hidden entity with an unknown location in a vast underwater search space was tackled. Two molecular messaging methods for location discovery were proposed: a chemical encoding messaging method and a Rosenbrock gradient ascent algorithm. The two methods were found to offer attractive performance trade-offs in complexity and robustness. When compared to conventional acoustic signals, the chemical methods proposed offered a significantly longer propagation distance (2 orders of magnitude) and longer signal persistence duration (3 orders of magnitude).

To conclude, the proposed channel model characterizations and performance analysis provide useful guidelines and potential solutions for the understanding of MC in future.

8.2 Future Work: Complex Geometric Environments Modelling

Many previous works assume infinite or random boundary conditions. However, the confined environment in the real world (e.g., mine tunnel) can be more complex with defined regular geometries. For example, traditional EM communication studied in such environment have pointed out that the signal strength and other communication performance (e.g., BER, delay, channel capacity, etc.) can be significantly affected by tunnel cross section, bend, incline. MC has been proved to be

used in confined environment, but there has been little research to establish proper channel models and analyse the communication performance for the environments with consideration of the shape of cross section, number of bends or slope of the incline. Thus, to the best of the author's knowledge, complex geometric environment modelling is expected to be a promising future research area.

References

[1] T. Nakano, A. Eckford, and T. Haaguchi, *Molecular Communication*. Cambridge University Press, 2013.

[2] R. P. Feynman, "Plenty of room at the bottom," *Engineering and Science*, vol. 23, no. 5, pp. 22–36, Dec. 1959.

[3] B. Bassler, "How bacteria talk to each other: Regulation of gene expression by quorum sensing," vol. 2, no. 1, pp. 582–587, Sep. 1999.

[4] M. B. Miller and B. Bassler, "Quorum sensing in bacteria," *Annual Review of Microbiology*, vol. 55, no. 1, pp. 165–199, Jan. 2001.

[5] S. Hiyama, Y. Moritani, T. Suda, R. Egashira, A. Enomoto, M. Moore, and T. Nakano, "Molecular communication," in *2005 NSTI Nanotechnology Conference*, Jun. 2005, pp. 33–40.

[6] N. Neave, *Hormones and Behavior: A Psychological Approach*. Cambridge Univ. Press, 2008.

[7] T. D. Wyatt, *Pheromones and Animal Behaviour: Communication by Smell and Taste*. Cambridge Univ. Press, 2003.

[8] M. E. Ortiz and D. Endy, *Engineered cell-cell communication via dna messaging*. Springer Journal of Biological Engineering, 2012.

[9] P. Collins and R. Ferrier, *Monosaccharides: Their Chemistry and Their Roles in Natural Products*. Academic Press, 1995.

[10] M. Thaysen-Andersen and N. H. Packer, *Advances in LCMS/MS-based glycoproteomics: Getting closer to system-wide site-specific mapping of the N-and O-glycoproteome*. Biochimica et Biophysica Acta (BBA), 2014.

[11] S. Hiyama and Y. Moritani, "Molecular communication: Harnessing biochemical materials to engineer biomimetic communication systems," *Elsevier Nano Communication Networks*, vol. 1, no. 1, pp. 20–30, Mar. 2010.

[12] N. Farsad, W. Guo, and A. Eckford, "Tabletop molecular communication: Text messages through chemical signals," *PLOS ONE*, vol. 8, Dec. 2013.

[13] M. Mukai, K. Maruo, J. Kikuchi, Y. Sasaki, S. Hiyama, Y. Moritani, and T. Suda, "Propagation and amplification of molecular information using a photoresponsive molecular switch," vol. 21, no. 3, pp. 284–291, Apr. 2009.

[14] Y. Sasaki, Y. Shioyama, W. Tian, J. I. Kikuchi, S. Hiyama, Y. Moritani, and T. Suda, "A nanosensory device fabricated on a liposome for detection of chemical signals," vol. 105, no. 1, pp. 37–43, Jan. 2010.

[15] M. J. Doktycz and M. L. Simpson, "Nano-enabled synthetic biology," vol. 3, no. 1, pp. 125–135, Jul. 2007.

[16] B. Alberts, D. Bray, A. Johnson, J. Lewis, M. Raff, and K. Sutoh, *Essential Cell Biology: An Introduction to the Molecular Biology of the Cell*. Garland, 1997.

[17] M. Chen and R. Weiss, "Artificial cell-cell communication in yeast saccharomyces cerevisiae using signaling elements from arabidopsis thaliana," vol. 23, no. 12, pp. 1551–1555, Dec. 2005.

[18] S. Basu, Y. Gerchman, C. H. Collins, F. H. Arnold, and R. Weiss, "A synthetic multicellular system for programmed pattern formation," vol. 434, no. 7037, pp. 1130–1134, Apr. 2005.

[19] L. You, R. S. Cox, R. Weiss, and F. H. Arnold, "Programmed population control by cell-cell communication and regulated killing," vol. 428, no. 6985, pp. 868–871, Apr. 2004.

[20] V. Mittal, *Encapsulation Nanotechnologies*. Wiley, 2013.

[21] T. S. Moon, C. Lou, A. Tamsir, B. C. Stanton, and C. A. Voigt, "Genetic programs constructed from layered logic gates in single cells," vol. 491, no. 7423, pp. 249–253, Nov. 2012.

[22] P. Siuti, J. Yazbek, and T. K. Lu, "Synthetic circuits integrating logic and memory in living cells," vol. 31, no. 5, pp. 448–452, May 2013.

[23] A. Gossler, T. Doetschman, R. Korn, E. Serfling, and R. Kemler, "Transgenesis by means of blastocyst-derived embryonic stem cell lines," vol. 83, no. 23, pp. 9065–9069, Dec 1986.

[24] G. M. Cooper and R. E. Hausman, *The Cell*. Sunderland, Sinauer Associates, 2000.

[25] S. Huang and M. Kamihira, "Development of hybrid viral vectors for gene therapy," vol. 31, no. 2, pp. 208–223, Apr. 2013.

[26] J. E. Toettcher, C. Mock, E. Batchelor, A. Loewer, and G. Lahav, "A synthetic-natural hybrid oscillator in human cells," vol. 107, no. 39, pp. 17 047–17 052, Sep. 2010.

[27] O. Mondragon-Palomino, T. Danino, J. Selimkhanov, L. Tsimring, and J. Hasty, "Entrainment of a population of synthetic genetic oscillators," vol. 333, no. 6047, pp. 1315–1319, Sep. 2011.

[28] D. Hymel and B. R. Peterson, "Synthetic cell surface receptors for delivery of therapeutics and probes," vol. 64, no. 9, pp. 797–810, Jun. 2012.

[29] H. Shankaran, H. Resat, and H. S. Wiley, "Cell surface receptors for signal transduction and ligand transport: A design principles study," vol. 3, no. 6, pp. 101–103, Jun. 2007.

[30] P. Cuatrecasas, "Membrane receptors," vol. 43, no. 1, pp. 169–214, July 1974.

[31] M. Pierobon and I. F. Akyildiz, "A physical end-to-end model for molecular communication in nanonetworks," *IEEE Journal on Selected Areas in Communications (JSAC)*, vol. 28, no. 4, pp. 602–611, 2010.

[32] ——, "Capacity of a diffusion-based molecular communication system with channel memory and molecular noise," *IEEE Trans. on Information Theory*, vol. 59, no. 2, pp. 942–954, 2013.

[33] S. Hiyama, Y. Moritani, R. Gojo, S. Takeuchi, and K. Sutoh, "Biomolecular-motor-based autonomous delivery of lipid vesicles as nano- or microscale reactors on a chip," *RSC Lab on a Chip*, vol. 10, no. 20, pp. 2741–2748, June 2010.

[34] H. Berg, *E. coli in Motion.* Springer Verlag, 2003.

[35] J. Berthier and P. Silberzan, *Microfluidics for Biotechnology 2nd Edition.* Artech House, 2009.

[36] H. Tyrrell and K. Harris, *Diffusion in Liquids: A Theoretical and Experimental Study (Monographs in Chemistry).* Butterworth-Heinemann, 1984.

[37] D. Arifler, "Connectivity properties of free diffusion-based molecular nanoscale communication networks," *IEEE Transactions on Communications*, vol. 65, no. 4, pp. 1686–1695, Apr. 2017.

[38] M. Kuran, H. Yilmaz, and T. Tugcu, "A tunnel-based approach for signal shaping in molecular communication," 2013.

[39] A. Eckford, "Nanoscale communication with brownian motion," 2007.

[40] S. Wang, W. Guo, S. Qiu, and M. McDonnell, "Performance of macro-scale molecular communications with sensor cleanse time," in *IEEE International Conference on Telecommunications (ICT)*, Jun. 2014, pp. 363–368.

[41] H. B. Yilmaz, A. C. Heren, T. Tugcu, and C.-B. Chae, "Three-dimensional channel characteristics for molecular communications with an absorbing receiver," *IEEE Communication Letter*, vol. 18, no. 6, pp. 929–932, 2014.

[42] A. Akkaya, H. Yilmaz, C. Chae, and T. Tugcu, "Effect or receptor density and size on signal reception in molecular communication via diffusion with an absorbing receiver," vol. 19, no. 2, pp. 155–158, Feb 2015.

[43] M. Kuran, H. Yilmaz, T. Tugcu, and B. Ozerman, "Energy model for communication via diffusion in nanonetworks," *Nano Communication Networks*, vol. 1, pp. 86–95, 2010.

[44] N. Farsad, N. Kim, A. Eckford, and C. Chae, "Channel and Noise Models for Nonlinear Molecular Communication Systems," *IEEE Journal on Selected Areas in Communications (JSAC)*, pp. 1–14, Nov. 2014.

[45] B. Atakan, "Optimal transmission probability in binary molecular communication," *IEEE Commun. Lett.*, vol. 17, no. 6, pp. 1152–1155, Jun. 2013.

[46] M. Gregori and I. F. Akyildiz, "A new nanonetwork architecture using flagellated bacteria and catalytic nanomotors," *IEEE Journal on Selected Areas in Communications*, vol. 28, no. 4, pp. 612–619, May 2010.

[47] L. C. Cobo and I. F. Akyildiz, "Bacteria-based communciation in nanonetworks," *Nano Communication Networks*, vol. 1, pp. 244–256, 2010.

[48] R. Macnab and D. Koshland, "The gradient-sensing mechanism in bacterial chemotaxis," *Proceedings of the National Academy of Sciences*, vol. 9, no. 69, pp. 2509–2512, 1972.

[49] H. Berg, *Random Walks in Biology.* Princeton, N.J.: Princeton University Press, 1993.

[50] P. D. Frymier, R. M. Ford, and P. T. Cummings, "Cellular dynamics simulations of bacterial chemotaxis," *Elsevier Chem. Eng. Sci*, vol. 48, no. 4, pp. 687–699, Feb. 1993.

[51] M. Gregori, I. Llatser, A. Cabellos-Aparicio, and E. Alarcon, "Physical channel characterization for medium-range nanonetworks using flagellated bacteria," *Elsevier Comput. Netw*, vol. 55, no. 3, pp. 679–791, Feb. 2011.

[52] Z. Wang, M. Kim, and G. Rosen, "Validating models of bacterial chemotaxis by simulating the random motility coefficient," *IEEE Int. Conf. on BioInformatics and BioEngineering (BIBE)*, Sept. 2008.

[53] P. Mullany, *The Dynamic Bacterial Genome.* Cambridge University Press, 2005.

[54] V. Petrov, D. Moltchanov, S. Balasubramaniam, and Y. Koucheryavy, "Incorporating bacterial properties for plasmid delivery in nano sensor networks," *IEEE Transaction on Nanotechnology*, vol. 14, no. 4, 2015.

[55] B. Atakan and O. B. Akan, "An information theoretical approach for molecular communication," Jun. 2007.

[56] ——, "On channel capacity and error compensation in molecular communication," *Transactions on Computational Systems Biology*, vol. 5410, no. 1, pp. 59–80, Sep. 2008.

[57] ——, "Single and multiple-access channel capacity in molecular nanonetworks," *Nano-Net.*, vol. 20, no. 1, pp. 14–23, Aug. 2009.

[58] ——, "Deterministic capacity of information flow in molecular nanonetworks," *Nano Commun. Netw.*, vol. 1, no. 1, pp. 31–42, May 2010.

[59] D. Arifler, "Capacity analysis of a diffusion-based short-range molecular nanocommunication channel," *Comput. Netw.*, vol. 55, no. 6, pp. 1426–1434, Apr. 2011.

[60] T. Nakano, Y. Okaie, and J. Liu, "Channel model and capacity analysis of molecular communication with brownian motion," *IEEE Commun. Lett.*, vol. 16, no. 6, pp. 797–800, Jun. 2012.

[61] M. Pierobon and I. F. Akyildiz, "Diffusion-based noise analysis for molecular communication in nanonetworks," *IEEE Transactions on Signal Processing*, vol. 59, no. 6, pp. 2532–2547, 2011.

[62] K. Srinivas, A. Eckford, and R. Adve, "Molecular communciation in fluid media: The additive inverse gaussian noise channel," *IEEE Trans. Inf. Theory*, vol. 58, no. 7, pp. 4678–4692, July 2012.

[63] H. Li, S. Moser, and D. Guo, "Capacity of the memoryless additive inverse gaussian noise channel," *IEEE J. Sel. Areas Commun.*, vol. 32, no. 12, pp. 2315–2329, Dec. 2014.

[64] C. Rose and I. Mian, "A fundamental framework for molecular communication channels: Timing and payload," Jun. 2015.

[65] M. U. Mahfuz, D. Makrakis, and H. T. Mouftah, "On the characterization of binary concentration-encoded molecular communication in nanonetworks," *Nano Commun. Netw.*, vol. 1, no. 4, pp. 289–300, Dec. 2010.

[66] M. S. Kuran, H. B. Yilmaz, T. Tugcu, and I. F. Akyildiz, "Modulation techniques for communication via diffusion in nanonetworks," Jun. 2011.

[67] ——, "Interference effects on modulation techniques in diffusion based nanonetworks," *Elsevier Nano Commun. Netw.*, vol. 3, no. 1, pp. 65–73, Mar. 2012.

[68] N. Garralda, I. Llatser, A. Cabellos-Aparicio, E. Alarcn, and M. Pierobon, "Diffusion-based physical channel identification in molecular nanonetworks," *Nano Commun. Netw.*, vol. 2, no. 4, pp. 196–204, Dec. 2011.

[69] I. Llaster, A. Cabellos-Aparicio, M. Pierobon, and E. Alarcon, "Detection Techniques for Diffusion-based Molecular Communication," *IEEE Journal on Selected Areas in Communications (JSAC)*, vol. 31, no. 12, pp. 726–734, Jan. 2014.

[70] Y. Hsieh, Y. Lee, P. Shih, P. Yeh, and K. Chen, "On the asynchronous information embedding for event-driven systems in molecular communications," *Nano Commun. Netw.*, vol. 4, no. 1, pp. 2–13, Mar. 2013.

[71] H. Arjmandi, A. Gohari, M. N. Kenari, and F. Bateni, "Diffusionbased nanonetworking: A new modulation technique and performance analysis," *IEEE Commun. Lett*, vol. 17, no. 4, pp. 645–648, Apr. 2013.

[72] B. Tepekule, A. E. Pusane, H. B. Yilmaz, and T. Tugcu, "Energy efficient isi mitigation for communication via diffusion," Sep. 2014.

[73] B. Tepekule, A. E. Pusane, M. S. Kuran, and T. Tugcu, "A novel pre-equalization method for molecular communication via diffusion in nanonetworks," *IEEE Commun. Lett.*, vol. 19, no. 8, pp. 1311–1314, Aug. 2015.

[74] A. Noel, K. Cheung, and R. Schober, "Improving receiver performance of

diffusive molecular communication with enzymes," *IEEE Trans. NanoBiosci.*, vol. 13, no. 1, pp. 31–43, Mar. 2014.

[75] H. ShahMohammadian, G. G. Messier, and S. Magierowski, "Optimum receiver for molecule shift keying modulation in diffusion-based molecular communication channels," *Nano Commun. Netw.*, vol. 3, no. 3, pp. 183–195, Sep. 2012.

[76] M. U. Mahfuz, D. Makrakis, and H. T. Mouftah, "Sampling based optimum signal detection in concentration-encoded molecular communication: Receiver architecture and performance," Jul. 2013.

[77] ——, "A generalized strength-based signal detection model for concentration-encoded molecular communication," Aug. 2013.

[78] D. Kilinc and O. B. Akan, "Receiver design for molecular communication," *IEEE J. Sel. Areas Commun.*, vol. 31, no. 12, pp. 705–714, Dec. 2013.

[79] A. Noel, K. Cheung, and R. Schober, "Optimal receiver design for diffusive molecular communication with flow and additive noise," *IEEE Trans. NanoBiosci.*, vol. 13, no. 3, pp. 350–362, Sep. 2014.

[80] C. Bai, M. Leeson, and M. Higgins, "Minimum energy channel codes for molecular communications," *Electronics Letters*, vol. 50, no. 23, pp. 1669–1671, Nov. 2014.

[81] Y. Lu, M. Higgins, and M. Leeson, "Comparison of channel coding schemes for molecular communications systems," *IEEE Trans. Commu.*, vol. 63, no. 11, pp. 3991–4001, Oct. 2015.

[82] ——, "Self-orthogonal convolutional codes(soccs) for diffusion-based molecular communication systems," Jun. 2015.

[83] W. Guo, T. Asyhari, N. Farsad, H. Yilmaz, A. Eckford, and C. Chae, "Molecular communications: channel model and physical layer techniques," *IEEE Wireless Commu.*, vol. 23, no. 4, pp. 120–127, Aug. 2016.

[84] P. Ko, Y. Lee, P. Yeh, C. Lee, and K. Chen, "A new paradigm for channel coding in diffusion-based molecular communications: Molecular coding distance function," May 2012.

[85] P. Shih, C. Lee, P. Yeh, and K. Chen, "Channel codes for reliability enhancement in molecular communication," *IEEE J. Sel. Areas Commun.*, vol. 31, no. 1, pp. 857–867, Jun. 2013.

[86] C. Chen, Y. Haik, and J. Chatterjee, "Development of nanotechnology for biomedical applications," May 2005.

[87] R. A. Freitas, "Nanotechnology, nanomedicine and nanosurgery," *International Journal of Surgery*, vol. 3, no. 4, pp. 243–246, Jan. 2005.

[88] K. B. Dving and D. Trotier, "Structure and function of the vomeronasal organ," *Journal of Experimental Biology*, vol. 201, no. 21, pp. 2913–2925, Mar. 1998.

[89] R. A. Freitas, "Pharmacytes: An ideal vehicle for targeted drug delivery," *Journal of Nanoscience and Nanotechnology*, vol. 6, no. 9, pp. 9–10, Jun. 2006.

[90] B. Wowk, "Cell repair technology," *Cryonics*, vol. 1, no. 1, pp. 21–30, Jan. 1988.

[91] ——, "24th century medicine," *Cryonics*, vol. 1, no. 2, pp. 16–34, Dec. 1988.

[92] J. W. Aylott, "Optical nanosensors? an enabling technology for intracellular measurements," *Analyst*, vol. 128, no. 4, pp. 309–312, Nov. 2003.

[93] D. Tessier, I. Radu, and M. Filteau, "Antimicrobial fabrics coated with nano-sized silver salt crystals," *NSTI Nanotech*, vol. 1, no. 1, pp. 762–764, Jun. 2005.

[94] M. S. Dresselhaus, G. Dresselhaus, and P. Avouris, *Carbon Nanotubes: Synthesis, Structure, Properties and Applications*. Springer-Verlag GmbH, 2005.

[95] M. Endo, T. Hayashi, Y. A. Kim, and H. Muramatsu, "Development and application of carbon nanotubes," *Japanese Journal of Applied Physics*, vol. 45, no. 6, pp. 4883–4892, Jun. 2006.

[96] J. Han, J. Fu, and R. B. Schoch, "Molecular sieving using nanofilters: Past, present and future," *Lab on a Chip*, vol. 8, no. 1, pp. 23–33, Jul. 2008.

[97] L. Munoz, N. Dimov, G. Carot-Sans, W. P. Bula, A. Guerrero, and H. J. G. E. Gardeniers, "Mimicking insect communication: Release and detection of pheromone, biosynthesized by an alcohol acetyl transferase immobilized in a microreactor," *PLoS One*, vol. 7, no. 11, pp. 477–510, Nov. 2012.

[98] R. K. V. Meer, M. D. Breed, K. E. Espelie, and M. L. Winston, *Pheromone Communication in Social Insects*. Boulder, 1998.

[99] R. A. Russell, "An odour sensing robot draws inspiration from the insect world," Feb. 1998.

[100] H. Ishida, T. Nakamoto, T. Moriizumi, T. Kikas, and J. Janata, "Plumetracking robots: A new application of chemical sensors," *Biol. Bull*, vol. 200, no. 2, pp. 222–226, Apr. 2001.

[101] A. W. Eckford, N. Farsad, S. Hiyama, and Y. Moritani, "Microchannel molecular communication with nanoscale carriers: Brownian motion versus active transport," Apr. 2010.

[102] E. Gul, B. Atakan, and O. B. Akan, "Nanons: A nanoscale network simulator framework for molecular communications," *Nano Commun. Netw.*, vol. 1, no. 2, pp. 138–156, Jun. 2010.

[103] L. Felicetti, M. Femminella, and G. Reali, "A simulation tool for nanoscale biological networks," *Nano Commun. Netw.*, vol. 3, no. 1, pp. 2–18, May. 2012.

[104] ——, "Simulation of molecular signaling in blood vessels: Software design and application to atherogenesis," *Nano Commun. Netw.*, vol. 4, no. 3, pp. 98–119, Sep. 2013.

[105] G. Wei, P. Bogdan, and R. Marculescu, "Efficient modeling and simulation of bacteria-based nanonetworks with bnsim," *IEEE J. Sel. Areas Commun.*, vol. 31, no. 12, pp. 868–878, Dec. 2013.

[106] A. Akkaya, G. Genc, and T. Tugcu, "Hla based architecture for molecular communication simulation," *Simul. Model. Pract. Theory*, vol. 42, no. 1, pp. 163–177, Mar. 2014.

[107] I. Llatser, D. Demiray, A. Cabellos-Aparicio, D. T. Altilar, and E. Alarcn, "n3sim: Simulation framework for diffusion-based molecular communication nanonetworks," *Simul. Model. Pract. Theory*, vol. 42, no. 1, pp. 210–222, Mar. 2014.

[108] H. B. Yilmaz and C. Chae, "Simulation study of molecular communication systems with an absorbing receiver: Modulation and isi mitigation techniques," *Simul. Model. Pract. Theory*, vol. 49, no. 1, pp. 136–150, Dec. 2014.

[109] R. Weiss and T. Knight, *Engineered Communications for Microbial Robotics*. Springer Berlin Heidelberg, 2001.

[110] R. Lentini, S. P. Santero, F. Chizzolini, D. Cecchi, J. Fontana, M. Marchioretto, C. D. Bianco, J. L. Terrell, A. C. Spencer, L. Martini, M. Forlin,

M. Assfalg, M. D. Serra, W. E. Bentley, and S. S. Mansy, "Integrating artificial with natural cells to translate chemical messages that direct e. coli behaviour," *Nat. Comm.*, vol. 5, no. 4012, pp. 1125–1145, May 2014.

[111] M. E. Ortiz and D. Endy, "Engineered cell-cell communication via dna messaging," *J. Biol. Eng.*, vol. 6, no. 1, pp. 16–17, Sep. 2012.

[112] M. Rahman, A. Ahammad, J.H.Jin, S. Ahn, and J. Lee, "A comprehensive review of glucose biosensors based on nanostructured metal-oxides," *Sensors*, vol. 10, no. 5, pp. 4855–4886, May 2010.

[113] L. Wang, N. Farsad, W. Guo, S. Magierowski, and A. W. Eckford, "Molecular barcodes: Information transmission via persistent chemical tags," Jun. 2015.

[114] C. Lee, B. Koo, N. Kim, H. B. Yilmaz, N. Farsad, A. Eckford, and C. Chae, "Molecular mimo communication link," May 2015.

[115] B. Koo, C. Lee, H. B. Yilmaz, N. Farsad, A. Eckford, and C. Chae, "Molecular mimo: From theory to prototype," *IEEE J. Sel. Areas Commun.*, vol. 34, no. 3, pp. 600–614, Mar. 2016.

[116] *ETRX357 Telegesis Development Kit for Zigbee Techlonogy Product Manual*. Telegesis, 2012.

[117] *ATmega328P Datasheet Summary*. Atmel, 2016.

[118] *Technical Data Sheet MQ3 Gas Sensor*. Hanwei Electronics, 2012.

[119] L. P. Kadanoff, *Statistical Physics: Statics, Dynamics and Renormalization*. World Scientific, 2000.

[120] L. Meng, P. Yeh, K. Chen, and I. Akyildiz, "MIMO communications based on molecular diffusion," in *IEEE Global Communications Conference (GLOBECOM)*, Dec. 2012, pp. 5380–5385.

[121] W. Guo, S. Wang, A. Eckford, and J. Wu, "Reliable communication envelopes of molecular diffusion channels," *Electronics Letters*, vol. 49, no. 19, pp. 1248–1249, Sep. 2013.

[122] J. Proakis, *Digital Communications*. London, UK: McGrall Hill, 2009.

[123] T. Cover and J. Thomas, *Elements of Information Theory*. New York: John Wiley and Sons, 2006.

[124] V. Jamali, A. Ahmadzadeh, C. Jardin, H. Sticht, and R. Schober, "Channel estimation techniques for diffusion-based molecular communications," May 2016.

[125] U. Chude-Okonkwo, S. Nunoo, and R. Ngah, "Diffusion-based Molecular Communication Concentration and Capacity Dependencies on Human Body Temperature Variation," in *IEEE International Colloquium on Signal Processing and its Applications (CSPA)*, April 2014.

[126] H. Lodish, A. Berk, and S. Z. et al., *Molecular Cell Biology, 4th Edition*. W. H. Freeman and Company, 2000.

[127] P. A. Mackowiak, S. S. Wasserman, and M. M. Levine, "A critical appraisal of 98.6 f, the upper limit of the normal body temperature, and other legacies of carl reinhold august wunderlich," *Jama*, vol. 268, no. 12, pp. 1578–1580, Sept. 1992.

[128] L. Wright, *Sea Level Rise, Coastal Engineering, Shorelines and Tides*. Nova Science Publishers, 2011.

[129] K. Srinivas, A. Eckford, and R. Adve, "Molecular Communication in Fluid Media: The Additive Inverse Gaussian Noise Channel," *IEEE Trans. on Information Theory*, vol. 8, no. 7, pp. 4678–4692, Jul. 2012.

[130] P. Kolios, V. Friderikos, and K. Papadaki, "Inter-cell interference reduction via store-carry and forward relaying," *IEEE Vehicular Technology Conference*, Sept. 2010.

[131] ——, "Load balancing via store-carry and forward relaying in cellular networks," *IEEE Global Telecommunications Conference*, Dec. 2010.

[132] H. Wu, Q. Chunming, S. De, and O. Tonguz, "An integrated cellular and ad-hoc relaying system: icar," *IEEE Journal on Selected Areas in Communications, SI on Mobility and Resource Management in Next Generation Wireless System*, vol. 19, no. 10, pp. 2105–2115, Oct 2001.

[133] R. Panst, "Relay based deployment concepts for wireless and mobile broadband radio," *IEEE Communications Magazine*, vol. 42, no. 9, pp. 80–89, Sept. 2004.

[134] P. Kolios, V. Friderikos, and K. Papadaki, "Energy efficient relaying via store-carry and forward within the cell," *IEEE Transactions on Mobile Computing*, vol. 13, no. 1, pp. 202–215, Oct 2014.

[135] S. M. Douglas, I. Bachelet, and G. M. Church, "A logic-gated nanorobot for targeted transport of molecular payloads," *Science*, vol. 335, Feb. 2012.

[136] I. F. Akyildiz, F. Brunetti, and C. Blzquez, "Nanonetworks: A new communication paradigm," *Computer Networks*, vol. 52, no. 12, pp. 2260 – 2279, 2008.

[137] S. Lujan, *Bacterial Conjugation and Its Inhibition*. UMI Microform, 2008.

[138] A. Eckford, T. Furubayashi, and T. Nakano, "Rna as a nanoscale data transmission medium: Error analysis," Apr. 2016.

[139] S. Qiu, N. Farsad, Y. Dong, A. Eckford, and W. Guo, "Underwater molecular signalling: a hidden transmitter and absent receivers problem," Jun. 2015.

[140] J. G. Mitchell, "The energetics and scaling of search strategies in bacteria," *The American Naturalist*, vol. 160, no. 6, pp. 727–740, Dec. 2002.

[141] H. Berg and L. Turner, "Chemotaxis of bacteria in glass capillary arrays. escherichia coli, motility, microchannel plate, and light scattering," *Biophysical Journal*, vol. 58, no. 4, pp. 919–930, Oct. 1990.

[142] N. Herman and T. Schneider, "High information conservation implies that at least three proteins bind independently to f plasmid incd repeats," *Biophysical Journal*, vol. 174, no. 11, pp. 3558–3560, Jan. 1992.

[143] A. Heren, H. Yilmaz, C. Chae, and T. Tugcu, "Effect of degradation in molecular communication: Impairment or enhancement," *IEEE Transactions on Molecular, Biological, and Multi-Scale Communications*, vol. 1, no. 2, 2015.

[144] S. Qiu, W. Guo, B. Li, Y. Wu, X. Chu, S. Wang, and Y. Dong, "Long range and long duration underwater localization using molecular messaging," *IEEE Transactions on Molecular, Biological, and Multi-Scale Communications*, vol. 1, no. 4, 2015.

[145] L. Mellefont and T. Ross, "The effect of abrupt shifts in temperature on the lag phase duration of escherichia coli and klebsiella oxytoca," *International Journal of Food Microbiology*, vol. 83, pp. 295–305, Aug. 2002.

[146] M. Rolfe and et.al, "Lag phase is a distinct growth phase that prepares bacteria for exponential growth and involves transient metal accumulation," *Journal of bacteriology*, vol. 194, no. 3, pp. 686–701, Aug. 2012.

[147] V. Petrov, D. Moltchanov, I. F. Akyildiz, and Y. Koucheryavy, "Propagation delay and loss analysis for bacteria-based nanocommunications," *IEEE Transactions on NanoBioscience*, vol. 15, no. 7, pp. 627–638, Oct. 2016.

[148] N. C. Kelland, "Deep-water black box retrieval," *Hydro International*, vol. 13, no. 1, pp. 15–20, Sept. 2009.

[149] K. Sakai and W. Peltier, "Influence of deep ocean diffusivity on the temporal variability of the thermohaline circulation," *The Ocean and Rapid Climate Change: Past, Present, and Future Geophysical Monograph*, vol. 126, no. 1, Jan. 2001.

[150] J. Murlis, J. S. Elkinton, R. T., and A. Card, "Odor Plumes and How Insects Use Them," *Annual Review of Entomology*, vol. 37, no. 1, pp. 505–532, Jun. 1992.

[151] H. C. Berg, "Bacterial microprocessing," in *Cold Springs Harbor Symp. Quant. Biol.*, vol. 55, no. 1, Mar. 1990, pp. 539–545.

[152] B. I. Shraiman and E. D. Siggia, "Scalar turbulence," *Nature*, vol. 405, no. 6787, pp. 639–646, Jun. 2000.

[153] G. Rosen and P. Hasler, "Chemical source localization in unknown turbulence using the cross-correlation method," in *IEEE International Conference on Acoustics, Speech and Signal Processing (ICASSP)*, vol. 3, May 2006.

[154] A. Atalla and A. Jeremic, "Localization of chemical sources using stochastic differential equations," in *IEEE International Conference on Acoustics, Speech and Signal Processing (ICASSP)*, Mar. 2008, pp. 2573–2576.

[155] R. L. Woodfin, *Trace Chemical Sensing of Explosives*. Wiley, 2007.

[156] A. Shrivastava and V. Gupta, "Methods for the determination of limit of detection and limit of quantitation of the analytical methods," *Chron. Young Sci.*, vol. 2, no. 21, p. 5, Jan. 2011.

[157] G. Bernardes, J. Chalker, J. Errey, and B. Davis, "Facile Conversion of Cysteine and Alkyl Cysteines to Dehydroalanine on Protein Surfaces: Versatile

and Switchable Access to Functionalized Proteins," *Journal of the American Chemical Society (JACS)*, vol. 130, no. 15, pp. 5052–5053, Jul. 2008.

[158] H. H. Rosenbrock, "An automatic method for finding the greatest or least value of a function," *The Computer Journal*, vol. 3, no. 3, pp. 175–184, Jan 1960.

[159] M. Stojanovic, "On the relationship between capacity and distance in and underwater acoustic communication channel," *ACM International Workshop on Underwater Networks*, vol. 1, no. 1, Dec. 2006.

[160] D. Anguita, D. Brizzolara, G. Parodi, and Q. Hu, "Optical wireless underwater communication for auv: Preliminary simulation and experimental results," in *IEEE International Conference on Oceans*, Jun. 2011, pp. 1–5.